A STUDY ON THE PRODUCTION AND PROPERTIES OF IN-SITU TITANIUM DIBORIDE PARTICULATE REINFORCED ALUMINUM A356 ALLOY COMPOSITE

A THESIS SUBMITED TO
THE GRADUATE SCHOOL OF NATURAL AND APPLIED SCIENCE
OF
MIDDLE EAST TECHNICAL UNIVERSITY

BY

OSMAN SERDARLI

IN PARTIAL FULFILLMENT OF THE REQUIREMENTS
FOR
THE DEGREE OF MASTER OF SCIENCE
IN
METALLURGICAL AND MATERIALS ENGINEERING

JUNE 2011

Approval of the thesis:

A STUDY ON THE PRODUCTION AND PROPERTIES OF IN-SITU TITANIUM DIBORIDE PARTICULATE REINFORCED ALUMINUM A356 ALLOY COMPOSITE

submitted by **OSMAN SERDARLI** in partial fulfillment of the requirements for the degree of **Master of Science in Metallurgical and Materials Engineering, Middle East Technical University** by

Prof. Dr. Canan Özgen
Dean, Graduate School of **Natural and Applied Sciences** ___________

Prof. Dr. Tayfur Öztürk
Head of Department, **Metallurgical and Materials Engineering** ___________

Prof. Dr. Naci Sevinç
Supervisor, **Metallurgical and Materials Engineering Dept., METU** ___________

Prof. Dr. Ali Kalkanlı
Co-Supervisor, **Metallurgical and Materials Engineering Dept., METU** ___________

Examining Committee Members:

Prof. Dr. Hakan Gür
Metallurgical and Materials Engineering Dept., METU _______________

Prof. Dr. Naci Sevinç
Metallurgical and Materials Engineering Dept., METU _______________

Prof. Dr. Ali Kalkanlı
Metallurgical and Materials Engineering Dept., METU _______________

Prof. Dr. Erdoğan Tekin
Metallurgical and Materials Engineering Dept., ATILIM UNI. _______________

Assoc. Prof. Dr. Arcan Dericioğlu
Metallurgical and Materials Engineering Dept., METU _______________

Date: 30.06.2011

I hereby declare that all information in this document has been obtained and presented in accordance with academic rules and ethical conduct. I also declare that, as required by these rules and conduct, I have fully cited and referenced all material and results that are not original to this work.

Name, Last name: OSMAN SERDARLI

Signature:

ABSTRACT

A STUDY ON THE PRODUCTION AND PROPERTIES OF IN-SITU TITANIUM DIBORIDE PARTICULATE REINFORCED ALUMINUM A356 ALLOY COMPOSITE

Serdarlı, Osman

M.Sc., Department of Metallurgical and Materials Engineering

Supervisor: Prof. Dr. Naci Sevinç

Co-Supervisor: Prof. Dr. Ali Kalkanlı

June 2011, 97 Pages

TiB_2 particle reinforced aluminum matrix composites have been the subject of several investigations. An M.Sc. thesis on production of TiB_2 reinforced aluminum composites by reaction between liquid aluminum and B_2O_3 and TiO_2 dissolved in cryolite has been completed in this Department in 2005. This study is a continuation of the mentioned M.Sc.study. Composition of the starting cryolite-B_2O_3-TiO_2 system, temperature and time were used as experimental variables. The resulting composite was squeeze cast and its microstructure was examined. Mechanical properties of the produced composite were measured and how mechanical properties of the composite vary with TiB_2 content of the composite was determined.

Keywords: In-Situ TiB_2, Metal Matrix Composite, Particles Reinforcement Composite

ÖZ

TİTANYUM DİBORÜR PARÇACIK TAKVİYELİ A356 ALÜMİNYUM ALAŞIM KOMPOZİTİNİN ÜRETİM ÇALIŞMASI

Serdarlı, Osman

Yüksek Lisans., Metalurji ve Malzeme Mühendisliği Bölümü
Tez Yöneticisi: Prof.Dr.Naci Sevinç
Ortak Tez Yöneticisi: Prof.Dr.Ali Kalkanlı

Haziran 2011, 97 Sayfa

TiB_2 parçacık takviyeli aluminyum matrisli kompozitler çeşitli çalışmalara konu olmuştur. Bölümümüzde 2005 yılında biten bir M.Sc. çalışmasında sıvı aluminyum ile kriyolit içinde çözünmüş B_2O_3 ve TiO_2 nin reaksiyonu sonucu TiB_2 parçacık takviyeli aluminyum kompozitlerin üretimi çalışılmıştır. Bu çalışma bahsedilen M.Sc. çalışmasının devamıdır. Kriyolit-B_2O_3-TiO_2 sisteminin başlangıç bileşimi, sıcaklık ve süre deneysel değişkenler olarak kullanılmıştır. Elde edilen TiB_2 takviyeli aluminyum kompozit ezme döküm yöntemi ile dökülmüş ve kompozitin içyapısı incelenmiştir. Elde edilen kompozitin mekanik özellikleri ölçülmüş ve mekanik özelliklerin kompozitin içerdiği TiB_2 miktarı ile değişimi belirlenmiştir.

Anahtar Kelimeler: Yerinde Üretilmiş TiB_2, Metal Matriksli Kompozit, Partikül Takviyeli Kompozit

To my parents

AKNOWLEDGMENTS

I wish to express here my deep and sincere gratitude to my professors: Dr.Ali KALKANLI and Dr.Naci SEVİNÇ for their valuable guidance and encouraging supports during this research.

Also offer my especial thank to Prof. Dr. Erdoğan TEKİN for her pure, honest, benefited hints, without which I may not have been able to complete my master. Mr. Salih TÜRE and all respectful staff of department’s laboratory are gratefully acknowledged for their friendly helps.

My sincere and special gratitude for my parents who supported enlightened me through the whole long way of my study.

Finally, I would never be able to thanks my real true friends Barış AKGÜN and Pelin MARADİT their help in editing my research.

My appreciation to all of my friends who gave me hope and courage.

TABLE OF CONTENTS

CHAPTERS

LIST OF TABLES

TABLES

LIST OF FIGURES

FIGURES

CHAPTER I

INTRODUCTION

In recent years, popularity of composite materials has drastically increased, against to the conventional monolithic alloys. Today, efficient materials, in terms of high specific strength and elastic modulus with light weight, are desired by aerospace, automotive and military applications. Savings in weight result in savings in fuel which translates directly into substantial increase in payload capabilities. A 10% saving in aircraft structural weight increases the available reserve payload by 4% [1]. Metal Matrix Composites, are composed of metallic matrix which provides ductility and toughness and generally ceramic reinforcements which provide high strength and high modulus. They offer a wide range of attractive material properties, both mechanical and physical, that cannot be achieved using conventional engineering alloys. These enhanced materials properties are the direct result of the interaction between the metallic matrix and the reinforcement [2].

Early studies on Metal Matrix Composites (MMCs) have especially concentrated on continuous fiber or short fiber reinforced MMCs. Even though, they have excellent mechanical and physical properties, production cost, complex production routes, reinforcement-particle interface integrity and anisotropic physical and mechanical properties cause some limitations. On the other hand, discontinuous particulate reinforced MMCs achieve some restrictions that continuous reinforced MMCs cannot succeed. Discontinuously reinforced MMCs can be manufactured either in solid state (powder metallurgy.) or in liquid state (stir casting, in-situ) processes and they can be subjected to secondary forming operations (extrusion, rolling, forging). Furthermore, they exhibit isotropic mechanical properties (especially UTS, Yield S.) . More recently, this class of metal matrix composites has attracted considerable attention as result of: (a) availability of various type of reinforcements at competitive costs, (b) the successful development of manufacturing processes to produce metal matrix composites with reproducible structures and properties, and (c) the availability of standard or near standard metal working methods which can be utilized to form theses metal matrix composite [3].

In this study, in-situ TiB_2 particulate reinforced Aluminum alloy matrix composites were produced via reaction of liquid Al with a slag produced from TiO_2, H_3BO_3 and Na_3AlF_6. Composition of the starting slag and reaction time were used as a experimental variables and TiB_2 reinforced aluminum composites having different volume percentages of TiB_2 were produced. Microstructural and mechanical properties of the produced composites were determined and their relationship with the TiB_2 amount and distribution was discussed.

Existing and potential Applications of Al-alloy/TiB_2 Particulate Reinforced Composites

(a) Prototype Parts and Alloys:

(a1) Automobile conrod: Wrought Alloy 2618 + TiB_2 Fatigue tests on forged demonstrator parts

(b) Aerospace & Automotive Applications

(b1) Helicopter Blade Sleeve Application: Wrought Alloy 2618 + TiB_2 Tests on pancake samples and forged I-beam

(b2) Seat Track Application: Wrought Alloy 7075 + TiB_2 Continuous cast and extruded; heat-treated

(c) Wear Resistance Applications: Casting Alloy A356 + TiB_2 Cylinder liners for automotive engines produced by high-pressure die casting and tested under realistic conditions in co-operation with Al producer and automotive companies.

CHAPTER II

LITERATURE SURVEY

2.1 Introduction

Metal Matrix Composites (MMCs), which are new and important class of materials for aerospace, automotive and structural wear applications, have become popular in the last decades. They offer a wide range of attractive material properties, both mechanical and physical, that cannot be achieved using conventional engineering alloys. These enhanced materials properties are the direct result of the interaction between the metallic matrix and the reinforcement [4].

In general, three common synthesizing routes are available for Metal Matrix Composites; Solid-State process, Liquid-State process and Two-Phase process. Among these, the liquid-state process yields better physically and chemically stable matrix-reinforcement interface and fine microstructural homogeneity. These two terms directly affect ambient and high temperature mechanical properties of metal matrix composite. Therefore, the clear interface is directly related with mechanical properties. In addition to these advantages, fast, low cost, single step composite synthesizing is achieved by the liquid-state process.

In-Situ Process is a novel technique that does not require any secondary process parameters. In this process the required reinforcing phases are produced by chemical reaction among the appropriate ingredients at suitable temperatures. During the last decade new in-situ fabrication technologies for processing metal and ceramic composites have been developed by chemical reactions generating very fine, thermodynamically stable reinforcing ceramic phases [5]. In-situ process also results in uniform distribution of the reinforcement and clean interface between matrix and reinforcement.

2.2 Metal Matrix Composite

Composites are commonly classified at two distinct levels. The first level of classification is usually made with respect to the matrix constituent. The major composite classes include organic-matrix composites (OMCs), metal-matrix Composites (MMCs), and ceramic-matrix composites (CMCs). The term “organic-matrix composite” is generally assumed to include two classes of composites: polymer-matrix composites (PMCs) and carbon-matrix composites (commonly referred to as carbon-carbon composites).

The second level of classification refers to the reinforcement form: particulate reinforcements, whisker reinforcements, continuous fiber laminated composites, and woven composites (braided and knitted fiber architectures are included in this category), as depicted in Figure 2.1 [6].

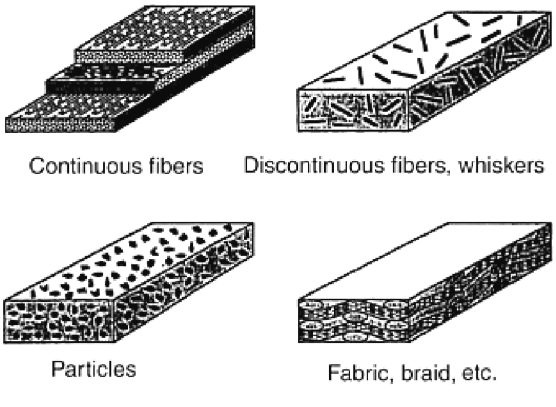

Figure 2. 1 Common forms of fiber reinforcement. In general, the reinforcements can be straight continuous fibers, discontinuous or chopped fibers, particles or flakes, or continuous fibers that are woven, braided, or knitted [6].

Reinforcement is considered to be a “particle” if all of its dimensions are roughly equal. Thus, particulate-reinforced composites include those reinforced by spheres, rods, flakes, and many other shapes of roughly equal axes. Whisker reinforcements, with an aspect ratio typically between approximately 20 to 100, are often considered together with particulates in MMCs. Together, these are classified as “discontinuous” reinforcements, because the reinforcing phase is discontinuous for the lower volume fractions typically used in MMCs [6].

“Reinforcement of metals can have many different objectives. The reinforcement of light metals opens up the possibility of application of these materials in areas where weight reduction has first priority. The precondition here is the improvement of the component properties. The development objectives for light metal composite materials are” [7]:

- Increase in yield strength and tensile strength at room temperature and above while maintaining the minimum ductility and toughness,
- Increase in creep resistance at higher temperatures compared to that of conventional alloys,
- Increase in fatigue strength, especially at higher temperatures,
- Improvement of thermal shock resistance,
- Improvement of corrosion resistance,
- Increase in Young’s modulus,
- Reduction of thermal elongation.

Important physical and chemical properties of three main materials are shown in Figure 2.2. Metal matrix composite materials are intersections of these properties

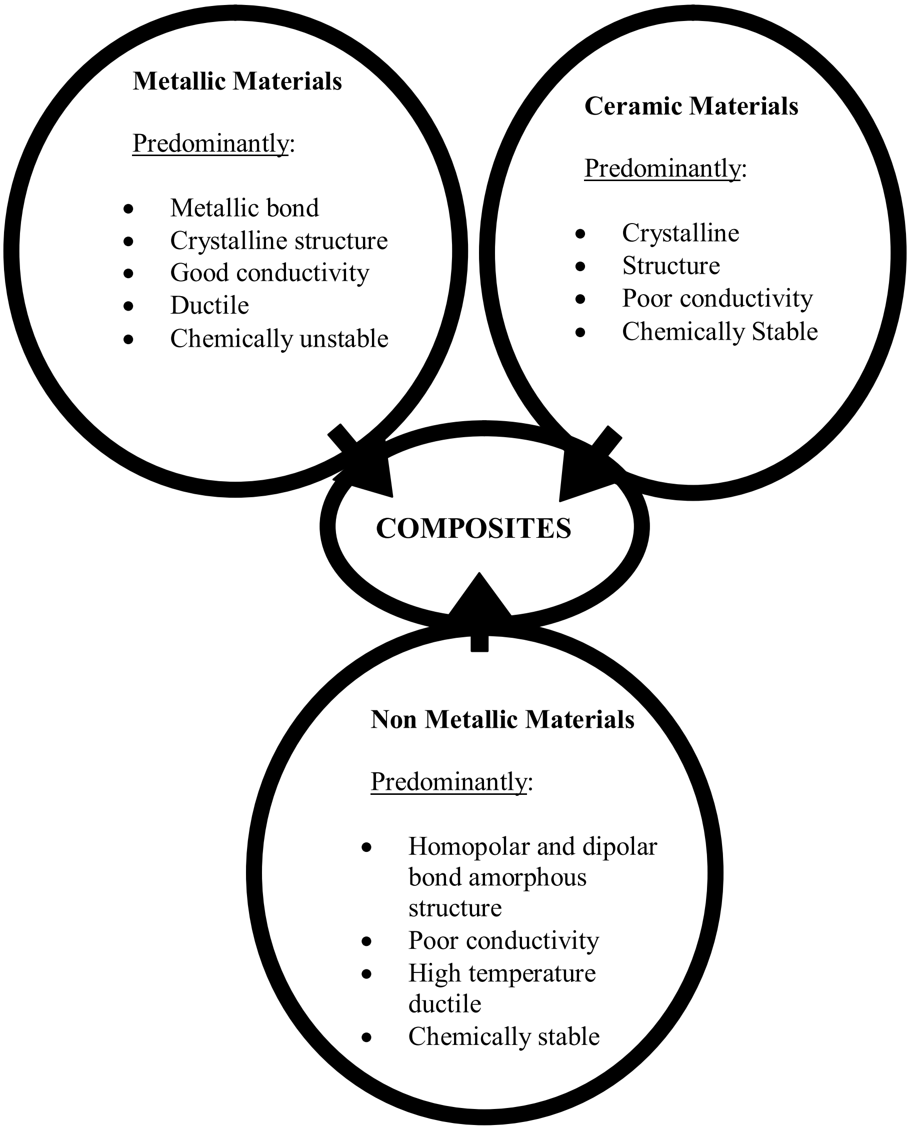

Figure 2. 2 Classification of the composite materials within the group of materials [8].

Discontinuous term usually refers to particulate reinforced composites because the ceramic phase discontinuously reinforced metal matrix. In a DRMMC (Discontinuously Reinforced Metal Matrix Composite) materials system, the reinforcement strengthens the metal matrix both extrinsically, by load transfer to the ceramic reinforcement, and intrinsically, by increasing dislocation density [9]. The interaction between the particulate reinforcement and the metallic matrix is the basis for the enhanced physical and materials properties associated with DRMMC materials systems. Composite materials properties can be tailored to meet specific engineering requirements by selecting a particular reinforcement and varying the amount added to the metal matrix. In this fashion, the physical and mechanical properties of the composite materials system can be controlled with some independence.

Increasing the reinforcement volume in a composite system increases mechanical properties, such as elastic modulus, ultimate strength, and yield strength, while reducing the thermal expansion and, in some cases, the density of the composite system. Unfortunately materials properties such as ductility and fracture toughness typically decrease with increasing reinforcement volume. The increase in both the elastic modulus and strength (ultimate and yield) is believed to be due to the difference in thermal expansion between the ceramic reinforcement particles and the metallic matrix during processing. During the production of these composites, both the reinforcement and matrix are heated to processing temperature, brought to thermomechanical equilibrium, and then allowed to cool. The thermal contraction of the metallic matrix during cool down is typically much greater than that of the reinforcement, which leads to a geometric mismatch. At the ceramic-metal interface, this geometrical disparity creates mismatch strains that are relieved by the generation of dislocations in the matrix originating from sharp features on the ceramic reinforcement [10].

2.3 Materials Selection

2.3.1 Matrix Selection

Wide range of metals can be used for the matrix of the composites whereas lightweight and compatibility with the ceramic reinforcements restricts choice of matrix metal. The common material candidates are Aluminum, Magnesium, Titanium, Copper, Zinc, Nickel and Lithium. Another restriction is that chemical reactions should not take place between matrix and reinforcement. Such a reaction deteriorates reinforcement-matrix interface properties hence the mechanical properties are reduced. Aluminum is the best option to produce in-situ TiB_2 reinforcement composite due to reasonable mechanical, casting properties and good compatibility of TiB_2 reinforcement.

The requirements of low density, with reasonably high thermal conductivity, have made aluminum and magnesium alloys the most commonly used matrices. Regarding alloying additions, the result of several studies have shown that low matrix alloying additions result in metal matrix composites with attractive combinations of strength, ductility and toughness. Minor alloying elements commonly used in wrought alloys as grain refiners, are unnecessary in discontinuous reinforced metal matrix composites. Furthermore, these additions should be avoided, since they may result in the formation of coarse intermetallic compounds during consolidation and subsequence processing, thus impairing the ductility of the composite [11],[12].

It is convenient to divide aluminum alloys into two major categories: casting compositions and wrought compositions. Cast and wrought alloy nomenclatures have been developed. The Aluminum Association system is most widely recognized in the United States. Their alloy identification system employs different nomenclatures for wrought and cast alloys, but divides alloys into families for simplification [13].

For wrought alloys a four-digit system is used to produce a list of wrought composition families as follows:

- 1xxx Controlled unalloyed (pure) compositions,
- 2xxx Alloys in which copper is the principal alloying element, though other elements, notably magnesium, may be specified,
- 3xxx Alloys in which manganese is the principal alloying element,
- 4xxx Alloys in which silicon is the principal alloying element,
- 5xxx Alloys in which magnesium is the principal alloying element,
- 6xxx Alloys in which magnesium and silicon are principal alloying elements,

- 7xxx Alloys in which zinc is the principal alloying element, but other elements such as copper, magnesium, chromium, and zirconium may be specified,
- 8xxx Alloys including tin and some lithium compositions characterizing miscellaneous compositions,
- 9xxx Reserved for future use.

2.3.1.1 Aluminum Casting Alloys

Aluminum casting alloys are the most versatile of all common foundry alloys and generally have the highest castability ratings. As casting materials, aluminum alloys have the following favorable characteristics [14]:

- Good fluidity for filling thin sections,
- Low melting point relative to those required for many other metals,
- Rapid heat transfer from the molten aluminum to the mold, providing shorter casting cycles,
- Hydrogen is the only gas with appreciable solubility in aluminum and its alloys, and hydrogen solubility in aluminum can be readily controlled by processing methods,
- Many aluminum alloys are relatively free from hot-short cracking and tearing tendencies,
- Chemical stability,
- Good as-cast surface finish with lustrous surfaces and little or no blemishes.

Casting compositions are described by a three-digit system followed by a decimal value. The decimal .0 in all cases pertains to casting alloy limits. Decimals .1 and .2 concern ingot compositions, which after melting and processing should result in chemistries conforming to casting specification requirements. Alloy families for casting compositions are:

- 1xx.x Controlled unalloyed (pure) compositions, especially for rotor manufacture,

- 2xx.x Alloys in which copper is the principal alloying element, but other alloying elements may be specified,
- 3xx.x Alloys in which silicon is the principal alloying element, but other alloying elements such as copper and magnesium are specified,
- 4xx.x Alloys in which silicon is the principal alloying element,
- 5xx.x Alloys in which magnesium is the principal alloying element,
- 6xx.x Unused,
- 7xx.x Alloys in which zinc is the principal alloying element, but other alloying elements such as copper and magnesium may be specified,
- 8xx.x Alloys in which tin is the principal alloying element,
- 9xx.x Unused.

2.3.1.2 Al-Si Casting alloys

Some 238 compositions for foundry aluminum alloys have been registered with the Aluminum Association. Although only 46% of this total consists of aluminum-silicon alloys, this class provides nearly 90% of all the shaped castings manufactured. The reason for the wide acceptance of the 3xx.x alloys can be found in the attractive combination of physical properties and generally excellent castability. Mechanical properties, corrosion resistance, machinability, hot tearing resistance, fluidity, and weldability are considered the most important [15]. This is why Al-Si casting alloy is selected as a matrix alloy in the presnt study. The compositions of most common casting alloys are summarized in Table 2.1 While these alloys exhibit excellent wear resistance, pressure tightness, fluidity, and shrinkage, their machinability and weldability characteristics are not as good [16].

Table 2.1. The Composition of Common Al-Si Alloys * [16]

Alloy	Fabrication Method ǂ	Element (wt.%)					
		Si	Cu	Mg	Fe	Zn	Others
350 Series	S/PM	5-7	<0.2-1.25	0.35-0.55	<0.06-<0.2	<0.1-<0.35	----
380 Series	D	8.5-11.0	2.0-3.5	<0.1-<0.3	<1.3	<3.0	<0.3Sn
390 Series	D	<7.5	4.5	0.55	<1.3	<0.1	<0.1Mg
400 Series	S/PM/D	5.25-12.0	<0.1-<0.3	<0.5-<0.1	<0.8-<2.0	<0.5	----

* The remainder of the composition is aluminum and impurities.
ǂ S- Sand casting; PM-Permanent mold casting; D-Pressure die casting

Aluminum-Silicon phase diagram is shown below. (Figure 2.3) Alloy compositions and phase identifications are made according to this diagram.

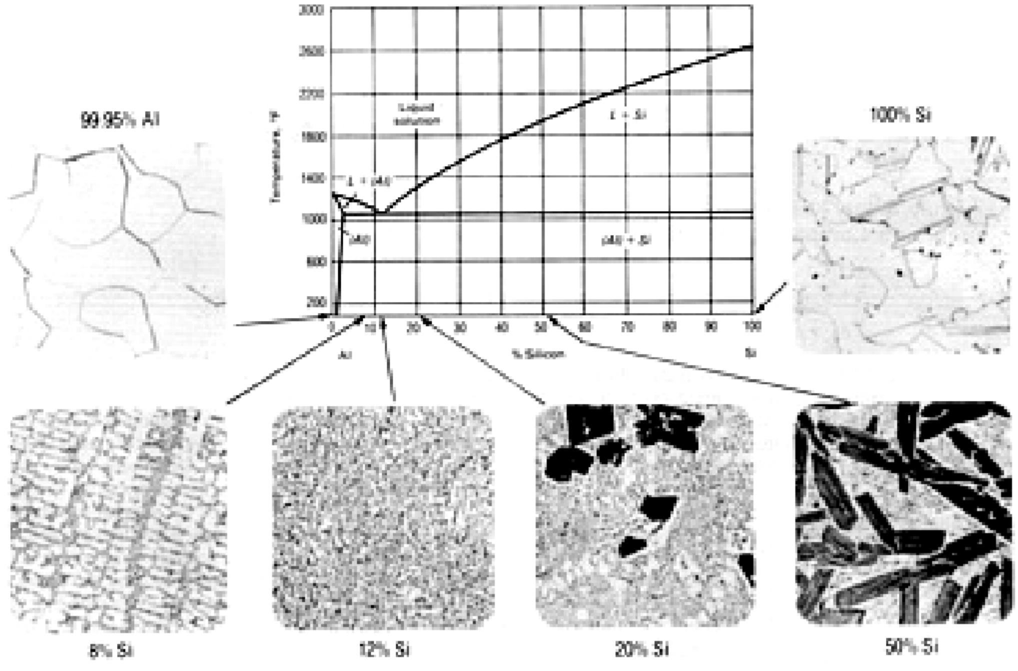

Figure 2.3 Aluminum-silicon phase diagram and cast microstructures of pure components and of alloys of various compositions. Alloys with less than 11.6% Si are referred to as hypoeutectic, those with close to 11.6% Si as eutectic, and those with over 11.6% Si as hypereutectic.

Selection of suitable aluminum cast matrix alloy is 356.0. Chemical compositions is shown below at the Table 2.2

Table 2.2. The Chemical Composition of 356.0 Al-Si casting alloy

Element (wt.%)							
Si	**Mg**	**Cu**	**Mn**	**Zn**	**Fe**	**Ti**	**Al**
6.5- 7.5	0.25-0.45	< 0.20	<0.10	< 0.10	<0.20	< 0.20	Balance

Alloy 356.0 (7 Si, 0.3 Mg) has excellent casting characteristics and resistance to corrosion. This justifies its use in large quantities for sand and permanent mold castings. Several heat treatments are used and provide the various combinations of tensile and physical properties that make it attractive for many applications. This includes many parts in both the automotive and aerospace industries. The companion alloy of A356.0 with lower iron content affords higher tensile properties in the premium-quality sand and permanent mold castings. [17]. Casting characteristics, specific strength and wide commercial practice are main reasons for selection of A356 alloy as a matrix.

2.3.2 Reinforcement Selection

The primary duty of reinforcement particles in metal matrix composites (MMCs) is resisting and transferring the external load acting on the composite at the boundary of particle and matrix [18]. Suitable wetting is a fundamental condition for the combination of reinforcement particles with the aluminum matrix throughout the composite casting. This favors the transfer and distribution of stresses in the solid state without fracture of the composite. These combinations could be formed by dissolution or chemical reaction of reinforcement particles with matrix metal. However, chemical reactions are usually harmful to the mechanical properties [19].

Selection criteria for the ceramic reinforcement include:

- elastic modulus,
- tensile strength,
- hardness
- density,
- melting temperature,
- thermal stability,
- coefficient of thermal expansion,
- size and shape,
- compatibility with matrix material, and
- cost.

Some selected properties of commonly used ceramic reinforcements are shown in Table 2.3. The structural efficiency of discontinuously reinforced metal matrix composites is a function of the density, elastic modulus, and tensile strength of the reinforcing phases [20] .

Table 2. 3. Essential Properties of Selected Reinforcements [21],[11],[22].

Reinforcement	Density (g/cm^3)	CTE (µm/m K)	Melting point (°C)	Strength (MPa)	Modulus (Gpa)
Al_2O_3	3.98	7.92	2015	221(1090°C)	379(1090°C)
AlN	3.26	4.84	2069	2069(24°C)	310(1090°C)
BeO	3.01	7.38	2570	24(1090°C)	190(1090°C)
BN	3.48	7.50	2327	2500	195
B_4C	2.52	6.08	2450	2759(24°C)	448(24°C)
C	2.18	-1.44	3527	-	690
CeO_2	7.13	12.42	2600	589(24°C)	185(24°C)
HfC	12.2	6.66	3928	-	317(24°C)
MgO	3.58	11.61	2620	41(1090°C)	317(1090°C)
$MoSi_2$	6.31	8.91	2030	276(1090°C)	276(1260°C)
Mo_2C	8.90	5.81	2500	-	228(24°C)
NbC	7.60	6.84	3500	-	338(24°C)
Si	2.33	3.06	1414	-	112
SiC	3.21	5.40	2830	-	324(1090°C)
Si_3N_4	3.18	1.44	1900	-	207
SiO_2	2.66	<1.08	1610	-	73
TaC	13.90	6.46	3880	-	366(24°C)

Table 2.3 (cont'd)

$TaSi_2$	9.1	10.80	2200	-	338(1260°C)
ThO_2	9.86	9.54	3300	193(1090°C)	200(1090°C)
TiB_2	**4.50**	**8.28**	**2920**	**-**	**414(1090°C)**
TiN	5.44	8.10	2950	1298	390
TiC	4.93	7.60	2830	55(1090°C)	296(24°C)
UO_2	10.96	9.54	2847	-	172(1090°C)
VC	5.77	7.16	2699	-	434(24°C)
WC	15.63	5.09	2800	-	669(24°C)
WSi_2	9.40	9.00	2165	-	248(1090°C)
ZrB_2	6.09	8.28	1845	-	503(24°C)
ZrC	6.73	6.66	1852	90(1090°C)	359(24°C)
ZrN	7.35	7.0	2952	-	328
ZrO_2	5.89	12.01	2700	83(1090°C)	132(1090°C)

Reinforcements used in the composites include carbides, nitrides, borides and oxides. Among these reinforcements, titanium diboride (TiB_2) can interact well with the matrix, and it does not react with aluminum, which avoids the formation of brittle interfacial products at the particle/matrix interface. Furthermore, the TiB_2 particles exhibit very high stiffness and hardness. Given these favorable properties, the TiB_2 particles have received more attention than other reinforcements [23], [24].

2.4 Physical and Mechanical Properties of Metal Matrix Composites

2.4.1 Physical Properties

Thermal Expansion Coefficient

"Reinforcement of light metal alloys with ceramic fibers or particles entails a reduction in the thermal expansion coefficients. Simple models are available to estimate the thermal expansion coefficients with the help of the characteristics of the individual components" [25].

The simplest model is the rule of mixture (ROM) which is shown below in Equation 2.1;

$$\alpha_c = \alpha_m V_m + \alpha_r V_r \tag{2.1}$$

where α is the thermal expansion coefficient, V is the volume fraction and the subscripts c, m, r denote to the composite, matrix and reinforcing phase. The ROM has some limitations and more complex models are available; Tuener [26] takes into account the effects of isostatic stress in Equation 2.2;

$$\mathrm{CTE_c} = \frac{\mathrm{CTE_m}\, K_m V_m + \mathrm{CTE_r}\, K_r V_r}{K_r V_r + K_m V_m} \tag{2.2}$$

where K is the bulk modulus, V is the volume fraction and the subscripts c, m, r denote the composite, matrix and reinforcing phase. This model gives more precise results in the calculation of CTE than the ROM. Kener [27] offers the most complex model that includes the effect of shear stress between matrix and (isotropic and spherical) reinforcements which is shown below in Equation 2.3;

$$\mathrm{CTE_c} = \mathrm{CTE_m} - V_r\,(\mathrm{CTE_m} - \mathrm{CTE_r}) \times \frac{A}{B} \tag{2.3}$$

where;

$$A = K_m\,(3K_r + 4\mu_m)^2 + (K_r - K_m) \times (16\mu_m{}^2 + 12\mu_m K_r)$$

$$B = \left(3K_r + 4\mu_m\right)\left[\,4V_r\,\mu_m\,(K_r - K_m) + \;3K_mK_r + 4\mu_m\,K_r\right]$$

"where μ and K are the shear and bulk modulus respectively and the subscripts m, r denote matrix and reinforcing phase. The results of this model are between the Tuener's model and the ROM." [28]

2.4.2 Mechanical Properties

2.4.2.1 Strengthening by Particles

"High modulus ceramic particles significantly increase hardness and strength of the ductile aluminum matrix. One micromechanical model showing this effect is described [29], [30] by Equation 2.4":

$$\Delta R_{p,C} \;=\; \Delta\sigma_\alpha + \Delta\sigma_{KG} \;+ \Delta\sigma_{SKG} + \Delta\sigma_{KF} \tag{2.4}$$

where $\Delta R_{p,C}$ is the boost in tensile strength of aluminum matrix by the presence of ceramic reinforcement; $\Delta\sigma_\alpha$ etcetera are described below

The effect of induced dislocations, $\Delta\sigma_\alpha$,is given by Equation 2.5:

$$\Delta\sigma_\alpha = \;\alpha\, G\, b\, p^{1/2} \tag{2.5}$$

with;

$$p = 12\Delta T\frac{\Delta C\Phi_P}{bd} \tag{2.6}$$

"where $\Delta\sigma_\alpha$ is the yield strength contribution due to geometrical necessary dislocations and inner tension, α is a constant (values 0.5–1), G is the shear modulus, b is the Burger's vector, p is the dislocation density, ΔT is the temperature difference, ΔC is the difference in thermal expansion coefficient between matrix and particle, Φ_P is the particle volume content and d the particle size."

The effect of the grain size, $\Delta\sigma_{KG}$, is given by Equation 2.7:

$$\Delta\sigma_{KG} = k_{Y1} D^{-1/2} \tag{2.7}$$

with

$$D = d\left(\frac{1-\Phi_P}{\Phi_P}\right)^{1/3} \tag{2.8}$$

where $\Delta\sigma_{KG}$ is the yield strength contribution from changes in grain size; k_{Y1} is a constant, D is the resulting grain size and Φ_P is the particle volume content.

The effect of the grain size $\Delta\sigma_{SKG}$ is given by Equation 2.9:

$$\Delta\sigma_{SKG} = k_{Y2} {D_s}^{-1/2} \tag{2.9}$$

with

$$D_s = d\left(\frac{\pi d^2}{6\Phi_P}\right)^{\frac{1}{2}} \tag{2.10}$$

“where $\Delta\sigma_{SKG}$ is the yield strength contribution due to changes in subgrain size (for instance in a relaxation process during thermomechanical treatment of composite), k_{Y2} is a constant (typical value 0.05 MN $m^{-3/2}$), D_s is the resulting subgrain size and Φ_P is the particle volume content.”

The yield point is the yield strength at the 0.2 % elongation. The considerable strain hardening is seen which is dependent on the particle diameter and content.

The strain hardening contribution $\Delta\sigma_{KF}$ is given in equation 2.11;

$$\Delta\sigma_{KF} = KG\Phi_P \left(\frac{2b}{d}\right)^{1/2} \varepsilon^{1/2} \tag{2.11}$$

“where K is a constant, G the shear modulus, Φ_P the particle volume content, b the Burger’s vector, d the particle diameter and Ɛ the elongation.”

“Generally higher hardening contributions are made by smaller particle diameters than by coarser particles. For smaller particle diameters the work hardening and the grain size influence contribute the most to the increase in the yield strength ” [28].

2.4.2.2 Young’s Modulus (Modulus of Elasticity)

“A significant increase in the elastic modulus is observed with addition of discontinuous reinforced ceramic particles. Reinforcement amount, geometry, distribution and type affect the modulus. The suitable rules for the determination of the modulus in the composite materials are given below” [31].

Inverse mixture rule: Reuss-model (IMR) is given by Equation 2.12

$$E_C = \left(\frac{\Phi_P}{E_P} + \frac{1-\Phi_P}{E_M}\right)^{-1} \tag{2.12}$$

“where Φ_P is the volume content of particles or fibers, E_c the Young’s modulus of the composite material, E_P the Young’s modulus of the particle or fiber and E_M the Young’s modulus of the matrix.”

“An advancement of these models, which is also applicable for short fibers or particles, is the model by Tsai Halpin. By implementing an effective geometry factor, which can be determined from the structure of the composite materials as a function of the load direction, the geometry and the orientation of the reinforcement can be considered” [32]:

$$E_C = \frac{E_M(1+2Sq\Phi_P)}{1-q\Phi_P} \tag{2.13}$$

with;

$$q = \frac{(E_P/E_M)-1}{(E_P/E_M)+2S} \tag{2.14}$$

where S is the geometry factor of the fiber or particle (1/d).

“The critical requirement for the application of such models is the presence of a composite material with an optimal structure, i.e. without pores, agglomerates of particles or nonreinforced areas” [28].

2.5 Thermodynamics of Aluminum Matrix Composites

In spite of many processing techniques developed, mechanisms of the reactions that occur in the process are not well understood. For example, in Al-Ti-B system, several different reactions have been proposed between Al, Ti and B [33]. Maxwell and Hellawell [34] suggested a ternary peritectic reaction of L (liquid) + Al_3Ti + TiB_2 = (Al) above 665°C and a ternary eutectic reaction of L (liquid) = (Al) + Al_3Ti + TiB_2 below 659°C.

Abdel Hamid and Durand [35] proposed two transition reactions of L + Al_3Ti = (Al) + TiB_2 and L + TiB_2 = (Al) + AlB_2 to take place within the temperature range of 659±665°C. Thermodynamic calculations [36] have consistently revealed the existence of compounds AlB_2, TiB_2, Al_3Ti and mixed boride phase of (Al, Ti)B_2. Several studies on Al based metal matrix composites (MMCs) reinforced by TiB_2 were restricted to experimental investigations. A long traditional debate has been made [37],[38] on whether AlB_2 and TiB_2 be present as two separate phases or as a continuous series of solid solution of the form (Al,Ti)B_2. A number of investigators [39],[38] have reported that AlB_2 and TiB_2 can coexist together. Both AlB_2 and TiB_2 are of the same crystal structures and they have lattice parameters that are very similar.

TiO_2 and B_2O_3 are dissolved in cryolite based slag and overall reaction, between the dissolved species; TiO_2, B_2O_3 and liquid Al, is given below:

$$\mathbf{TiO_2\,(\mathit{s}) + B_2O_3\,(\mathit{l}) + 10/3\ Al\,(\mathit{l}) = TiB_2\,(\mathit{s}) + 5/3\ Al_2O_3\,(\mathit{s})}$$

with;

$\mathbf{\Delta G^\circ = -\,1855133.3+331.3T}$ [40],

Temperature range of the reaction is 933°K-1939°K (660^0C -1680^0C). ΔG° is negative at all temperatures in the range. According to reaction which is shown above, TiB_2(s) particles can be produced. This reaction takes place either in single step or multiple steps. TiO_2 and B_2O_3 are reduced subsequent to the reaction given above, Al_2O_3 remains at the system and will not involve in further chemical reaction. In this system, only Al, Ti and B are available to take part in further reactions. Ti and B are soluble in Al (l) . In the liquid aluminum bath, Ti and B can react and such a reaction is given below:

[Ti]+2[B] =TiB_2 (s) with $\Delta G = -284{,}500 + 20.5T$ [41]

ΔG of this intermediate reaction is negative at 1273°K (1000°C). According to reaction is shown above, TiB_2 (s) particles can be formed in the liquid aluminum.

2.6 Solubilities of Phases in Cryolite and Liquid Aluminum

2.6.1 Al_2O_3–Na_3AlF_6 and TiO_2–Na_3AlF_6 binary systems

The solubility of alumina (=Al_2O_3) in the liquid cryolite is very important aspect for the production of Aluminum via the famous Hall-Heroult process.

In Figure 2.4, the phase diagram of cryolite - alumina system is shown. Solubility of Al_2O_3 can be determined for each temperature from the phase diagram [42].

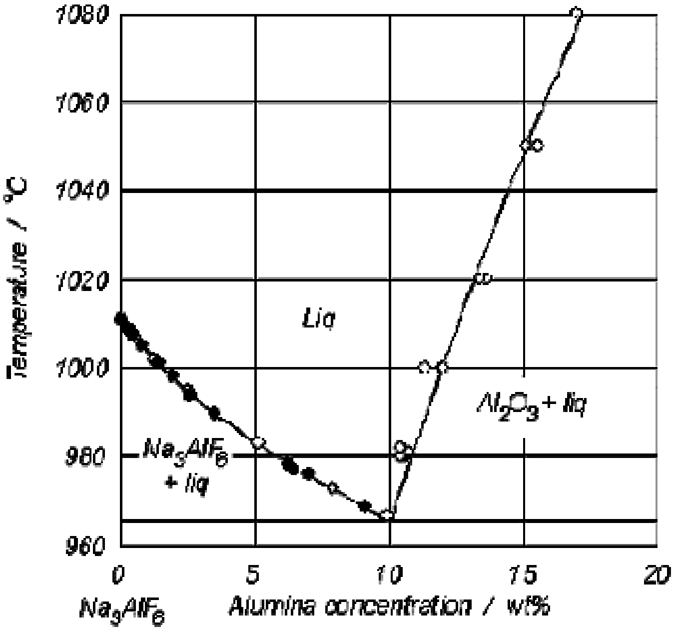

Figure 2. 4 Alumina Solubility in Cryolite [42]

The solubility of TiO_2 in Na_3AlF_6 can find out with phase diagram of Cryolite – TiO_2 The binary phase diagram is shown in Figure 2.5 [43].

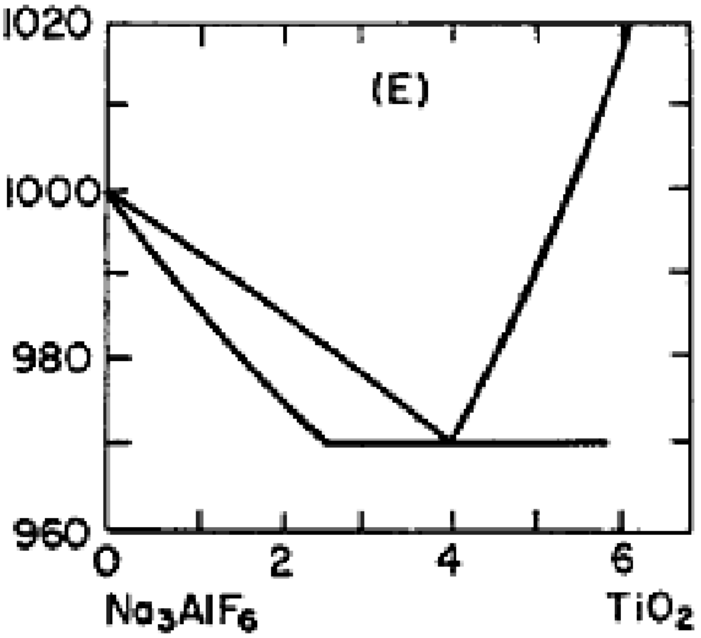

Figure 2. 5 Cryolite-Titanium dioxide System [43]

2.6.2 TiB_2—Al system

At 1300°K the solubility of TiB_2 in molten Aluminum is $6X10^{-3}$ %wt. The equilibrium is established within 10h between TiB_2 and liquid Aluminum in a library cell. At 1300°K, the aluminum solubility in TiB_2 is trace amount so that it is unmeasured [44] . Therefore, according to reaction given below produced $TiB_2(s)$ particles are directly precipitated in liquid Aluminum.

$[Ti]+2[B] = TiB_2\ (s)$ with $\Delta G = -284{,}500 + 20.5T$ [41]

[] denotes that species are dissolved in liquid aluminum.

2.6.3. Al—Ti, Al—B, Ti—B binary systems and Al—Ti—B ternary system

Titanium has some solubility in liquid aluminum at temperatures between 850°C and 1200°C. Above 1200°C solubility of Ti increases rapidly but experimental temperature range is limited at 1100°C.

In binary Al-Ti phase diagram, solubility limits and solid phases are shown in Figure 2.6

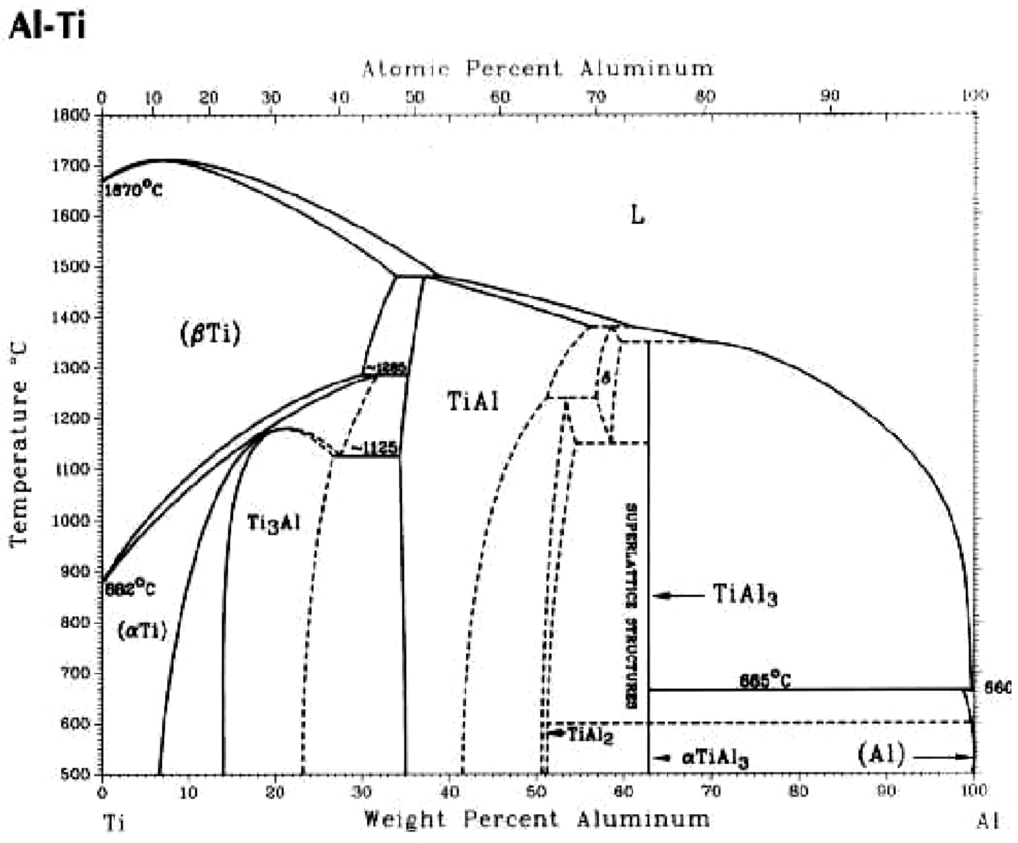

Figure 2. 6 Al-Ti binary phase diagram [36].

Boron also has some solubility in liquid aluminum. From the Al-B phase diagram given below, solubility of boron in liquid aluminum is seen to increase significantly with increase in temperature.

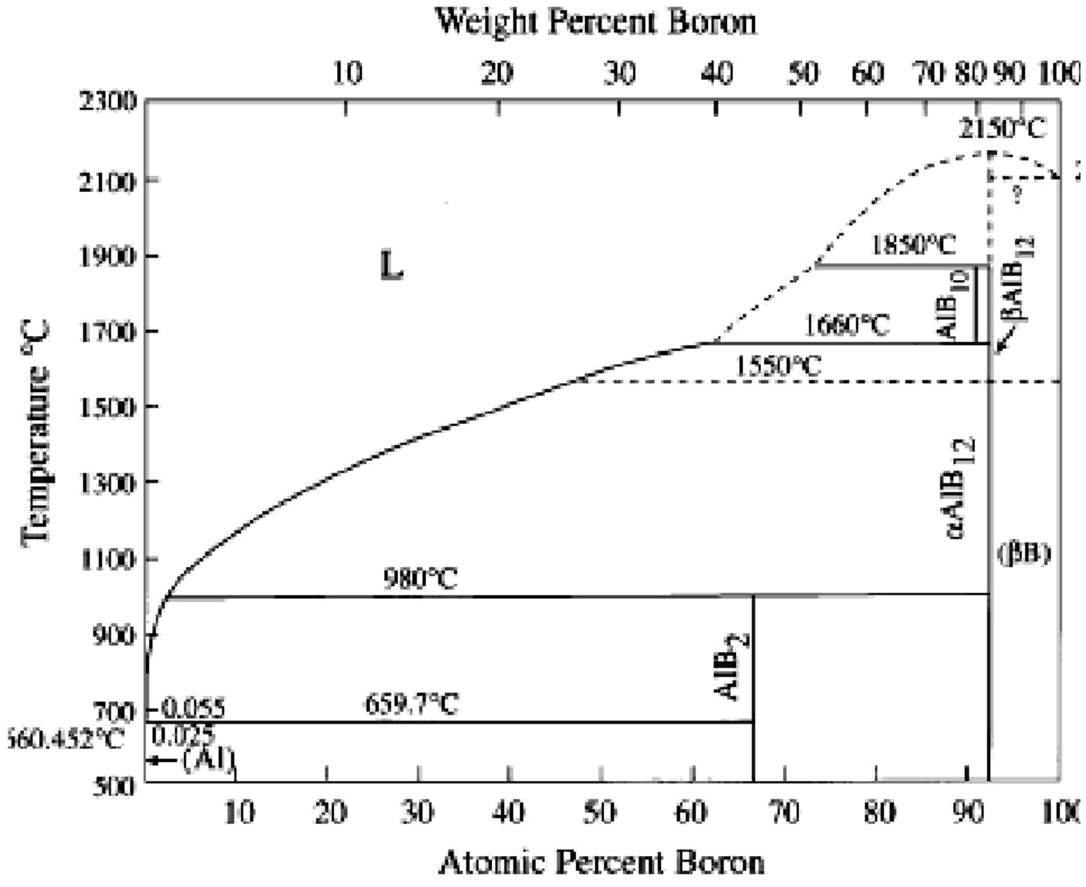

Figure 2. 7 Al-B binary phase diagram [45].

In Ti-B binary phase diagram, which is given in Figure 2.8, TiB_2(s) phase is stable at between 30.1 and 31.1 weight % boron from 25°C to 2201°C. Ti_3B_4(s) and TiB(s) phases will be formed with decreasing weight % boron. On the other hand, elemental boron and TiB_2(s) will be formed with increasing weight % boron.

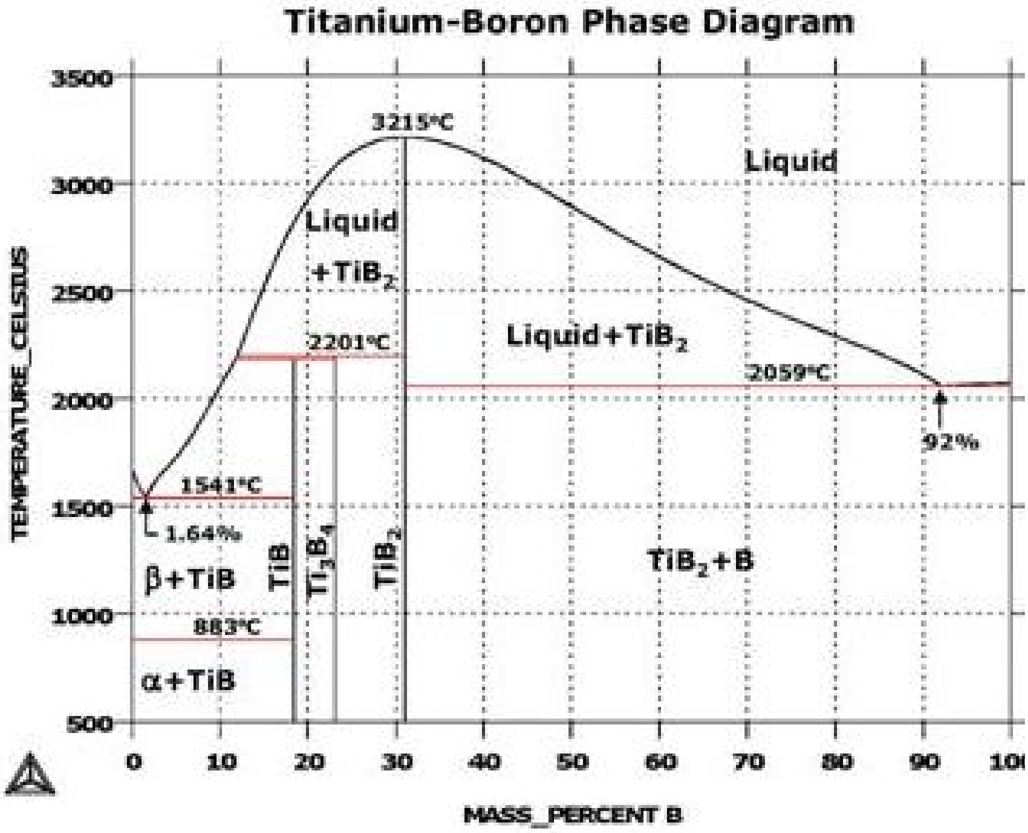

Figure 2. 8 Ti-B binary phase diagram [45].

Al-Ti-B ternary phase diagram is given below in Figure 2.9:

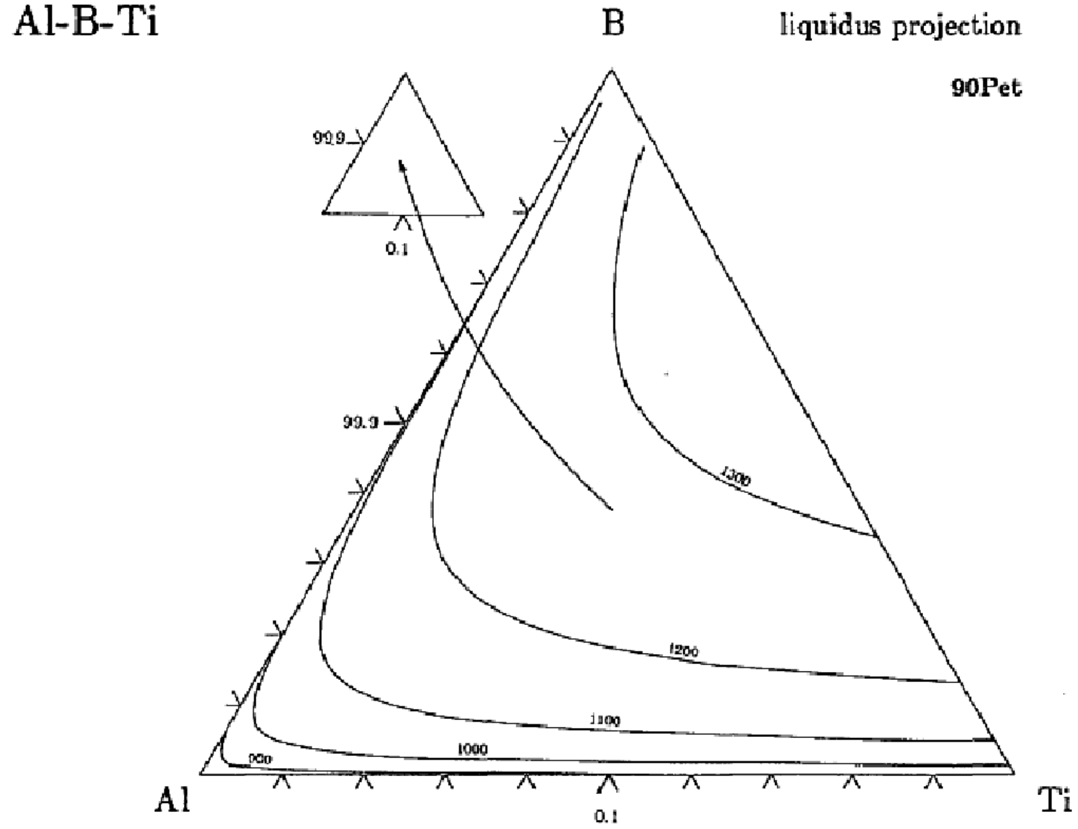

Figure 2. 9 Al-B-Ti Ternary phase diagram [45].

2.7 Processing Methods for Particulate Reinforced Al Alloy Matrix MMCS

The early studies are concentrated on the fiber (continuously) reinforced aluminum matrix composites however present studies are focused on particle or whisker (discontinuously) reinforced aluminum matrix composites. They have uncomplicated manufacture, low cost production, and isotropic mechanical properties [46].

Classification of processing are made by synthesis of reinforcing phase for particle reinforced MMCs. The processes can be divided two main classes;

- External production of the reinforcement and its addition to matrix (Ex-Situ),
- Internal production of reinforcement (In-Situ).

In the ex-situ production, the reinforcing phase is produced separately out of the matrix phase and it is introduced to the matrix with a secondary process. To the contrary, in in-situ production, the reinforcing phase is produced directly within the matrix.

Physical state of matrix is also accepted as a classification criterion. Three general processing techniques are available according to physical state of matrix. These are solid phase, liquid phase, and two phases. Classification is given in Figure 2.10

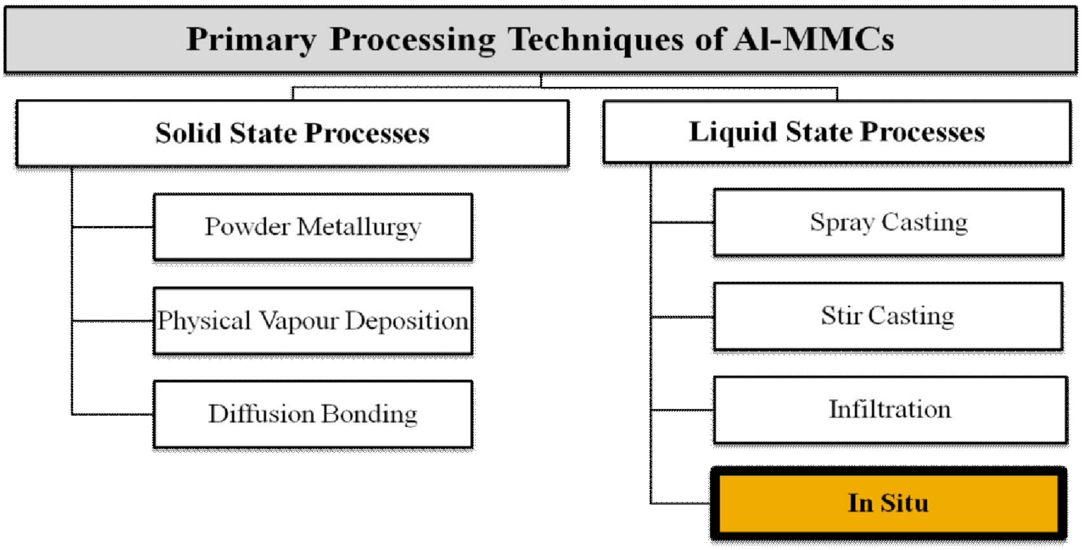

Figure 2. 10 Primary processing techniques of Al-MMCs according to physical state of matrix

2.7.1 Liquid State Processes

2.7.1.1 Casting

There are some basic different modifications between the conventional aluminum casting and the high-quality composite casting. The differences in composite foundry practices are:

- The inert gas coverage can be applied because common degassing procedures, such as gas injection or plunging tablets, can cause gas bubble nucleation on the reinforcement particles and dewetting of the reinforcement.
- Temperature control is sensitive for the reinforcement phase, for example, if overheating takes place, aluminum carbide will form in SiC reinforced aluminum according to reaction; $4Al + 3SiC \rightarrow Al_4C_3 + 3Si$. Aluminum carbide forms slightly above 750°C, and the reaction is fast in the 780-800°C temperature range.
- Stirring is crucial for the uniform distribution of ceramic particles. The ceramic reinforcing particles neither melt nor dissolved in the liquid aluminum matrix. Furthermore some ceramic particles are denser than the liquid metal so the sinking of the particles can take place to the bottom of the crucible.
- Turbulence throughout the casting process can cause gas entrapment [46] .

Melting of Aluminum MMCs is identical to the conventional aluminum alloys. Gas or oil fired, electric-resistance, and induction furnaces can be used. The furnace is charged with dry composite ingots and then protective inert gas is applied prior the melting. All equipments, such as ladles, skimmers, thermocouples, also should be fully dried and preheated prior to use [46].

Generally density of ceramic reinforcements is higher than the aluminum alloys. For instance the density of TiB_2 is ~4.8 g/cm^3 while density of aluminum alloys is around 2.7 $g/cm^{3.}$ The recommendation is that the suitable stirring method is applied for dispersing the reinforcements throughout the liquid metal. Speed of the string is also important. Vortex formation can cause contamination from the dross and entrapment of gas from the ambient atmosphere [46] .

2.7.1.2 Pressure Infiltration Casting

Pressure infiltration casting (PIC) is a unique MMC production technique. An isostatical gas pressure, which is subjected to liquid metal, is used in order to fill the particulate or fiber preform. Near-net shape production ,which can be made with PIC, is crucial for decreasing machining requirement [46] .

Numerous methods are available with PIC for the discontinuously reinforced MMCs. All of them include liquid metal infiltration into evacuated and free standing preform by an external isostatically applied inert gas. The reinforcement preform is placed into a mold, which is in the outer metal canister, prior to starting of the PIC process. The metal canister serves to vacuum both inside of the mold and preform during the applied pressure. Molten aluminum is placed at the entry part of the mold and it is sealed. Schematic illustration of top-fill pressure infiltration casting machine is shown below in Figure 2.11 [46].

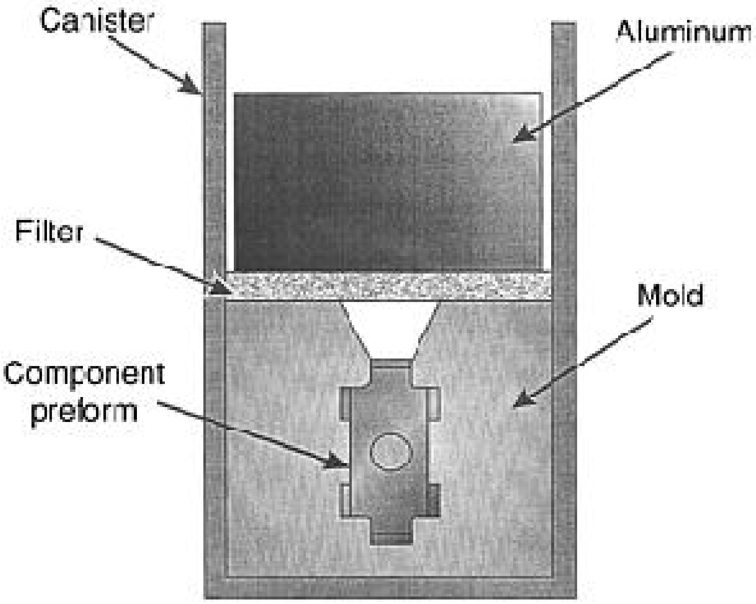

Figure 2. 11 Schematic of structure of the top-fill PIC method

In the top-fill method, aluminum is melted in different crucible and liquid is poured into the canister. After sufficient vacuum is maintained, the tube is sealed and process started [46].

Generally the reinforcement amount changes from a minimum of 30% over than 70% because current technology limits the production of lower amounts. These amounts serve stable geometrical shapes of preforms. SiC and Al_2O_3 are the most common used reinforcement types for the PIC process [46].

2.7.1.3 In-Situ

In the in-situ production of composites, reinforcing phases (generally ceramic materials) are produced directly within the aluminum matrix. To the contrary, ex-situ composites, reinforcing phases are separately produced and at least one secondary process is required to incorporation step [47]. There are numerous in situ production techniques which are adopted from the conventional casting or powder metallurgy [48].

The potential advantages of in situ production are uniform size and distribution of reinforcements, clean interface between the reinforcement and matrix which provides excellent interfacial bonding. Moreover, in this method, very fine reinforcement sizes are achieved, about 0.5-5μm, which improves mechanical properties of MMCs [47].

In ex-situ process, preserving and handling of micro-sized reinforcement are main problems. Small sized particles (around ~ 1μm) are extremely reactive. This may cause contamination of interface and unwanted brittle intermetallics can be produced. Moreover, agglomeration of particles depresses mechanical properties [49].

2.7.1.4 Wettability between Reinforcement and Matrix

“Wettability can be represented by an edge angle adjustment of a liquid droplet on a solid substrate which is given by Young equation :

$$\gamma_{SA} - \gamma_{LS} = \gamma_{LA} \cdot \cos\theta \tag{2.18}$$

where θ is the edge angle, γ_{SA} is the surface energy of the solid phase, γ_{LS} is the interface energy between the liquid and solid phases, and γ_{LA} is the surface energy of the liquid phase” [50].

Figure 2.12 illustrates the edge angle change of liquid droplet on the solid substrate for various interfacial energy values. “ The wettable system is described at an angle of <π/2. On the contrary, the nonwettable system is described at an angle of >π/2. The critical angle value is π/2. The wettability increases with decreasing the edge angle values” [50].

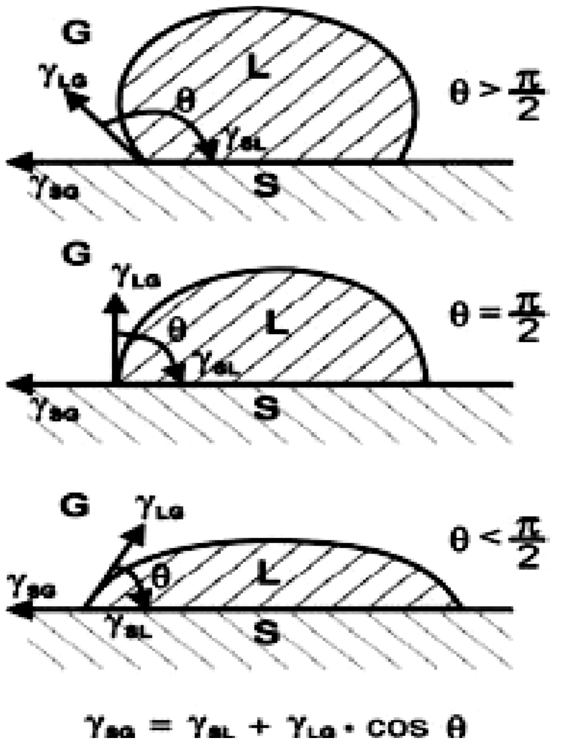

Figure 2. 12 Edge angle adjustment of a melt drop on a solid base for various values of the interface energy (after Young) [50].

In Table 2.7 surface and interface stresses of special metal-ceramic systems are given at different temperatures.

Table 2.4 Surface and interface strains of selected metal–ceramic systems at different temperatures

Alloy, Ceramic, Systems	**Temperature (°K)**	γ_{la} **(mJ m^{-2})**	γ_{sa} **(mJ m^{-2})**	γ_{ls} **(mJ m^{-2})**
Al	953	1050		–
Mg	943	560	–	–
Al_2O_3	0	–	930	–
MgO	0	–	1150	–
Cu/Al_2O_3	1370	1308	1485	2541
Cu/Al_2O_3	1450	1292	1422	2284
Ni/Al_2O_3	1843	1751	1114	2204
Ni/Al_2O_3	2 03	176	9	1598
Al/SiC	973	851	2 69	2949
Al/SiC	1073	840	2414	2773
Al/SiC	1173	830	2350	2684

“As the contact develops, for example at the beginning of an infiltration, adhesion occurs. The adhesion work W_A for separation is” [51]:

$$W_A = \gamma_{SA} - \gamma_{LA} = \gamma_{LS} \tag{2.19}$$

$$W_A = \gamma_{LA} \cdot (1 + \cos\theta) \tag{2.20}$$

“In the case of immersion the interface between the solid and the atmosphere disappears, while the interface between the solid and the liquid forms. The immersing work W_I is” [50]:

$$W_I = \gamma_{LS} - \gamma_{SA} \tag{2.21}$$

"In the case of spreading the liquid is spread out on a solid surface. During this procedure the solid surface is reduced as well as a new liquid surface being formed and hence a new solid/liquid interface is formed. The spreading work W_S is" [50]:

$$W_S = \gamma_{SA} - \gamma_{LS} - \gamma_{LA} \tag{2.22}$$

2.8 Solidification of Aluminum Matrix Composites and Distribution of Ceramic Particles

Particulate reinforced hypoeutectic Al-Si matrix composites have important micro-structural properties such as, eutectic Si morphology, primary α secondary dendrite arm spacing, and distribution of reinforcing particles. Microstructures directly affect the mechanical properties of composites. There are critical relationships between solidification mechanisms and microstructural properties. Solidification process of aluminum-TiB_2 composites is more complex than the monolithic aluminum alloys. Size, shape, and distribution of the reinforcement particles are crucial for mechanical properties and also ceramic particles act as suitable heterogeneous nucleation sites. Therefore, average grain size and secondary dendrite arm spacing of primary hypoeutectic α can be reduced.

The distribution of reinforcement particles in the aluminum alloy matrix is directly related with solidification. If the density difference between the liquid alloy and the reinforcement particle is over 2 g/cm^3, 2 μm diameter particles have a 10^{-4} cm/min sinking rate, therefore 1-2 μm diameter particles can be assumed as suspending in the liquid metal [52]. In addition, the wetting phenomenon among the reinforcement and liquid metal also cause preventing the sinking of reinforcing particles within the liquid aluminum. If the reinforcing particles are distributed uniformly in the liquid, agglomerations could be prevented.

In aluminum matrix composites growth of the solid is encountered under two different reinforcement types. These are mobile and stationary reinforcements. Generally fibers or monofilaments are stationary ones and whisker or particulates are mobile reinforcements. In this study solidification takes place with the mobile reinforcements. A growing solid-liquid boundary encounters mobile reinforcing particles which are suspended in the liquid metal. The reinforcement can either be engulfed or rejected. If the first case takes place, the distribution of reinforcement in the newly formed solid will be uniform but slightly different than that in the liquid. However in some cases, little redistribution may take place. On the other hand, if reinforcements are pushed by the solid-liquid boundary, redistribution occurs and final liquid regions will collect the whole reinforcing particles.

If the interface is planar, the reinforcing particles are not dragged and segregation of particles in the latest solidification area is prevented. If cellular interface growth takes place, particle segregations occur at the grain boundaries. In conclusion, Interdendritic (nonuniform) segregation is a result of the nonplanar solid-liquid interface and presence of convection in the liquid metal. reference [53].

Three conclusions can be made according to the experimental studies:

1. If the net Gibbs free energy change is negative (the particle liquid interfacial energy is higher than the particle solid interfacial energy), the particles are engulfed in all growth circumstances [54].
2. If the growth velocity is lower than the critical one, $V_{C,}$ particle is rejected. On the contrary, at higher growth velocities than the V_C, engulfing is achieved. V_C is dependent on the interface chemistry, thermal conductivities of particles and matrix, temperature gradient, and liquid viscosity [54].
3. Some reinforcing particles and matrix pairs usually reject and push the particles at any growth situation. For instance, most of Al_2O_3, SiC, TiB_2 and ZrB_2- reinforced hypoeutectic Al alloys have nonplanar interfaces [54].

2.9 Interfaces in Aluminum Matrix Composites

In theory, interfaces are volumeless, two-dimensional regions where at least two different materials meet and discontinuities occur in one or more material. Nevertheless in reality there is always some volume existing within the interface over which a gradual transition in material properties is present. Two major points that emphasize the significance of interfaces in composites [55]:

- Composites have significant interface area.
- In ceramic reinforced MMC, excessive physical and mechanical property differences are available between reinforcing particles and metallic matrixes.

Thermal expansion coefficient and elastic modulus are the main discontinuities of the ceramic-metal system. During temperature changes resulting from solidification or heat treatment, tension stress fields develop due to expansion of metal matrix being larger than the ceramic reinforcement [55].

For an efficient load transfer between matrix and reinforcement, clean interface must be established and preserved during the service conditions. Chemical or physical bonds can be established. Chemical bonds are stronger but at perfect wetting situations, physical bonds for instance Van Der Waals types might be enough to produce a well bonded interface [56]. The interfacial reactions between the reinforcement and the matrix deteriorate the interface quality. Unwanted brittle intermetallic products such as Al_3Ti and Al_2B are source of the micro-structural corruption. It is essential to understand the thermodynamic, kinetic, mechanical and micro-structural aspects of interface in order to optimize the production to achieve excellent interfaces in MMC's [55].

CHAPTER III

EXPERIMENTAL PROCEDURE

3.1 Introduction

In this study, starting ingredients are TiO_2, H_3BO_3, Na_3AlF_6 powders and commercially pure Aluminum metal. They were charged into graphite crucible and melted in an induction furnace.

The two-liquid phase system was maintained, in which liquid aluminum phase was on the bottom and TiO_2, H_3BO_3, and Na_3AlF_6 mixture slag phase was on the top. TiB_2 was formed through the overall slag-metal Reaction 3.1 as is shown below:

$$(B_2O_3) + (TiO_2) + 10/3\ Al\ (l) = TiB_2(s) + 5/3\ (Al_2O_3) \qquad (3.1)$$

where; the () denotes the species dissolved in the slag phase. After formation of $TiB_2(s)$ particles, penetration of $TiB_2(s)$ to liquid metal takes place. (Al_2O_3) dissolves in the slag phase and does not enter the liquid metal. After the reaction was complete, the slag phase was removed carefully by a steel pot. Then the composite, $Al+TiB_2$, was poured and solidified into a graphite mold. Specimens were carefully cut then X-Ray studies were carried out.

Afterwards coarse powder silicon and bulk magnesium additions were applied to remelted $Al+TiB_2$ in order to obtain A356, Al-(7 %wt.) Si-(0.3 %wt.) Mg alloy matrix+TiB_2 composite. Then, resulting A356 Aluminum alloy + TiB_2 reinforced composite was cast via squeeze casting method.

The squeeze cast samples were carefully prepared by suitable metallographical techniques. And then, optical, scanning electron microscopic, and x-ray examinations were carried out. Finally, mechanical tests such as Vickers microhardness, tensile and, 3-point bending tests were done according to relevant ASTM Standards.

3.2 Starting Materials

Commercial purity of aluminum ingots (> 99.7%wt.), rutile (TiO_2, high purity > 99.8%wt.), boric acid (H_3BO_3, 1μm > particle size, high purity > 99.8%wt.), and cryolite (Na_3AlF_6, 1μm > particle size, high purity > 99.8%wt.) were starting ingredients for this study. Boric acid and rutile powders were obtained from the Merck and the cryolite powder was obtained from Etibank. Information about the powder products was obtained from the companies, and they indicated that the size distributions for rutile and boric acid powders are similar and classified as fine.

3.3 Production Parameters

The starting materials, in powder form, TiO_2, H_3BO_3, and Na_3AlF_6 and aluminum ingots, were weighed according to the stoichiometry of reactions which are shown below:

$$2H_3BO_3 = 3H_2O + B_2O_3 \tag{3.2}$$

$$TiO_2 + B_2O_3 + 10/3\ Al = TiB_2 + 5/3\ Al_2O_3 \tag{3.3}$$

Three powder mixtures were prepared for the different, 5, 7.5, and 10 volume percent TiB_2 reinforcements. The raw powders, were carefully mechanically mixed and then dried at 150°C for 4 hours in order to remove the humidity thoroughly. Then the dried powder mixture and aluminum ingots were placed in conductive graphite crucible. The nonconductive powders cannot be heated at induction furnace (Figure 3.1) without conductive crucible. After the heating of crucible had taken place by the secondary electric currents inside of the graphite, the powders were heated and finally melted. Meanwhile, boric acid was calcined to water vapor (H_2O) and boric oxide (B_2O_3). Temperature was increased up to 1050°C-1100°C; the two-phase system was maintained: at the bottom, liquid aluminum and at the top, liquid slag (TiO_2, B_2O_3, Na_3AlF_6). The schematic illustration of the slag-metal system is shown in Figure 3.1.

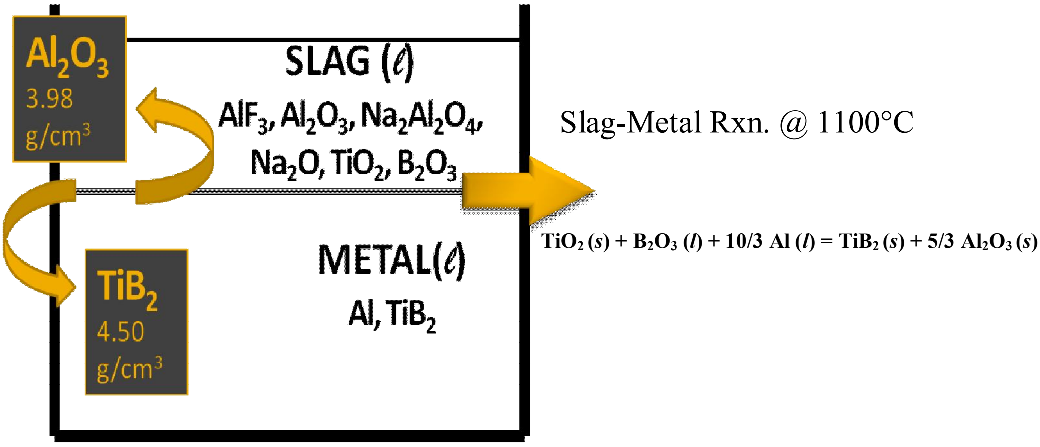

Figure 3. 1 The schematic illustration of the slag-metal system in the graphite crucible

Tiny sparks were observed when the exothermic metal slag reactions started. In order to prevent excessive heating of the system, the furnace was turned down when the reaction started. The system was carefully stirred for increasing the contact between the slag and the metal. The stirring was continued until no sparks were observed which was a sign of the completion of the reaction.

During the reaction, TiB_2 particles were produced and then entered into the aluminum melt. Aluminum oxide was formed and dissolved in the cryolite based slag. The removal of aluminum oxide (Al_2O_3) was achieved by high alumina solubility of cryolite based slag and in addition, the density difference of slag and aluminum melt. For each three %vol. TiB_2, three different reaction times were applied, which were 15 min., 45 min, and 70 min . The temperature of the system was fixed at 1100°C. After the reaction was complete, the slag phase was removed carefully by a steel pot. Then the composite was poured and solidified in a graphite mold.

In order to examine the produced TiB_2 reinforcing particles, the commercially pure aluminum matrix+TiB_2 composite was leached with a suitable acid solution, which dissolved Al but did not affect TiB_2. Hydrochloric acid (HCl) was used to accomplish this. In order to extract TiB_2 particles from the aluminum matrix, leaching was carried out at 100°C, for 4 hours, and stirring was applied. After dissolving the composite material in 6 molar HCl solutions, undissolved residue was separated by filtration. Then TiB_2 residue was washed, dried and then weighted.

The residue was then subjected to XRD analysis. The XRD pattern of the residue indicated that it did not contain any compound in any appreciable quantity other than TiB_2. The residue was considered to be pure TiB_2 and its weight was found to be close to the weight of TiB_2 expected to form on the basis of stoichiometric considerations. Moreover, after the pouring of commercially pure aluminum matrix+TiB_2 composite, the weighing was carefully applied in order to determine TiB_2 amount in the matrix.

Alloying procedure was carried out; silicon and magnesium were added to liquid composite prior to the squeeze casting. Chemical compositions of matrix were determined with FOUNDARY MASTER Model, optical emission spectrometric device. The matrix alloy was well-known commercial aluminum casting alloy A356 which consisted of the following major alloying elements; 7% wt. Si, 0.3% wt. Mg.

3.4 Casting Practice and Squeeze Casting Machine

Prior to the casting, the temperature of the liquid A356 alloy- TiB_2 composite was kept at around 700-750°C. The hot worked tool steel die, which is designed for two tensile specimens and four bending specimens, was pre-heated to 230-290°C.

The special die is shown in Figure 3.2.

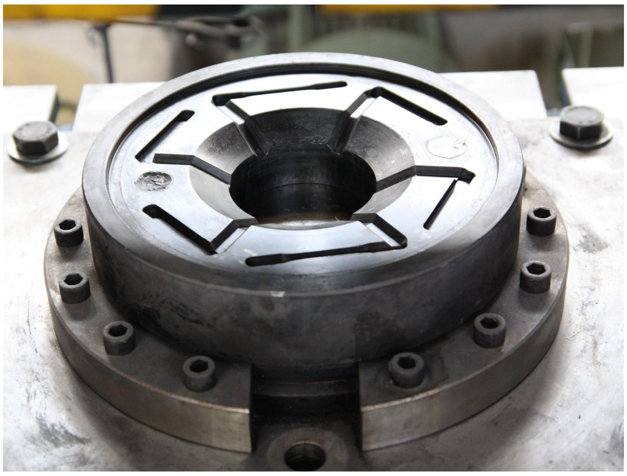

Figure 3. 2 The hot worked tool steel die is designed for two tensile specimens and four bending specimens

In order to obtain fine microstructure and better mechanical properties, squeeze casting of A356+TiB_2 was applied under the 90 X 10^3 kgf for approximately 90 seconds to complete solidification before the composite was ejected. Squeeze casting machine is shown below in Figure 3.3.

Figure 3. 3 Squeeze casting machine with hot worked steel die

Preheating of mold is crucial for the fluidity of liquid composite within the die. In each casting practice, temperature of die was measured with special laser based thermometer and temperature values of the die for prior to each casting is given below in Table 3.1.

Table 3. 1 Pre-heating Die Temperatures

	Reference Alloy (A356)	**A356+5%vol TiB_2**	**A356+7.55%vol TiB_2**	**A356+10%vol TiB_2**
Casting No	Temperature °C	Temperature °C	Temperature °C	Temperature °C
1	235	240	235	255
2	240	245	240	260
3	255	255	250	260
4	255	260	255	270
5	260	260	255	270
6	270	275	260	275
7	265	275	270	280
8	265	280	275	280
9	275	275	275	275
10	270	275	275	275

Finally the two tensile and four three point bending testing samples were taken out from the steel die and cooled down in air.

3.5 Determination of Parent Phases in A356-TiB_2 Composite via X-Ray Diffraction Analysis

Bulk samples were carefully prepared with 120, 240, 320, 600, 800 and 1200 grid SiC emery papers respectively. Then x-ray studies were conducted prior to alloying and also after the alloying and squeeze casting. Therefore the phases were observed at every step of the process. Moreover, if alloying elements such as silicon and magnesium had formed any brittle intermetallic compounds with aluminum or TiB_2, they could be seen. RIGAKU X-Ray Diffraction equipment with with Cu Kα radiation at 40 kV and 40 mA was used to attain the XRD patterns.

3.6 Metallographic Examination

Metallographic samples were carefully cut from the edges of tension and bending specimens by A BUHLER Metallographic cutter. Then samples were mounted in bakalite in A METKON mounting machine. In order to apply metallographic examination, samples were prepared using standard SiC grinding papers 120, 240, 320, 500, 600, 800, 1000, 1200, and 2000 grid respectively and polishing is applied with 3 µm and 1 µm diamond suspension. Then etching was done with Keller' reagent (1 ml HF + 1.5 ml HCl + 2.5 ml HNO_3 + 95 ml H_2O) in order to observe grain structures and TiB_2-matal matrix interfaces. The prepared samples were investigated and photographed using NIKON ECLIPSE LV 150 special optical metallographic microscope. Then scanning electron microscope studies were carried out using JEOL 6400 scanning electron microscope and also energy dispersive X-rays spectroscopy (EDS) analysis were taken from the TiB_2 reinforcements with NORAN apparatus.

3.7 Secondary Dendrite Arm Spacing Distance (SDAS) Measurement

The common mechanical properties especially strength is directly related to secondary dendrite arm spacing distance (SDAS) of the Al-Si alloy. The same argument applies to the aluminum matrix composites. The strength increases with decreasing SDAS. X-Rays and optical digital imaging software were used for measurement of SDAS in the Al-Si+TiB_2 composites.

Strict diffraction condition was explained by Bragg`s law, which is shown below in Equation 3.4. In ideal case, infinitely thick crystal is one which contains no imperfections and truly monochromic X-ray source. Peak broadening takes place with increasing SDAS size. This occurs in such a manner that the width of peaks measured at half height B can be related to cell or subgrain size, t, “SDAS” with

$$t = 0.9\, \lambda / B \cos \theta_B \qquad 4(3.5)$$

where; λ is the wavelength of the X-ray, B is the structural broadening, and θ_B is the Bragg’s angle of the peak.

In this study, a wide angle range scan was applied for the first sample and the broadening peak was measured and selected. The (200) crystal plane peak was selected and shown on Figure 3.4 below. The broadening could be measured at half-height, but this is not enough as there were other factors that influence. One factor was that the X-Ray source was not monochromatic as K_α in the doubled $K_{\alpha1}$ and $K_{\alpha2}$, other factors were geometric and depended on the alignment and slit arrangement in the diffractometer. All these could be referred to as instrumental broadening. Simple way of evaluating the degree of instrumental broadening was to inspect a standard sample in the same setup. In the present experiment this was achieved by examining an annealed aluminum (at 450°C for 20 hour) for this purpose, which gave a SDAS size. Because SDAS were large, the broadening obtained in this sample is due solely to an instrumental broadening. With such standard sample, structural broadening, B, could be calculated in Equation 3.5 as follows:

$$B^2 = B_M^2 - B_S^2 \qquad (3.5)$$

Where; B_M is the broadening of the sample, and B_S is the broadening of the standard.

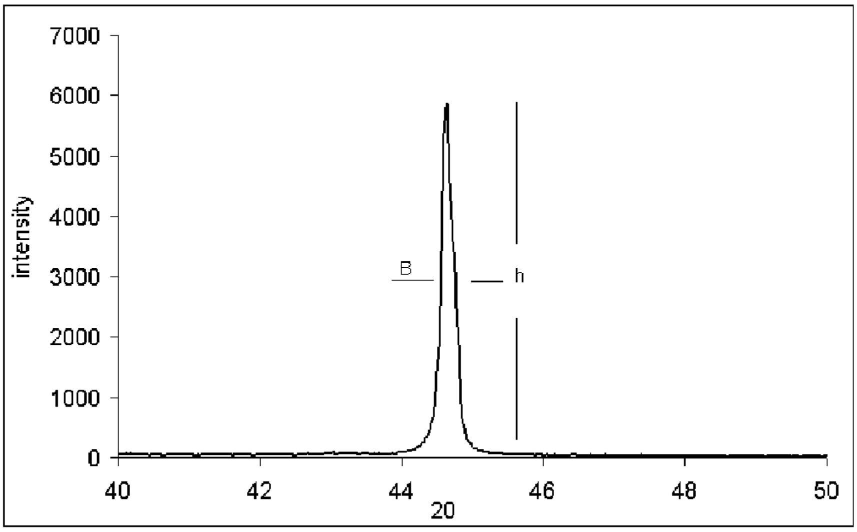

Figure 3. 4 (200) crystal plane peak of Aluminum

3.8 Mechanical Tests

3.8.1 Tensile Test

Test specimens, which were prepared according to ASTM D3552 “testing unidirectional or cross-piled metal matrix composites and discontinuous metal matrix composites in tension”, was prepared during the squeeze/pressure die casting. Tension test was applied for three different volume percentage of titanium diboride (% TiB_2 vol.). In Figure 3.5 the specimen geometry is shown clearly. The test was carried out with SCHMATZU TENSILE TESTER with 3mm/min test speed. In order to accurate elastic modulus calculations, the video was used during the all tension tests.

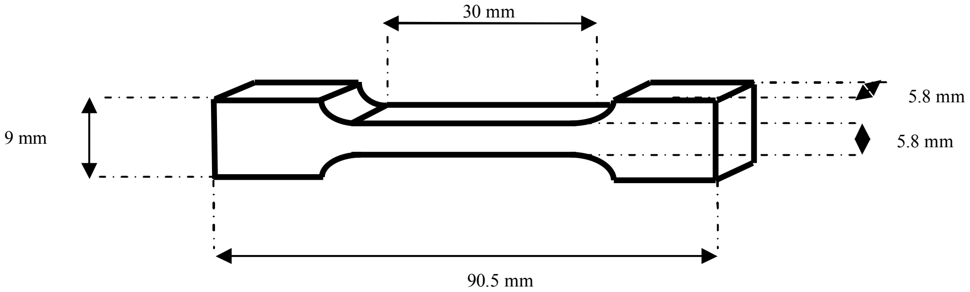

Figure 3.5 The schematic of the tensile test specimen produced by squeeze/pressure die casting machine

3.8.2 Three Point Bending Test

The test specimens, which were shown on Figure 3.6, were produced by squeeze/pressure die casting machine.Test was carried out according to ASTM E 290 – 97a Standard Test Methods for Bend Testing of Material for Ductility. The three point bending test is a well-known mechanical strength test especially discontinuously reinforced metal matrix composites. Three point bending tests were performed to observe the fracture behavior of aluminum matrix composite with three different volume percentage of titanium diboride (% TiB_2 vol.). The three point bending test, the maximum fracture loads were evaluated. These kilogram values were converted into flexural stress (MPa) values.

The flexural stress formula is given as in equation 3.6; $\sigma = My/I$ were σ flexural stress, M the bending moment, y the distance from the natural axis and I the moment of inertia. The maximum flexural surface occurs in the mid-point of the specimen.

Therefore:

$$M = \frac{P \times L}{4} \;;\; y = \frac{t}{2} \;;\; I = \frac{b \times t^3}{12} \;;\; \sigma = \frac{3 \times p \times t}{2 \times b \times t^2} \tag{3.6}$$

P : Load applied by the testing machine,

t : Thickness of the specimen,

b : Width of the specimen, and

L : span length, respectively.

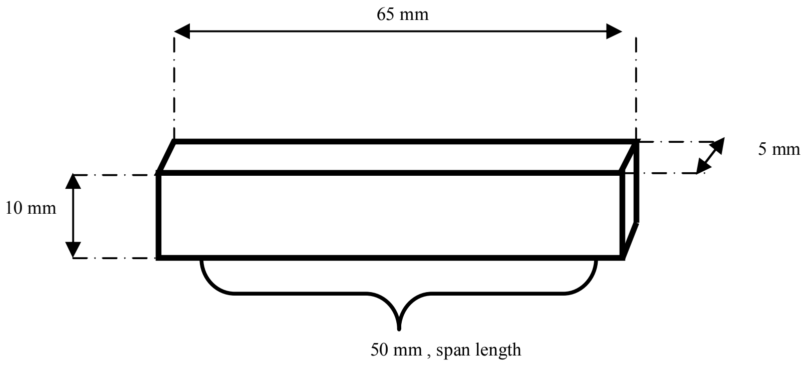

Figure 3. 6 The schematic of the three point bending test specimen specimens produced by squeeze/pressure die casting machine

3.8.3 Vickers Micro-Hardness Test

Vickers micro-hardness Test determined the hardness values of the metallic matrix composites. Hardness measurements were carried out according to ASTM standard E 92-82 (Reapproved 2003) describing standard test method for Vickers hardness of metallic materials. Hardness Numbers (HV) were obtained with a square pyramidal diamond indenter having included face angles of 136°, computed from equation 3.7. Test was carried out at X200 magnification under 0.2 kgf load for 15 seconds penetration time. Mounted, polished and etched specimens were conducted test with standard Vickers indenter and Zwick/Roell ZHV 10 Microhardness machine which is shown in Figure 3.5.

$$\mathrm{HV} = 2\mathrm{P}\left(\sin\frac{\alpha}{2}\right)\mathrm{d}^2 \; = \frac{1.8544\mathrm{P}}{\mathrm{d}^2} \tag{3.7}$$

where:

P= applied force, kgf,

d= mean diagonal of impression, mm, and

α= face angle of diamond = 136°.

CHAPTER IV

RESULTS AND DISCUSSION

4.1 Formation of In-Situ TiB_2 Reinforcing Particles and X-Ray Studies

Aim of the study was to produce in situ Al-TiB_2 composites via method of the slag metal reaction. Reactions were carried out with liquid aluminum, TiO_2, and B_2O_3. The cryolite (Na_3AlF_6) based slag contained TiO_2 and B_2O_3. Moderately low melting point and high Al_2O_3, TiO_2, and B_2O_3 solubility are important parameters for the cryolite based slag.

First of all, calcination of boric acid (H_3BO_3) took place during heating according to reaction 4.1 which is shown below:

$$2H_3BO_3\ (s) = 3H_2O\ (g) + B_2O_3\ (s) \qquad (4.1)$$

Second of all, melting of the slag phase took place at around 950°C and two liquid phases which were liquid aluminum and liquid Na_3AlF_6-TiO_2-B_2O_3 slag were formed.

Finally, overall reaction started which was between the slag and metal phases for the production of TiB_2 as given by reaction 4.2. The charges were prepared for 5, 7.5, and 10 volume percent TiB_2 reinforcement in aluminum matrix composites according to the stoichiometry of the overall reaction 4.2.

$$TiO_2\ (s) + B_2O_3\ (s) + 10/3\ Al\ (l) = TiB_2\ (s) + 5/3\ Al_2O_3(s) \qquad (4.2)$$

The produced TiB_2 particles entered the liquid aluminum and then became reinforcement of the composite. The unwanted Al_2O_3 entered the slag phase and dissolved in the cryolite according to Reaction 4.3.

$$2Al_2O_3 + 2Na_3AlF_6 = 4AlF_3 + Na_2Al_2O_4 + 2Na_2O \qquad (4.3)$$

Weights of the cryolite (Na_3AlF_6), rutile (TiO_2) and boric acid (H_3BO_3) powders and aluminum metal charges are given in Table 4.1.

Table 4 1 Weight of the powders and aluminum metal charges

Vol % TiB_2	**Na_3AlF_6 (gr)**	**TiO_2 (gr)**	**H_3BO_3 (gr)**	**Al (gr)**
5	1931	101	156	1114
7.5	2974	155	240	1174
10	4075	213	330.0	1240

Before the alloying procedure, the commercially pure aluminum matrix–TiB_2 composite was cast in a graphite mold. In order to identify produced phases in every step of the process, x-ray studies were conducted both on the as-cast composite and the alloyed squeeze cast composite. Then specimens obtained from the squeeze cast A356 Aluminum alloy - TiB_2 composite were subjected to optical microscopy and scanning electron microscopy examinations and microhardness, tensile and 3-point bending tests.

X-Ray diffraction pattern of commercially pure Aluminum, and commercially pure Al+5 vol. % TiB_2 samples are given below for three different reaction times 25 min., 45 min. , 70 min. in Figures 4.1 , 4.2, 4.3 and 4.4 ,respectively, while the diffractometric data for TiB_2 and Al given in Table 4.2 .

Table 4.2 Diffractometric Data for Pure Al-TiB_2 As-Cast Composite

Al	**●**	**TiB_2**	**♦**
2θ	**hkl**	**2θ**	**hkl**
38.324	111	27.469	001
44.563	200	33.949	100
64.948	220	44.652	101
78.069	311	56.748	002
82.263	222	60.999	110
		67.969	102
		68.357	111
		71.342	200
		78.672	201
		88.189	112

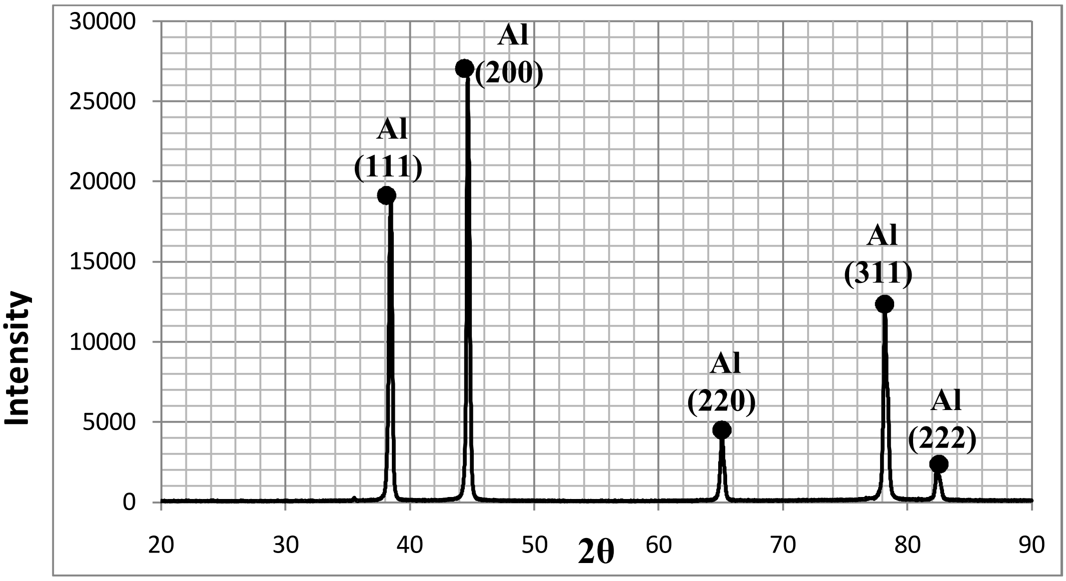

Figure 4. 1 Al- 0% vol. TiB_2 Commercially Pure Aluminum

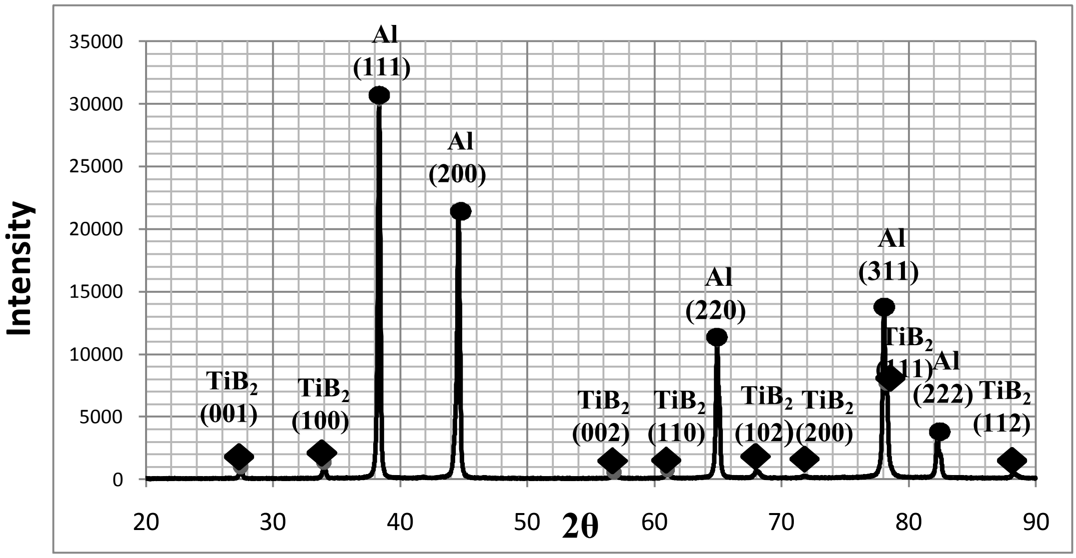

Figure 4. 2 Al- 5% vol. TiB_2 and 25 min. reaction time

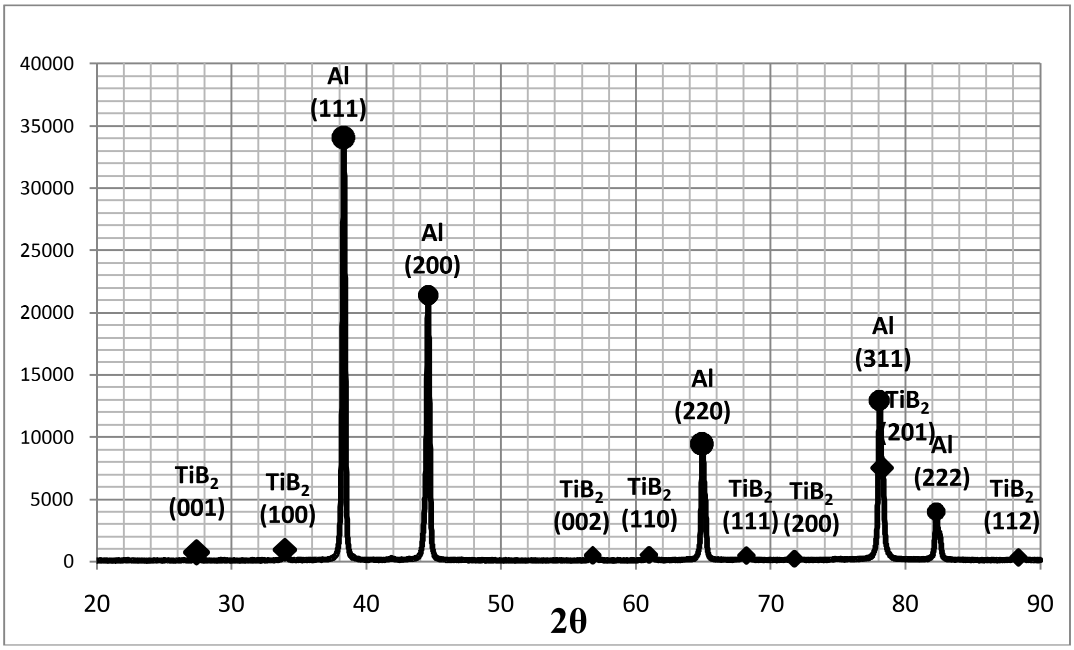

Figure 4. 3 Al- 5% vol. TiB_2 and 45 min. reaction time

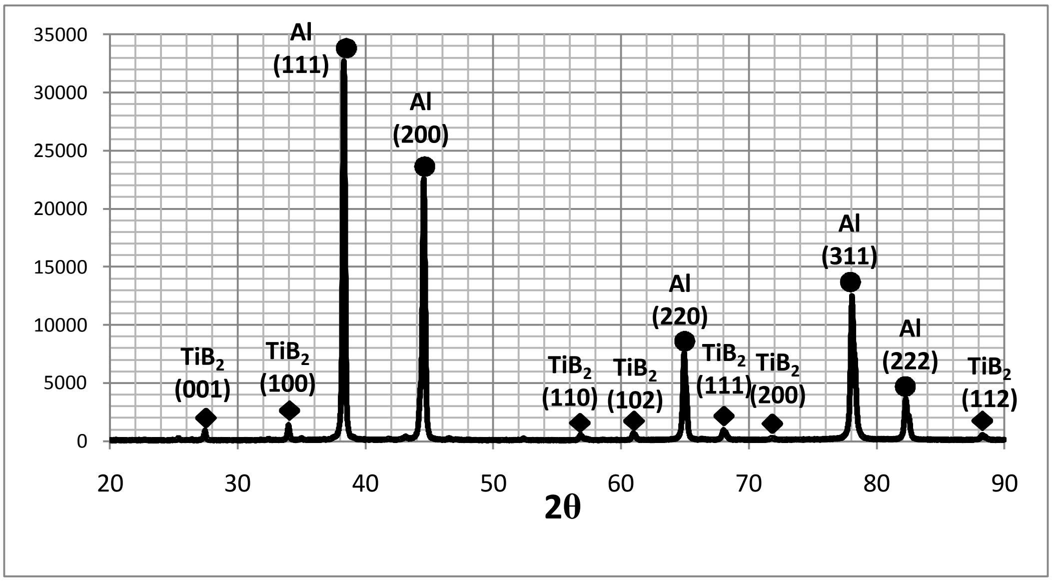

Figure 4. 4 Al- 5% vol. TiB_2 and 70 min. reaction time

X-Ray diffraction pattern of Al-7.5 vol. % TiB_2 samples are given for three different reaction times 25 min., 45 min. , 70 min. in Figures 4.5 , 4.6, and 4.7 respectively.

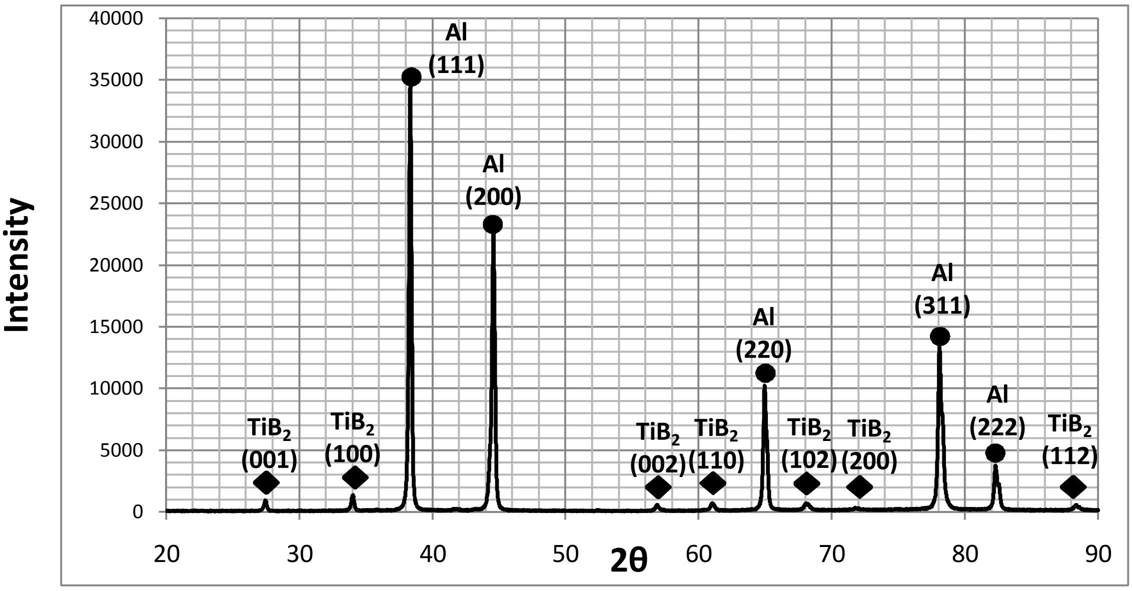

Figure 4. 5 Al- 7.5% vol. TiB_2 and 25 min. reaction time

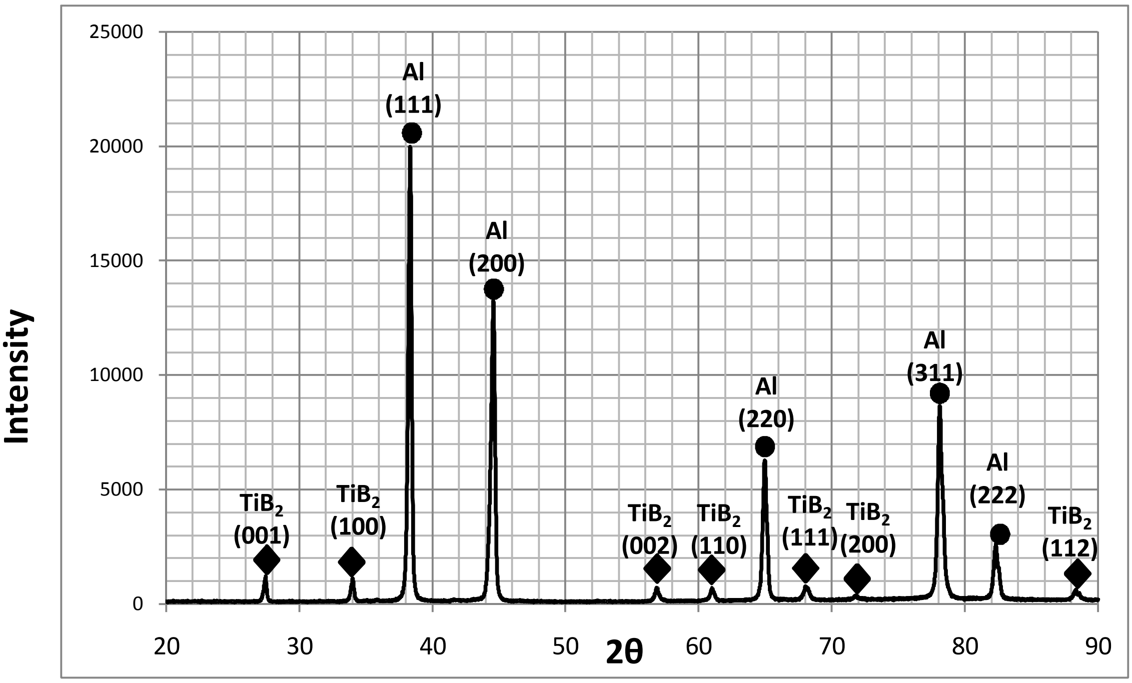

Figure 4. 6 Al- 7.5% vol. TiB_2 and 45 min. reaction time

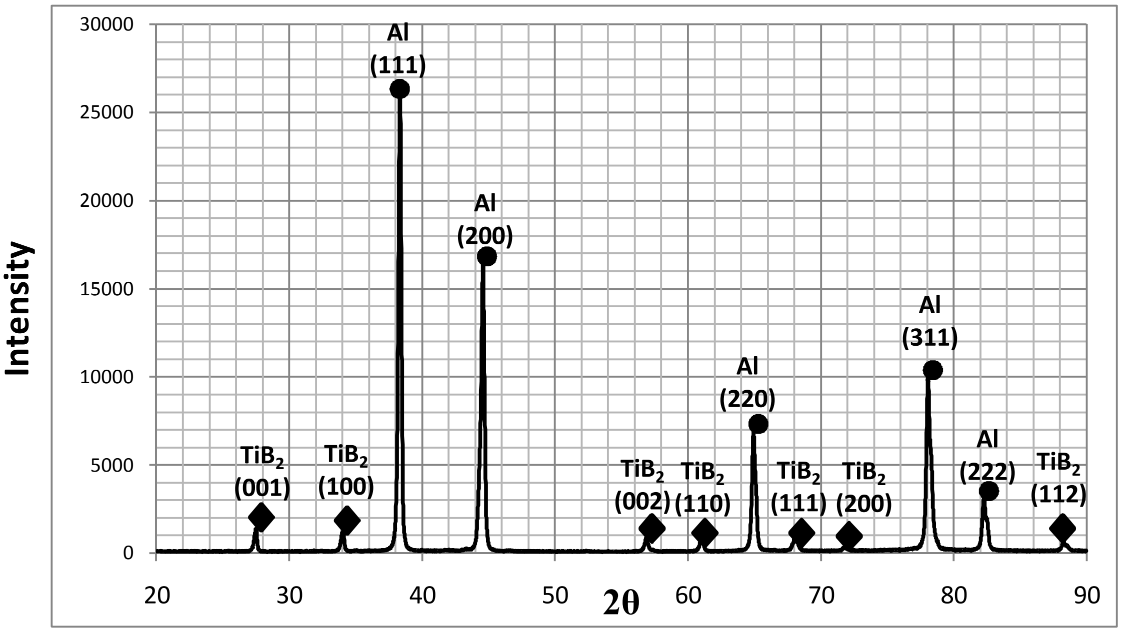

Figure 4. 7 Al- 7.5% vol. TiB_2 and 70 min. reaction time

X-Ray diffraction pattern of Al-10 vol. % TiB_2 samples are given for three different reaction times 25 min., 45 min. and, 70 min. respectively in Figures 4.8 , 4.9, and 4.10 respectively.

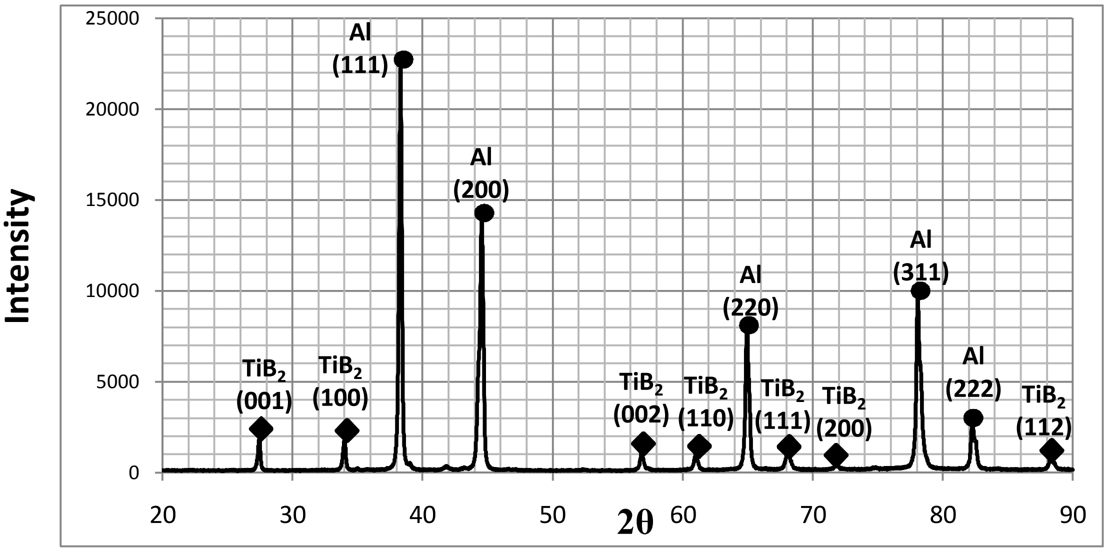

Figure 4. 8 Al- 10% vol. TiB_2 and 25 min. reaction time

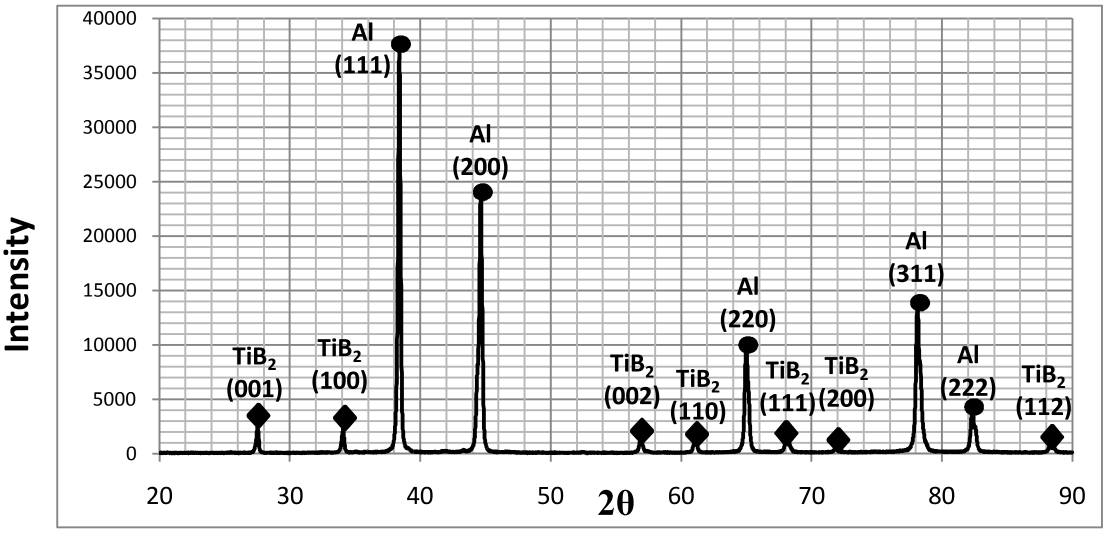

Figure 4. 9 Al- 10% vol. TiB_2 and 45 min. reaction time

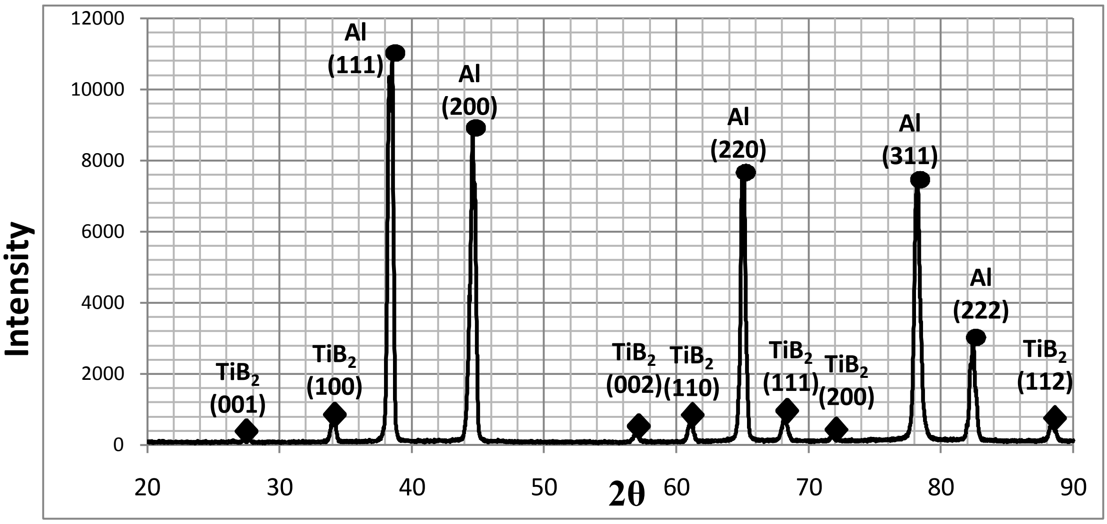

Figure 4. 10 Al- 10% vol. TiB_2 and 70 min. reaction time

X-Ray diffraction patterns given in Figures 4.2 to 4.10 clearly indicate that TiB_2 is present in the aluminum specimens, which clearly indicate that Al-TiB_2 composites have been successfully produced. Intermetallic Ti-Al, especially Al_3Ti, phases which may form in the system and have been observed to form in some studies, Al_2O_3 and any other compound could not be detected in the commercially pure aluminum-TiB_2 samples. This is proved by the XRD patterns which are shown in Figures 4.2 to 4.20. XRD patterns show that none or a negligible amount of Ti-Al intermetallic compound has formed and all Al_2O_3 forming has entered the liquid cryolite phase.

X-Ray diffraction patterns of A356 (Al7Si0.3Mg) -5% vol.TiB_2 , A356-7.5% vol.TiB_2 and A356-10% vol.TiB_2 squeeze cast samples are given in Figures 4.12, 4.13, and 4.14 respectively, while the diffractometric data for TiB_2 and A356 given in Table 4.3 .

Also the diffraction pattern of A356 alloy is given in Figure 4.11 in order to compare of the TiB_2 peaks in the alloy.

Table 4.3 Diffractometric Data for A356-TiB_2 Squeeze Cast Composite

TiB_2	**♦**	**Al**	**●**	**Si**	**■**
2θ	**hkl**	**2θ**	**hkl**	**2θ**	**hkl**
27.324	001	38.501	111	28.442	111
33.981	100	44.541	200	47.302	220
56.783	002	65.082	220	56.121	311
61.041	110	78.221	311	69.132	400
68.142	102	82.041	222	76.377	331
71.581	200			80.026	422
88.321	112				

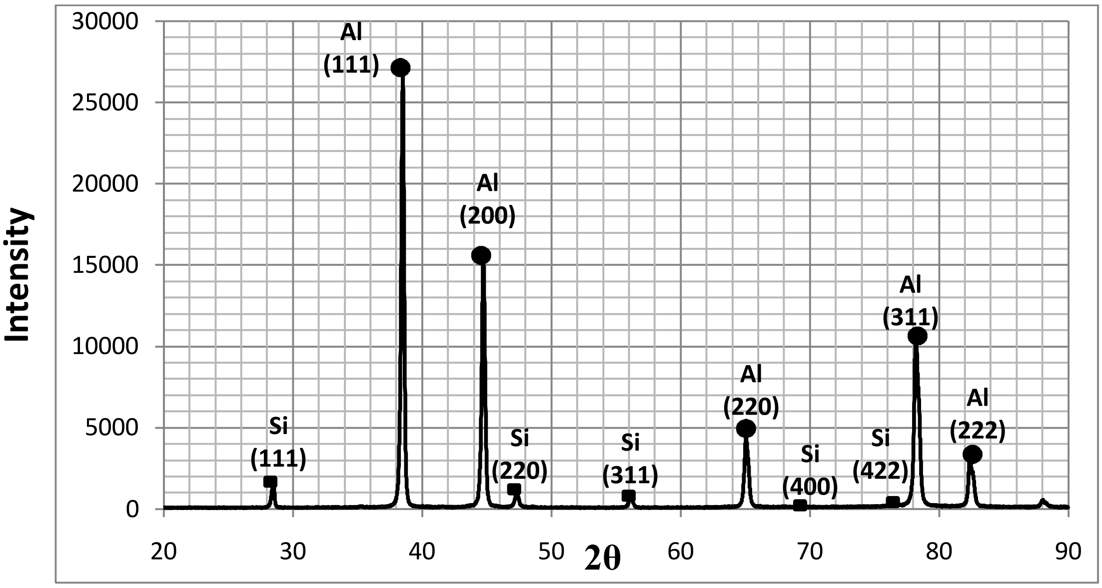

Figure 4. 11 A356 -0% vol.TiB_2

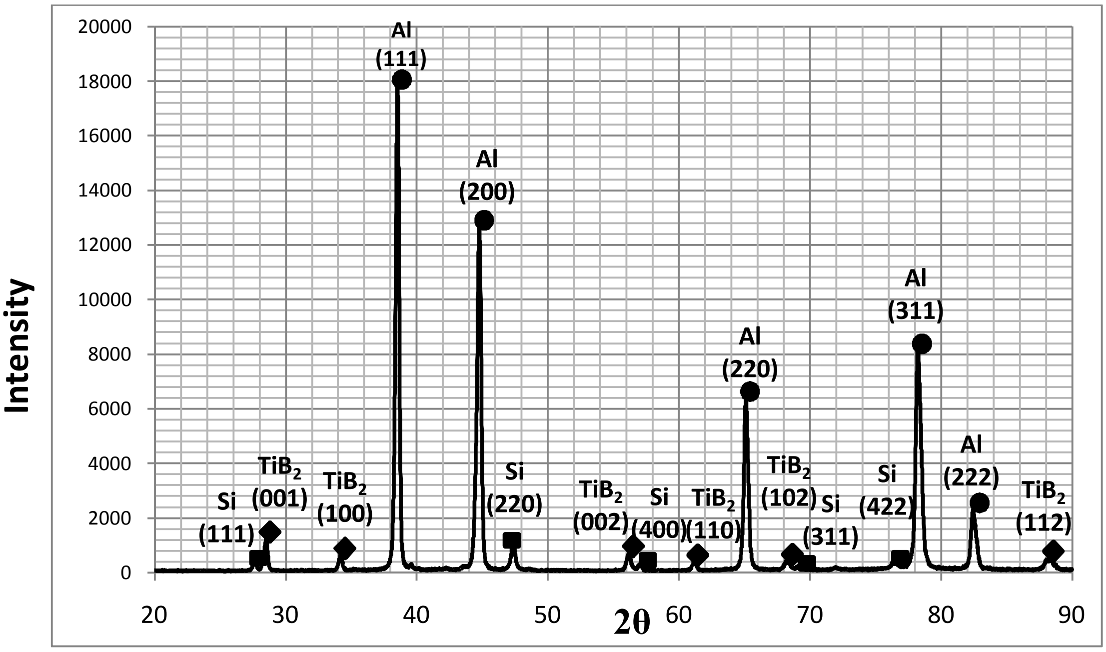

Figure 4. 12 A356 -5% vol.TiB_2

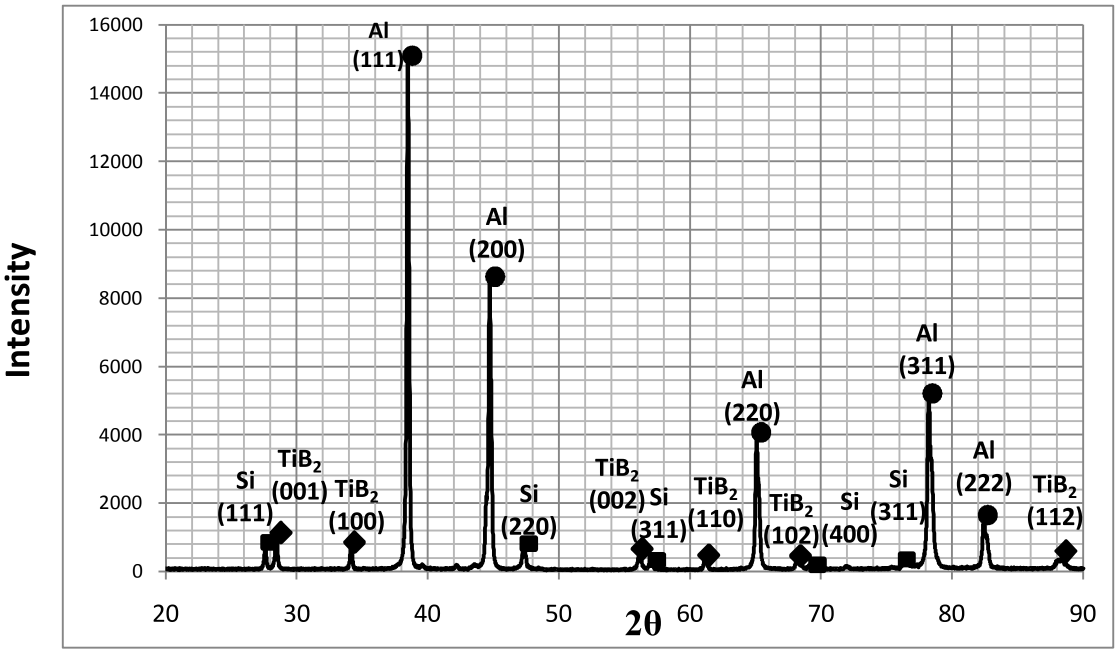

Figure 4. 13 A356 -7.5% vol.TiB_2

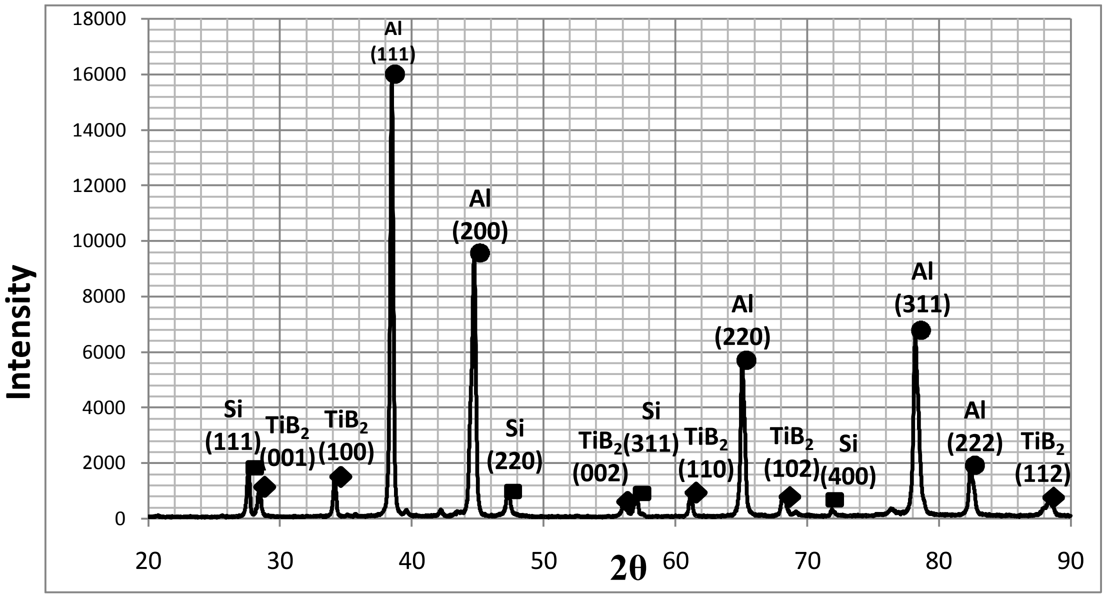

Figure 4. 14 A356 -10% vol.TiB_2

X-Ray diffraction patterns given in Figures 4.12 to 4.14 obviously point out that TiB_2 is present in the aluminum specimens, which clearly indicate that A356-TiB_2 squeeze cast composites have been successfully produced. Aluminum, Silicon, and TiB_2 peaks appear in the diffractogram, but magnesium peaks cannot be seen because of its low amount in the alloy system.

The alloying elements, Si and Mg do not form any intermetallic phases with TiB_2. According to the X-Ray patterns which are shown on Figures 4.12 to 4.14, the only appreciable phase is TiB_2 and any other ceramic or intermetallic phases are not present in the final metallic matrix composite system.

4.2 Determination the Amount of TiB_2 Reinforcement

In the present study, three different charges were prepared on the basis of stoichiometric considerations based on Reaction 4.2. X-Ray patterns indicate the presence of TiB_2; unfortunately it does not give information as to the amount of TiB_2 in the samples.

In order to determine the amount of TiB_2 in the matrix extraction of TiB_2 particles was applied. The method was leaching the bulk composite with a suitable agent, which would dissolve Al but would not affect TiB_2 reinforcement. Hydrochloric acid (HCl) was selected to fulfill this objective. After dissolving the bulk composite in HCl, undissolved residue was separated from the solution by filtering. The residue was washed with distilled water, dried at 120°C and then weighed. The residue was then subjected to XRD analysis. The XRD pattern of the residue and its diffractometric data are shown in Figure 4.15 and in Table 4.4. XRD analysis indicated that composite did not contain any compound in any appreciable quantity other than TiB_2.

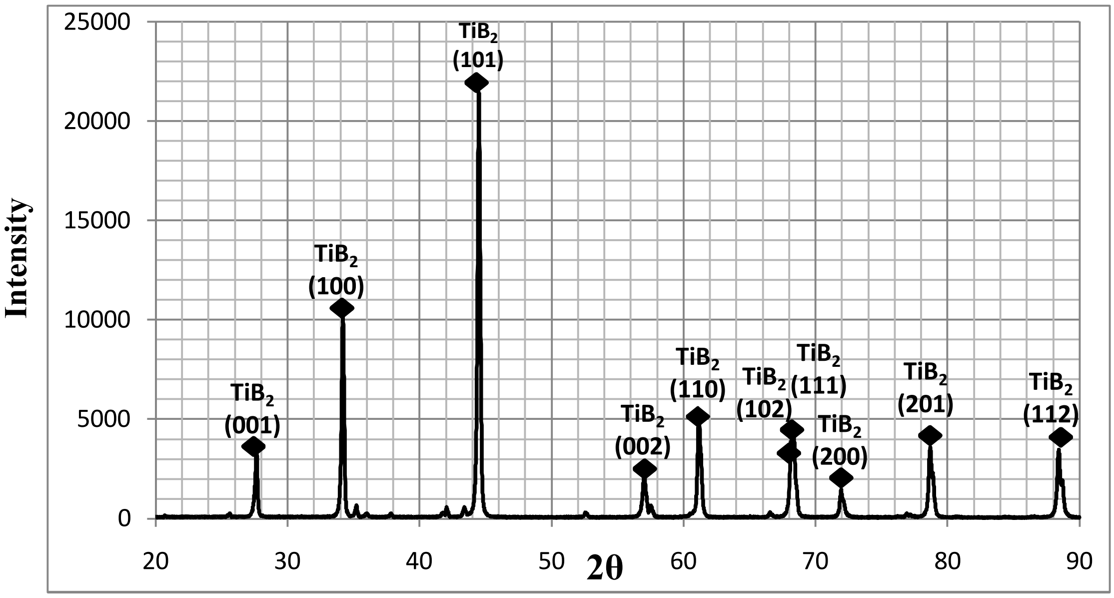

Figure 4. 15 XRD pattern of leach residue of TiB_2 powder

Table 4.4 Diffractometric Data of TiB_2 Leach Residue

TiB_2 ♦						
2θ	27.62	34.18	44.48	57.02	61.16	68.14
hkl	001	100	101	002	110	102
2θ	68.14	68.32	71.92	78.66	88.38	
hkl	102	111	200	201	112	

The residue was considered to be pure TiB_2 and its weight was taken as the weight of TiB_2 that has formed.

Efficiency of formation of TiB_2 was defined as:

$$Efficiency = \frac{\text{experimental weight of the produced amount of TiB}_2}{\text{stoichiometric amount of TiB}_2\text{ (according to reaction 4.2)}} x100$$

The X-ray studies of the slag phase clearly showed that slag does not have any significant amount of TiB_2. Figure 4.16 shows XRD pattern of slag phase. No TiB_2 peak is observed the XRD pattern of slag phase.

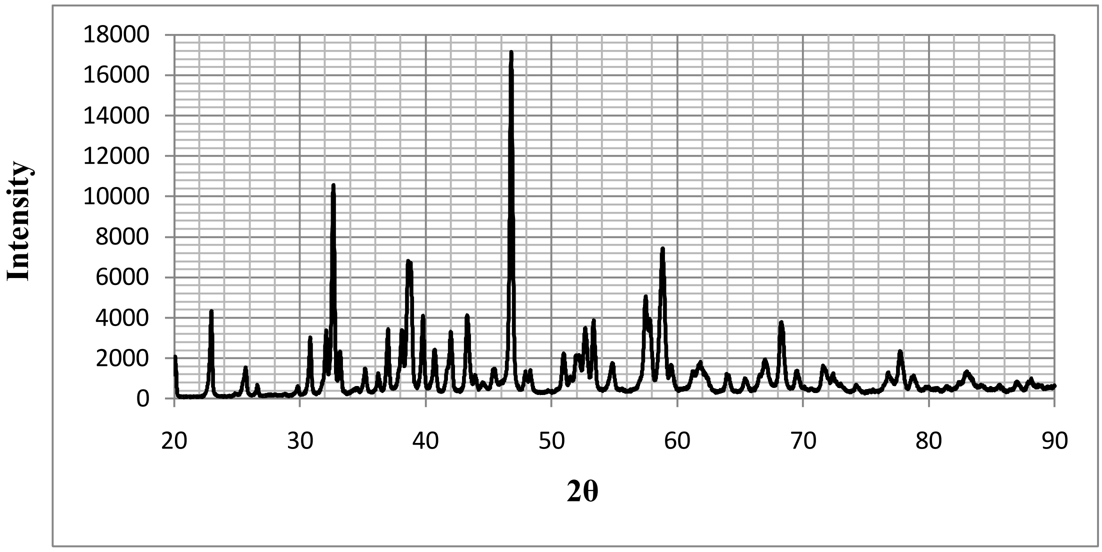

Figure 4. 16 XRD pattern of slag phase containing Al_2O_3 and Na_3AlF_6

Efficiency results are shown on Table 4.5 for each experiment. Efficiency of the TiB_2 production is increased with increasing reaction times which is an expected result.

Table 4.5 The Efficiencies of the TiB_2 production via Slag-Metal reaction

Experiment No	**Time (min)**	**Temperature (°C)**	**%vol. TiB_2**	**% Efficiency**
1	25	1100	5	83
2	45	1100	5	92
3	70	1100	5	97
4	25	1100	7.5	78
5	45	1100	7.5	89

Table 4.5 (cont'd)

6	70	1100	7.5	96
7	25	1100	10	80
8	45	1100	10	84
9	70	1100	10	92

4.3 Microstructures and Phase Relations

In this study TiB_2 is used as a discontinuous ceramic reinforcement and also an additive for grain refinement. All of the samples were ground using SiC grinding paper of 120, 220, 320, 600, 800 and 1200 grid and they were then polished with 3 micron and 1 micron oil based diamond suspension and then the surfaces were cleaned in alcohol with ultrasonic cleaner. Afterwards specimens were etched with Keller's reagent.

Optical emission spectroscopic analysis was used to determine chemical composition of the prepared aluminum silicon alloys. Results are given below in Table 4.6:

Table 4.6. Chemical Compositions of Prepared Metal Matrix Composite Samples

Element (Wt.%)	A356 Ref. Sample	A356-Vol. 5%TiB_2	A356-Vol. 7.5%TiB_2	A356-Vol. 10%TiB_2
Si	7.32	7.84	8.48	8.84
Mg	0.299	0.315	0.296	0.302
Fe	0.196	0.256	0.370	0.360
Cu	0.004	0.013	0.010	0.013

Table 4.6 (cont'd)

Mn	0.001	0.001	0.001	0.001
Zn	0.005	0.005	0.011	0.198
Cr	0.005	0.017	0.018	0.017
Ni	0.005	0.018	0.055	0.043
Al	Balance			

Optical and scanning electron microscopy studies were conducted on squeeze cast A356 alloy containing no TiB_2 and squeeze cast A356-TiB_2 composite samples containing different amounts of TiB_2. Micrographs are given in Figure 4.17 to 4.20.

The squeeze cast microstructure of A356 alloy containing no TiB_2, which is shown on Figure 4.17, consists of a eutectic phase located in between the fine primary α-aluminum dendrites.

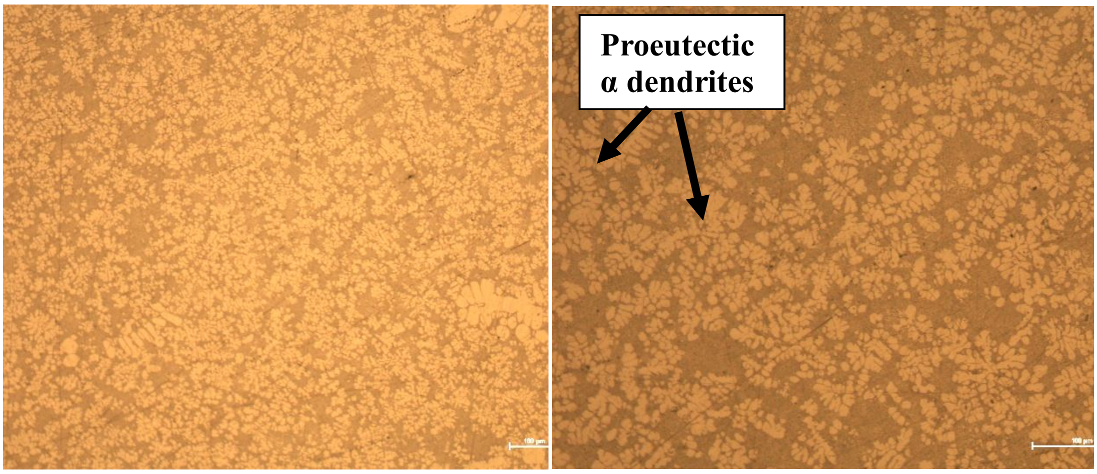

a X100 b X200

Figure 4. 17 Optical micrographs of A356 alloy with different magnifications respectively; (a) X100, (b) X200, (c) X500, and (d) X1000, Samples were etched with Keller's reagent

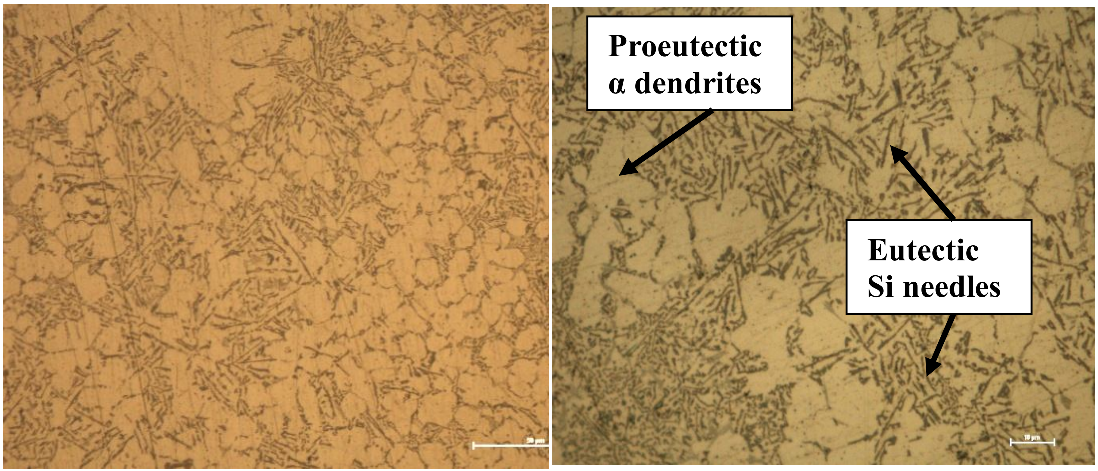

c X500 d X1000

igure 4. 17 Optical micrographs of A356 alloy with different magnifications respectively; (a) X100, (b) X200, (c) X500, and (d) X1000, Samples were etched with Keller's reagent **(continued)**

The optical photomicrographs of A356-5 vol. % TiB_2 squeeze cast composite is given in Figure 4.18 with four different magnifications.

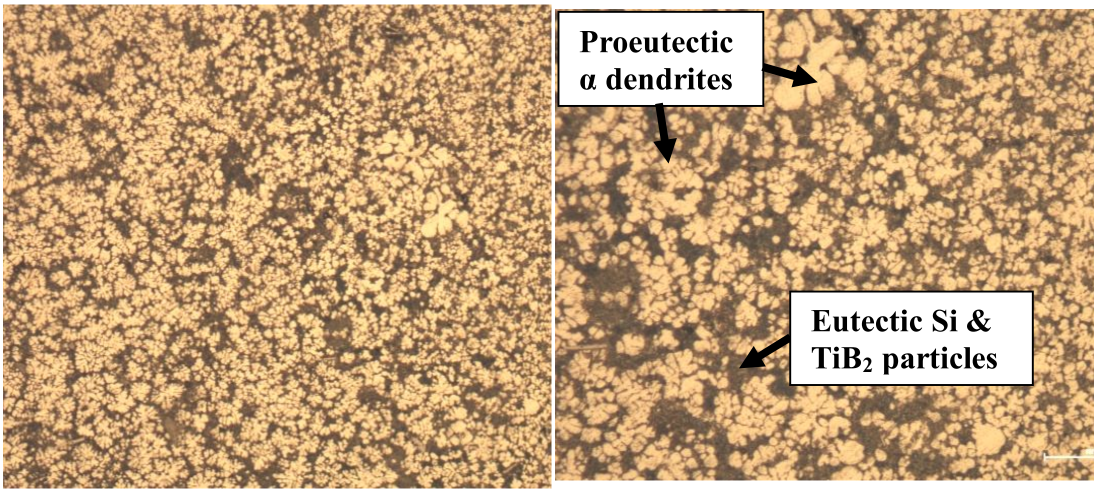

a X100 b X200

Figure 4. 18 Optical micrographs of A356-5vol. % TiB_2 with different magnifications respectively; (a) X100, (b) X200, (c) X500, and (d) X1000, Samples were etched with Keller's reagent

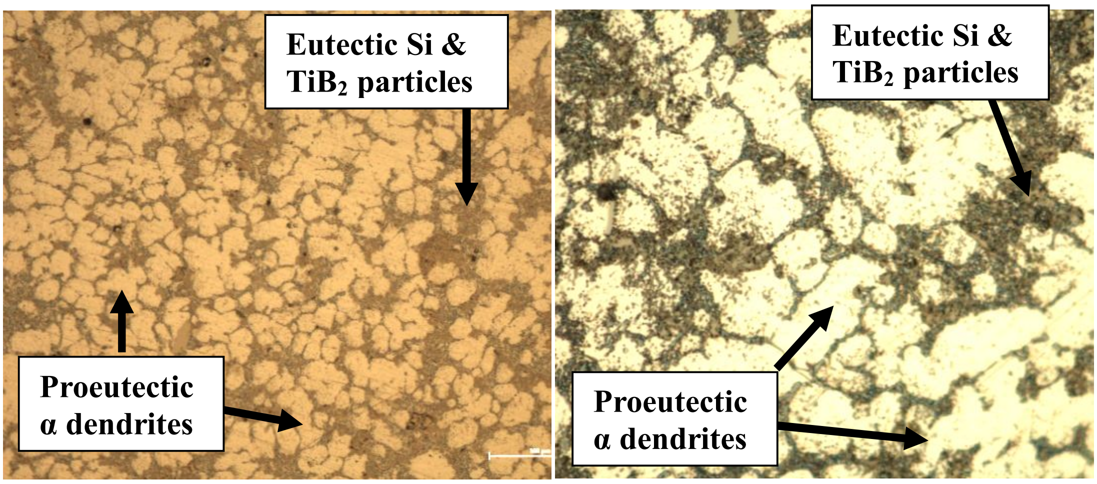

c X500 d X1000

Figure 4. 18 Optical micrographs of A356-5vol. % TiB_2 with different magnifications respectively; (a) X100, (b) X200, (c) X500, and (d) X1000, Samples were etched with Keller's reagent **(continued)**

The optical photomicrographs of A356-7.5 vol. % TiB_2 squeeze cast composite is given in Figure 4.19 with four different magnifications.

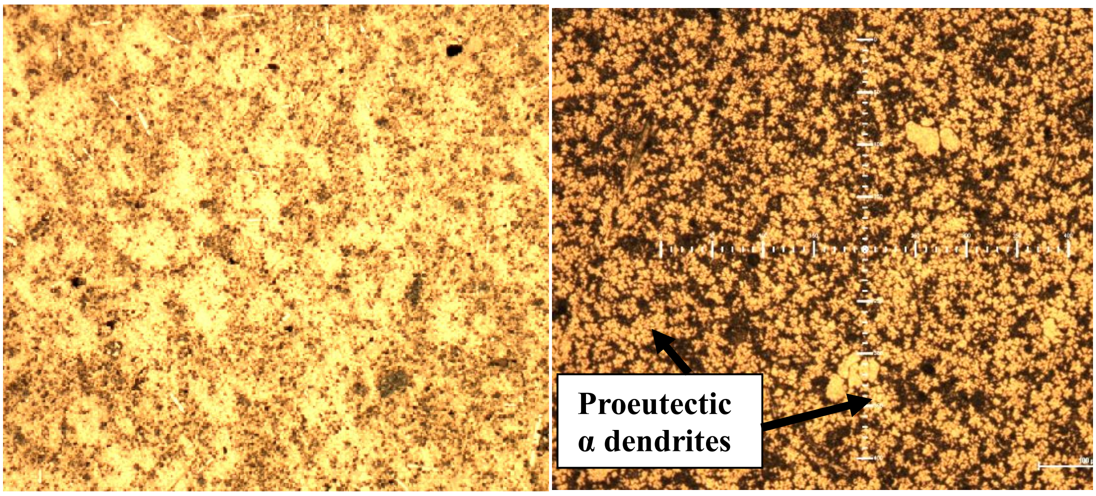

a X100 b X200

Figure 4. 19 Optical micrographs of A356-7.5 vol. % TiB_2 with different magnifications respectively; (a) X100, (b) X200, (c) X500, and (d) X1000 , Samples were etched with Keller's reagent

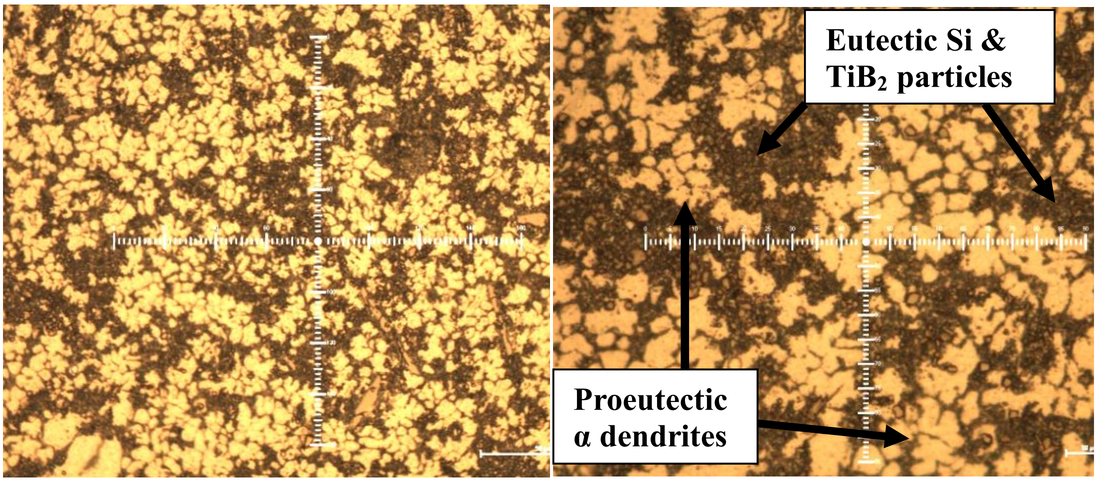

c X500 d X1000

Figure 4. 19 Optical micrographs of A356-7.5 vol. % TiB_2 with different magnifications respectively; (a) X100, (b) X200, (c) X500, and (d) X1000 , Samples were etched with Keller's reagent **(continued)**

The optical photomicrographs of A356-10 vol. % TiB_2 squeeze cast composite is given in Figure 4.20 with four different magnifications.

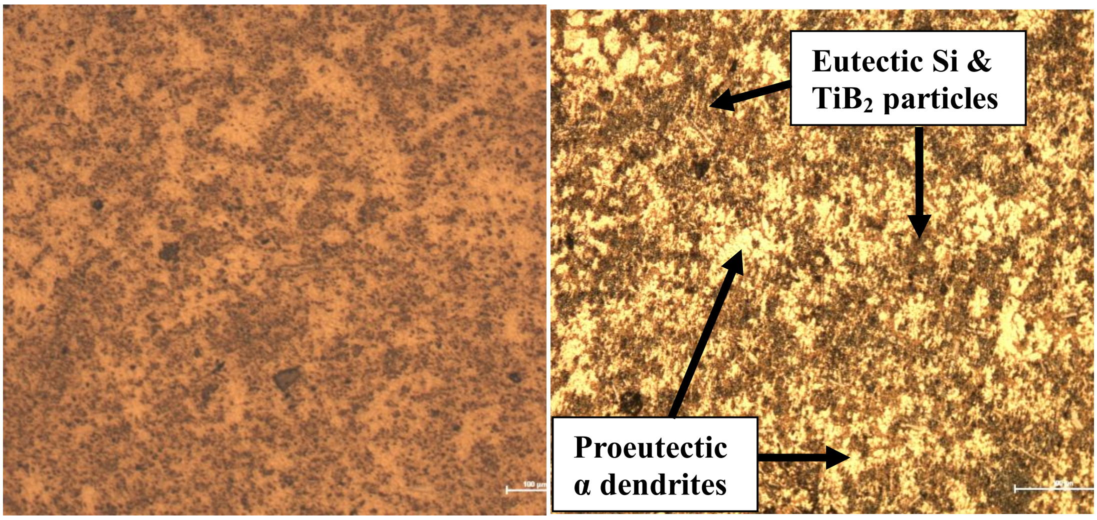

a X100 b X200

Figure 4. 20 Optical micrographs of A356-10 vol. % TiB_2 with different magnifications respectively; (a) X100, (b) X200, (c) X500, and (d) X1000 , Samples were etched with Keller's reagent

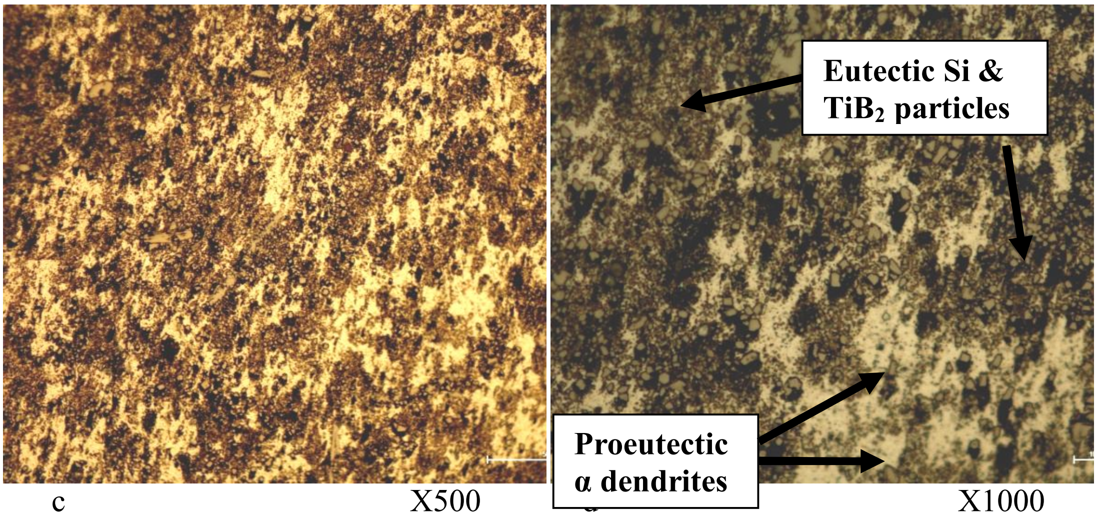

c X500 d X1000

Figure 4. 20 Optical micrographs of A356-10 vol. % TiB_2 with different magnifications respectively; (a) X100, (b) X200, (c) X500, and (d) X1000 , Samples were etched with Keller’s reagent **(continued)**

In order to observe coarse eutectic silicon around the large proeutectic α aluminum dendrites in plain A356 alloy. Annealing procedure was applied at 450°C for 20 hours. The main aim of the annealing was removal of the squeeze effect on the eutectic silicon. Sand-cast A356 alloy consists of coarse eutectic silicon needles around large proeutectic α-aluminum dendrites. Such a microstructure was not observed in the squeeze-cast samples of this study.

The optical photomicrograph of A356, which was annealed at 450°C for 20 hours, is given in Figure 4.21 with four different magnifications.

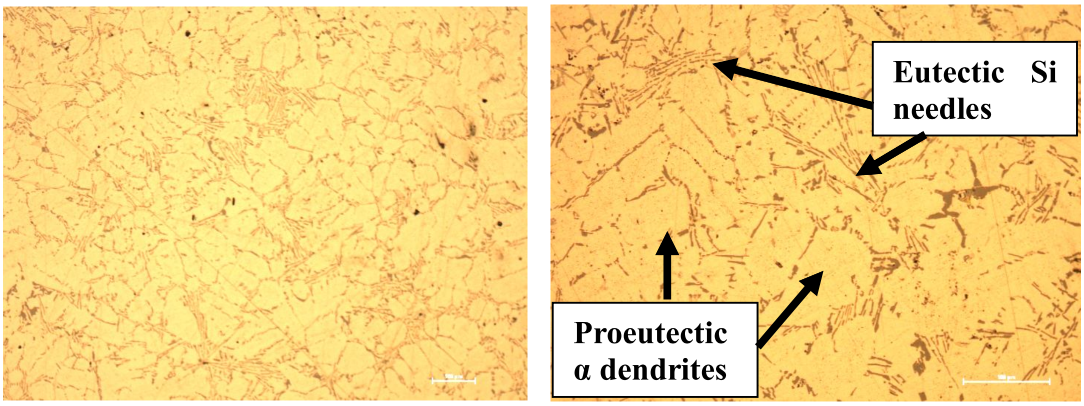

a X100 b X200

Figure 4. 21 Optical micrographs of annealed (at 450°C for 20 hours),A356 reference specimen with different magnifications respectively; (a) X100, (b) X200, (c) X500, and (d) X1000 , Samples were etched with Keller’s reagent

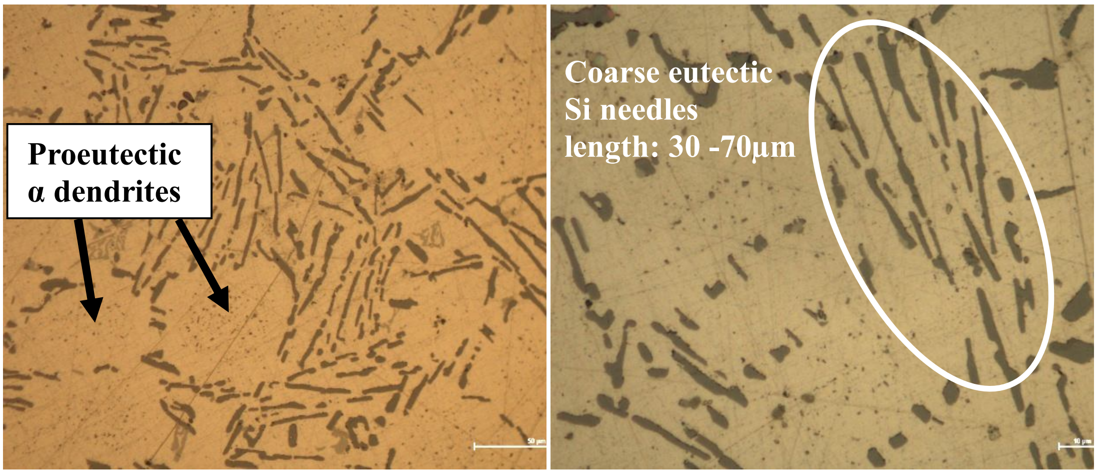

c X500 d X1000

Figure 4. 21 Optical micrographs of annealed (at 450°C for 20 hours),A356 reference specimen with different magnifications respectively; (a) X100, (b) X200, (c) X500, and (d) X1000 , Samples were etched with Keller's reagent **(continued)**

In Figure 4.21 the eutectic silicon needles are seen to be 30µm -70µm long; clearly seen especially at X500 and X1000 magnifications. The major differences between squeeze cast A356 alloy (Figure 4.17) and annealed A356 alloy (Figure 4.21) are the morphology of the eutectic silicon and the proeutectic α-Al dendrite size. In squeeze cast sample, the eutectic Si morphology was observed in moderately small rods around the fine proeutectic α dendrites. On the other hand, in annealed sample the long needle eutectic morphology is seen. In addition the proeutectic Al-dendrite size also decreased with the squeeze casting method.

In Figure 4.17, eutectic Si was observed as non modified small flakes in the squeeze cast A356 alloy. The modification action, which is shown in Figures 4.18 to 4.20, was performed by TiB_2 particles during solidification. Fine fibrous eutectic Si was obtained in eutectic Si modified composite samples.

Distribution of TiB_2 reinforcements is concentrated on the interdendritic regions (between the first solidified α-dendrites); the size of the reinforcement particles is smaller than 3-4 µm. The pro-eutectic α dendrites does not contain TiB_2 particles according to EDS point analysis results.

The optical micrographs suggest that while amount of the TiB_2 particles increases, the interdendritic regions become concentrated with TiB_2 particles. Moreover, size of the Si particles decreases progressively with TiB_2 addition within the interdendritic region. The reason should be; above the eutectic temperature, 577°C, the liquid contains first solidified parts which are proeutectic α-dendrites and TiB_2 reinforcing particles. Fine ceramic particles restrict the growth of α-dendrites. Furthermore, below the 577°C liquid contains α-dendrites, fine TiB_2 particles and eutectic Si. Again, ceramic particles restrict eutectic Si growth within the interdendritic regions.

A comparison of A356- vol. 5%TiB_2 (Fig. 4.18 c and d) and A356-vol. 10% TiB_2 composites (Fig. 4.20 c and d) clearly suggest that with the increasing number of TiB_2 particles, the primary α dendrite size and dendrite arm spacing decreases progressively. The continuous network structure comprising of "TiB_2 and Si particles" becomes more prominent in A356- vol. 10% TiB_2 composite which is shown clearly in Figure 4.20b, 4.20c and 4.20d.

The scanning electron microscopy studies are given in Figure 4.22 to 4.25. The photomicrographs clearly indicated that TiB_2 particles and fibrous eutectic Si were located around the primary α dendrites.

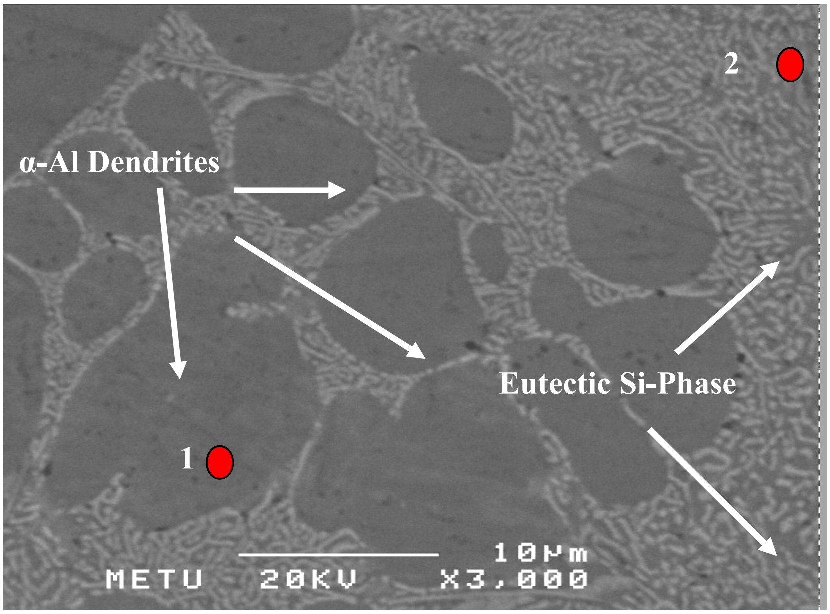

a X3000

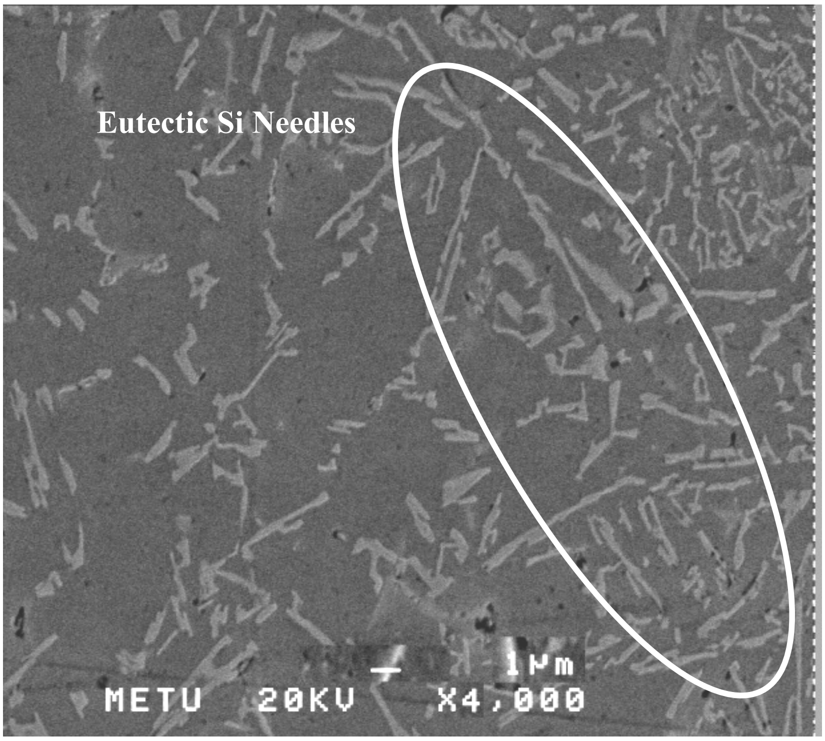

b X4000

Figure 4. 22 A356 0% vol TiB_2 Squeeze cast, Samples were etched with Keller's reagent

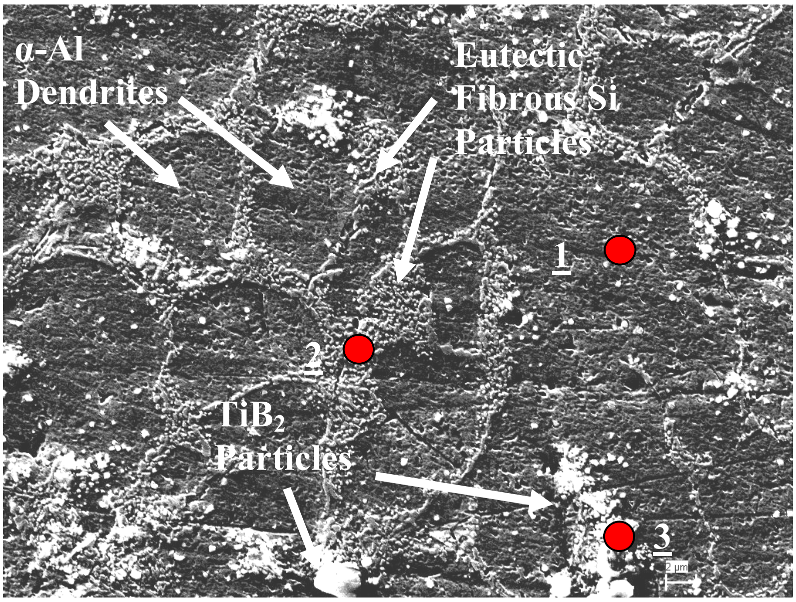

a X5300

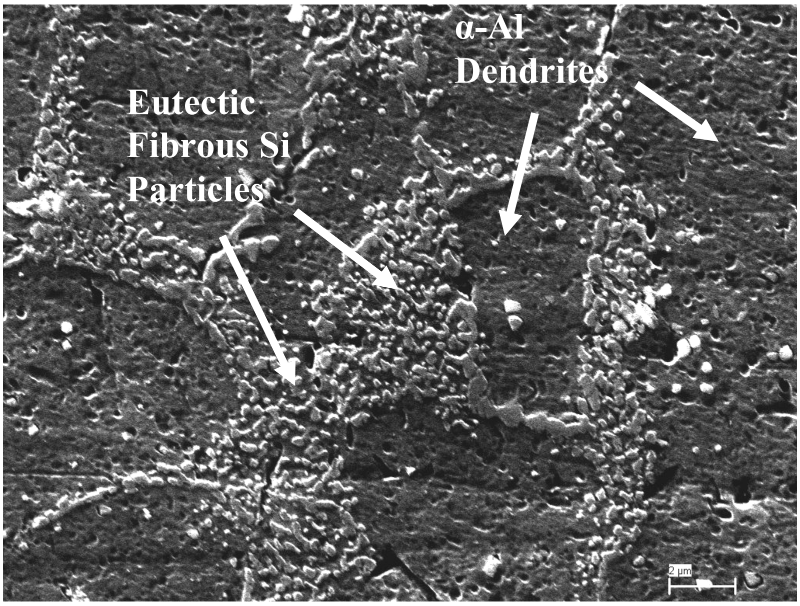

b X11800

Figure 4. 23 A356-5% vol TiB_2 , Squeeze cast Samples were etched with Keller's reagent

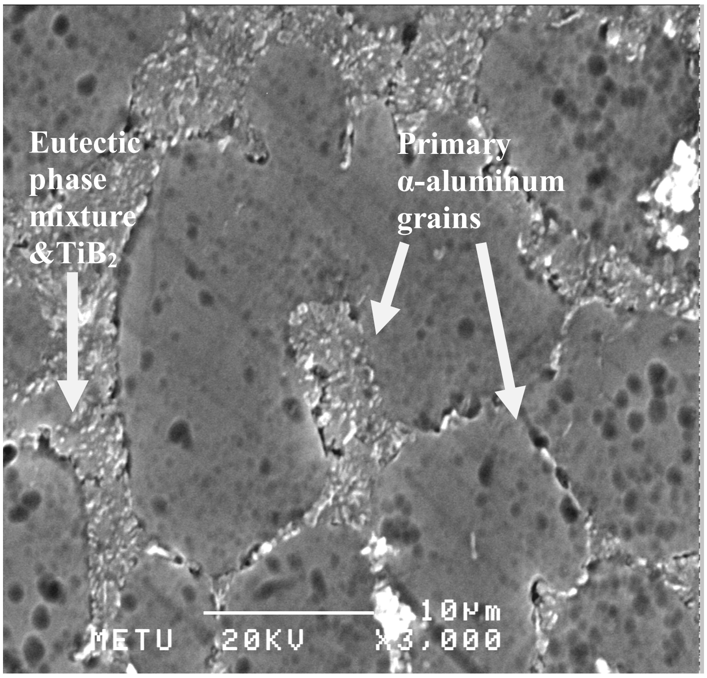

a X3000

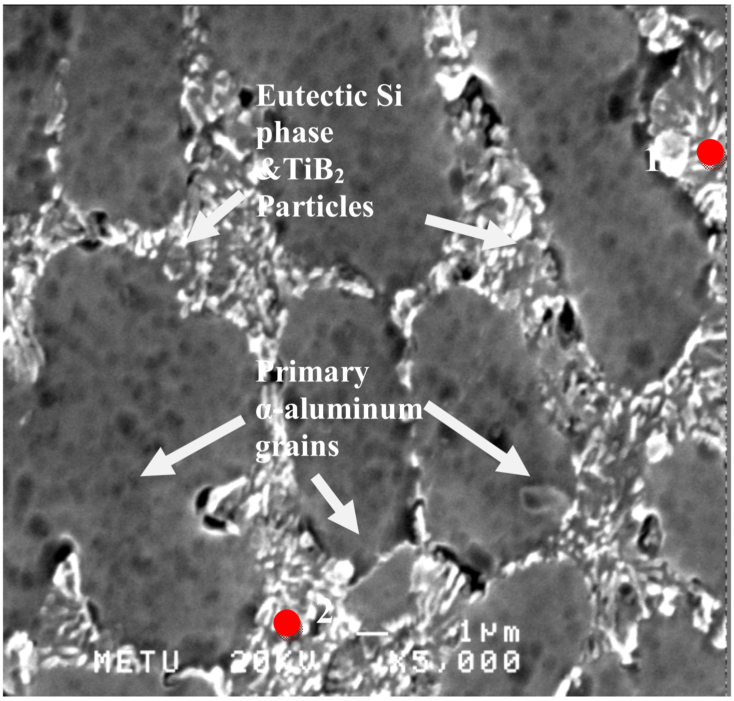

b X5000

Figure 4. 24 A356-7.5% vol TiB_2 , Squeeze cast, Samples were etched with Keller's reagent

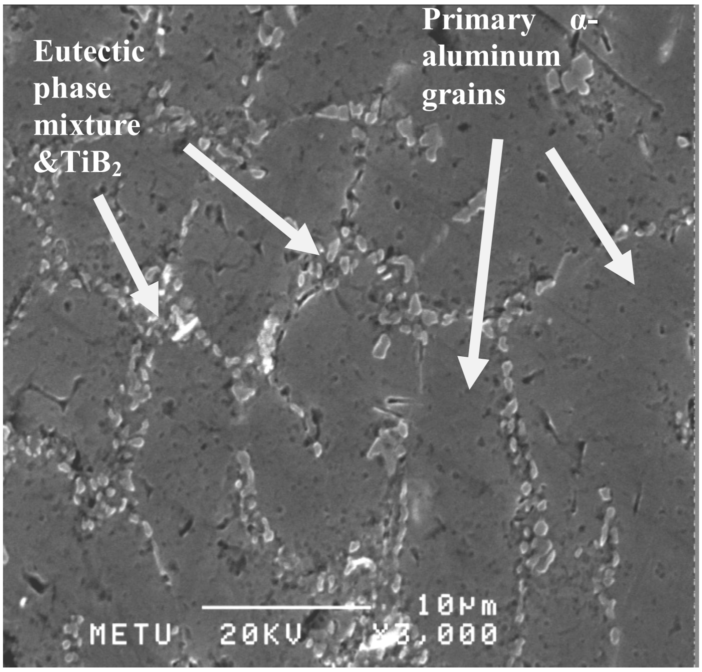

a X3000

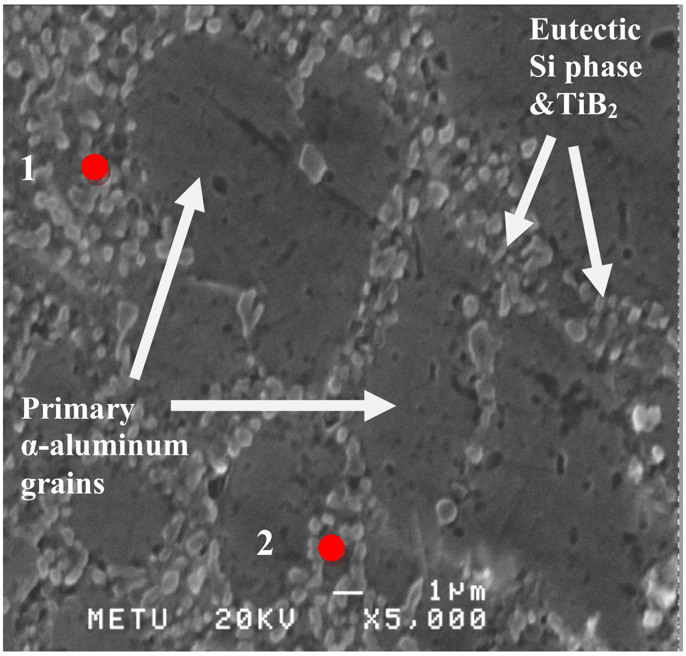

b X5000

Figure 4. 25 A356-10% vol TiB_2 , Squeeze cast Samples were etched with Keller's reagent

Primary α dendrites are clearly seen as dark regions on SEM micrographs. The dendrite size and arm spacing decreases progressively with increasing TiB_2 amount which is shown on Figure 4.22a, Figure 4.23a, Figure 4.24a and Figure 4.25a. In SEM micrographs Figure 4.24b and 4.25b with higher magnifications, TiB_2 reinforcements are clearly shown as white particles around the dendrites. Generally the size of the particles are less than 4 µm and around the 1 µm. Around the pro-eutectic α dendrites, TiB_2 distribution is mostly uniform and agglomeration of particles did not take place during the solidification, on the other hand TiB_2 particles cannot penetrate into the proeutectic Al dendrites. This is shown on Figures 4.23a, 4.24b and 4.25b.

In Figure 4.22a, Points 1 and 2 shows that EDS analyses were taken in SEM micrograph of A356 alloy. According to EDS Figures 4.26a and 4.26b, the black dendritic areas consist of Aluminum proeutectic dendrite was marked point 1 and between the black areas the eutectic silicon phase was marked point 2.

TiB_2 particles are observed in the SEM micrographs given in Figure 4.23a, 4.24 b and 4.25 b. EDS analysis, which are given in Figure 4.27, Figure 4.28 and Figure 4.29. They were indicated that points 1, 2 and 3 are TiB_2 particles on the three micrograph, (Figure 4.23a, Figure 4.24b, and Figure 4.25b). On the basis of XRD results of leach residue and EDS results of composite, these particles are titanium diboride reinforcements.

According to EDS analysis given in Figures 4.27b, 4.28b and 4.29b, eutectic fibrous Si and TiB_2 particles are in the form of fine particle mixture which are placed between the proeutectic α dendrites. The EDS analysis were taken on point 2 and 3, which are marked at Figures 4.23a, 4.24b and 4.25b

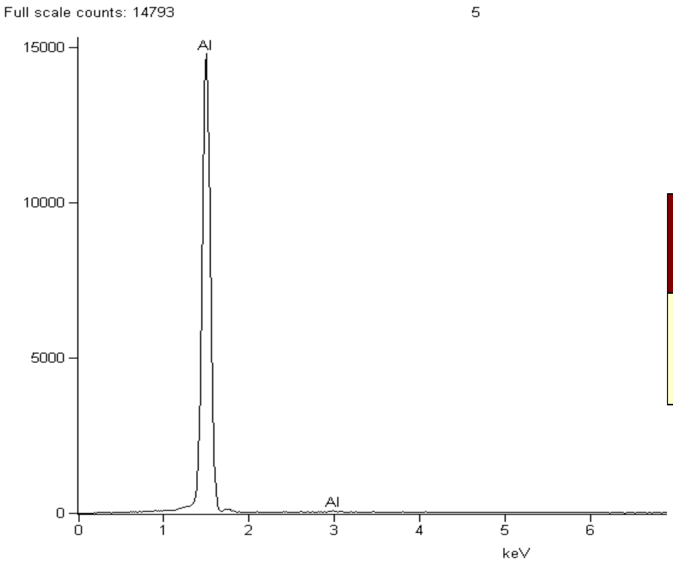

Element	*Weight Conc %*	*Atom Conc %*
Al	100.00	100.00

4.26 A A356 Primary Aluminum Dendrites at point 1

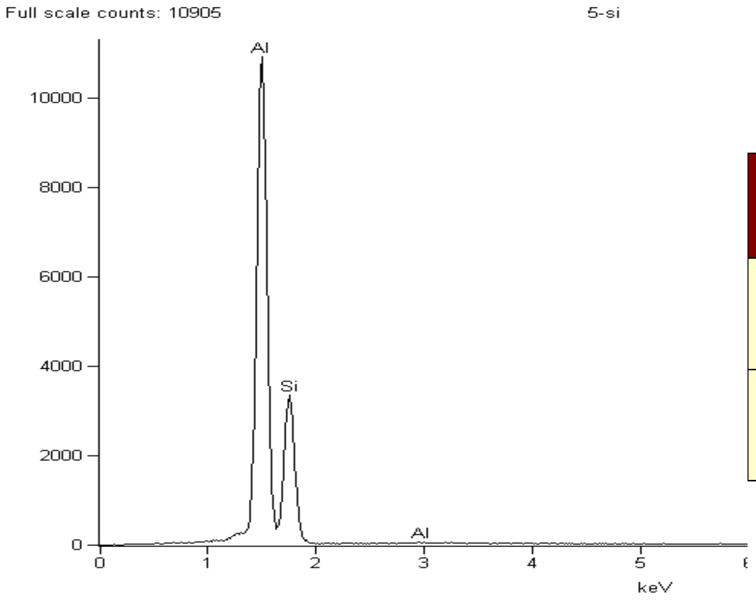

Element	*Weight Conc %*	*Atom Conc %*
Al	60.17	61.13
Si	39.83	38.87

4.26 B A356 Al-Si eutectic phase at point 2 on Figure 4.22a

Figure 4. 26 EDS point analyses on Figure 4.22a

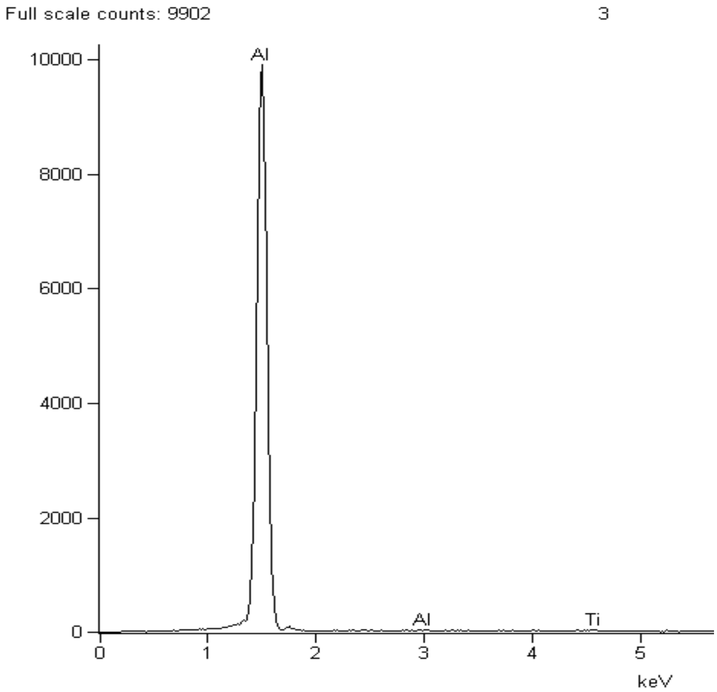

Element	*Weight Conc %*	*Atom Conc %*
Al	99.48	99.71
Ti	0.52	0.29

4.27 A %5vol TiB$_2$/A356 Primary Al-dendrites on point 1 at Figure 4.23a

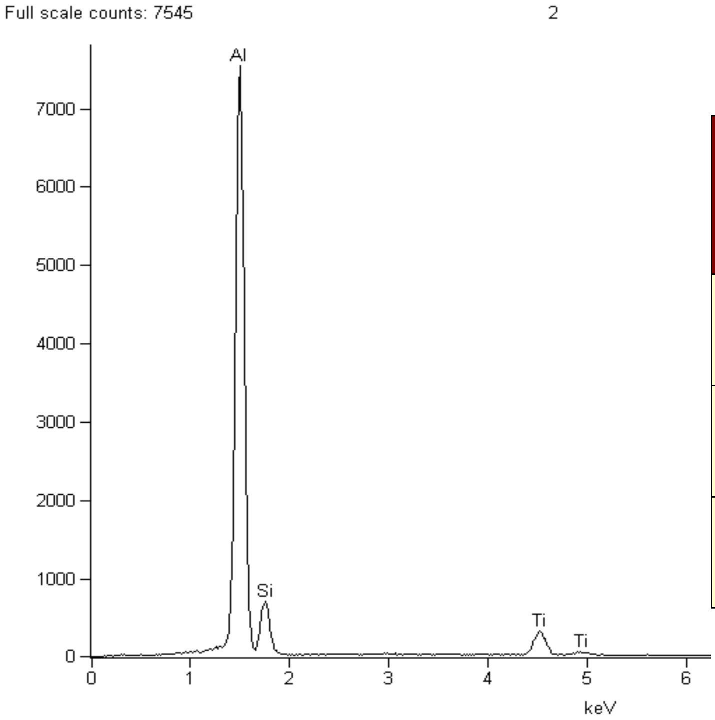

Element	*Weight Conc %*	*Atom Conc %*
Al	73.29	77.53
Si	15.60	15.86
Ti	11.10	6.61

4.27 B %5vol TiB$_2$/A356 Al-Si Eurectic Phase on point 2 at Figure 4.23a

Figure 4.27 EDS point analyses on vol.5% TiB$_2$-A356 Alloy at Figure 4.23a

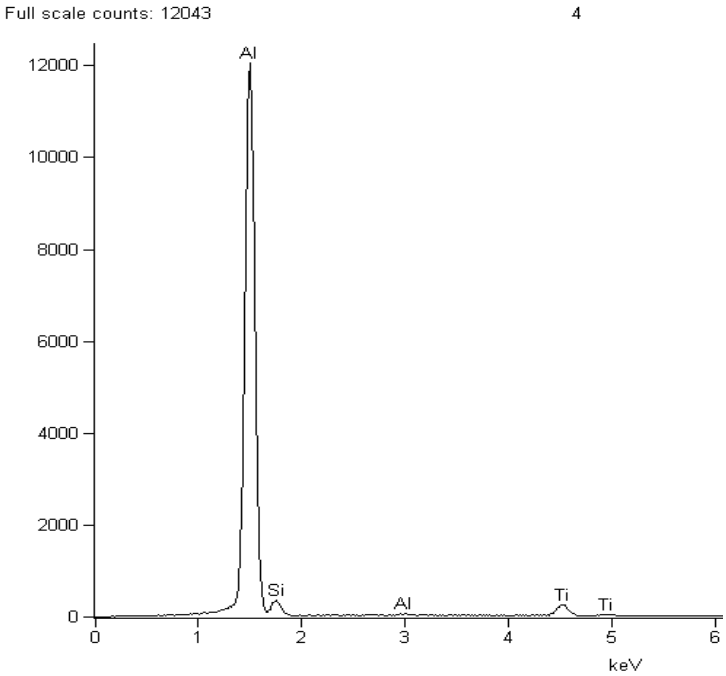

Element	*Weight Conc %*	*Atom Conc %*
Al	89.33	91.87
Si	4.78	4.72
Ti	5.89	3.41

4.27 C %5vol TiB_2/A356 TiB_2 particles on point 3 at Figure 4.23a

Figure 4. 27 EDS point analyses on vol.5% TiB_2-A356 Alloy at Figure 4.23a **(continued)**

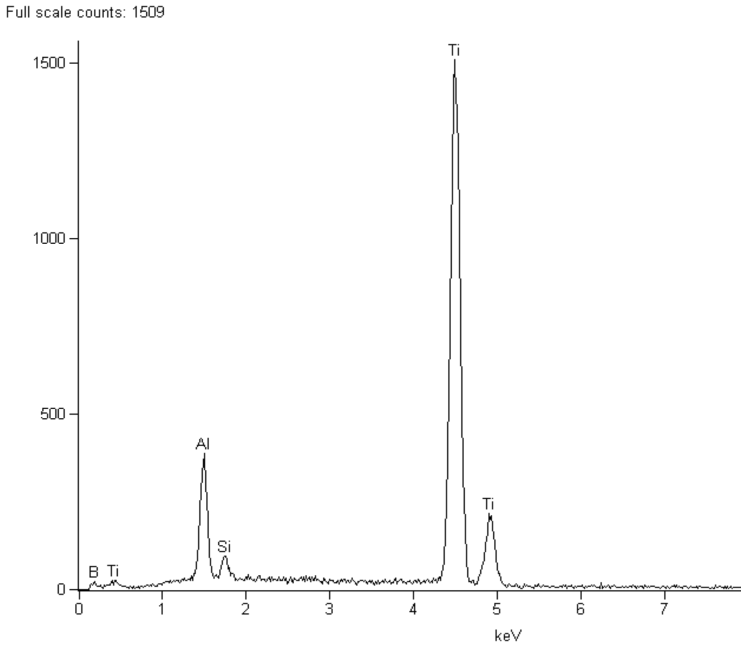

Element	**Weight Conc %**	**Atom Conc %**
B	12.27	36.21
Al	8.91	10.53
Si	1.58	1.80
Ti	77.24	51.45

4.28 A %7.5vol TiB_2/A356 TiB_2 particles on point 1 at Figure 4.24b

Figure 4.28 EDS point analyses on vol. 7.5% TiB_2-A356 Alloy at Figure 4.24b

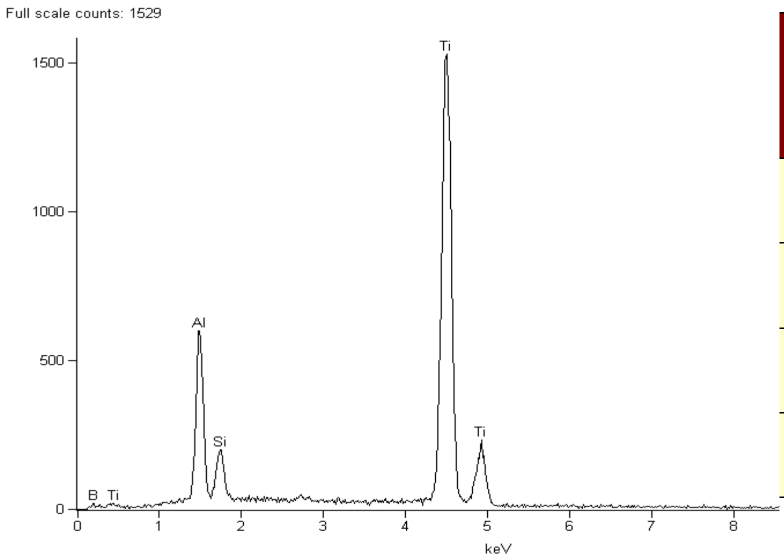

Element	Weight Conc %	Atom Conc %
B	10.23	30.64
Al	12.98	15.57
Si	3.95	4.56
Ti	72.84	49.23

4.28 B %7.5vol TiB_2/A356 TiB_2 particles on point 2 at Figure 4.24b

Figure 4. 28 EDS point analyses on vol. 7.5% TiB_2-A356 Alloy at Figure 4.24b **(continued)**

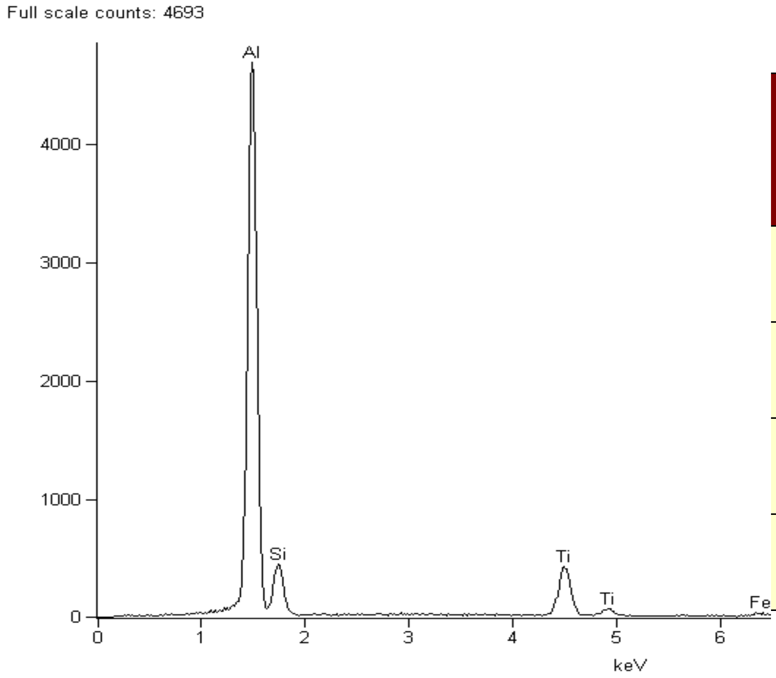

Element	Weight Conc %	Atom Conc %
B	65.80	73.02
Al	13.15	14.02
Si	18.74	11.71
Ti	2.31	1.24

4.29 A %10 vol TiB_2/A356 TiB_2 particles on point 1at Figure 4.25b

Figure 4.29 EDS point analyses on vol. 10% TiB_2-A356 Alloy at Figure 4.25b

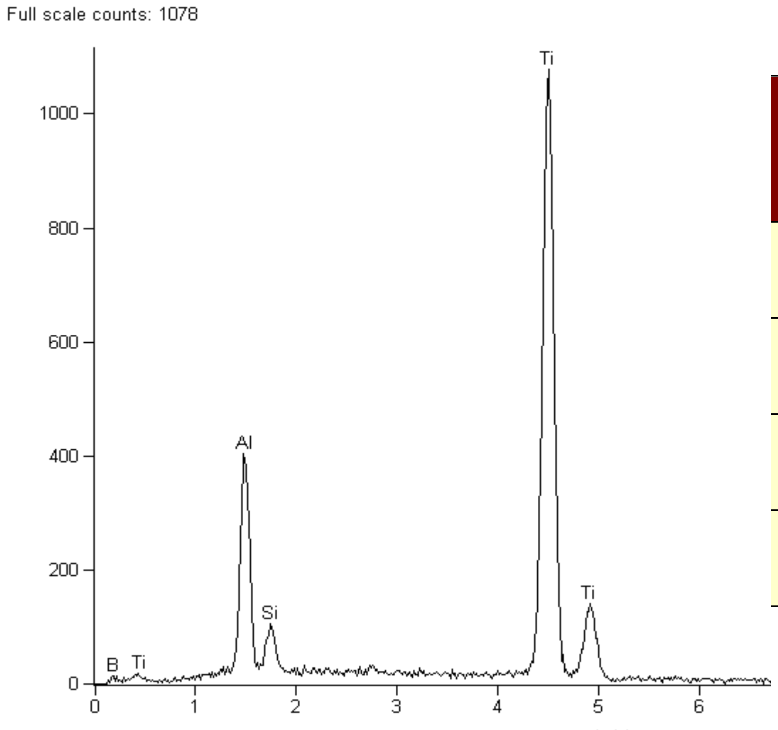

Element	Weight Conc %	Atom Conc %
B	10.23	30.74
Al	13.45	16.20
Si	2.74	3.16
Ti	73.58	49.90

4.29 B %10 vol TiB_2/A356 TiB_2 particles on point 2 at Figure 4.25b

Figure 4. 29 EDS point analyses on vol. 10% TiB_2-A356 Alloy at Figure 4.25b **(continued)**

4.4 Secondary Dendrite Arm Spacing (SDAS) Measurement

In chapter 3.7 the main principles of the grain size determination were explained in detail. Yield and ultimate tensile strengths and ductility increases with decrease in secondary dendrite arm spacing in metal matrixes.

In order to determine secondary dendrite arm spacings, the broadening of the X-ray diffraction peaks was measured. First of all, a reference sample which contained no reinforcement was used.

The X-Ray pattern maximum intensity (200) peak of reference sample is given in Figure 4.30 (a). Then, this sample was metallographically prepared by grinding, polishing and micro etching with 100ml H_2O + 200 ml HNO_3 + 180 ml HCl + 60 gr $FeCl_3$. In order to calculate the size of the grains, X50 micrograph of reference sample was used. Lines with 1 cm intervals were drawn on the micrograph and the number of grains that cut the lines was counted. The secondary dendrite arm spacing of this sample was measured as 23.66 µm.

In Figure 4.30 (b), 4.30 (c) and 4.30 (d) the X-Ray pattern of 5 %, 7.5 % and 10 % vol. TiB_2, are presented. To establish the variation in the grain size of aluminum alloy matrix by addition of 5 %, 7.5 % and 10 % vol. TiB_2, the broadening of the (200) peaks were measured.

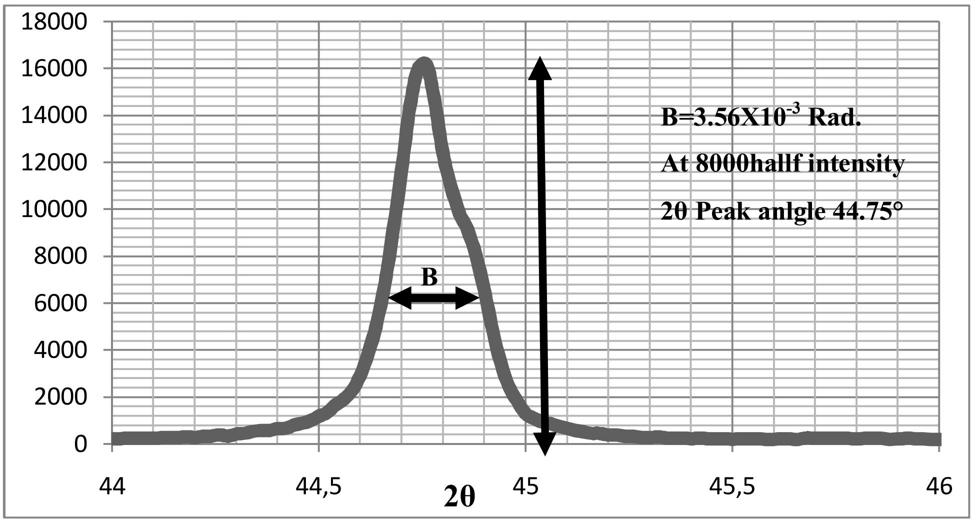

a %0TiB_2-A356 Reference Sample

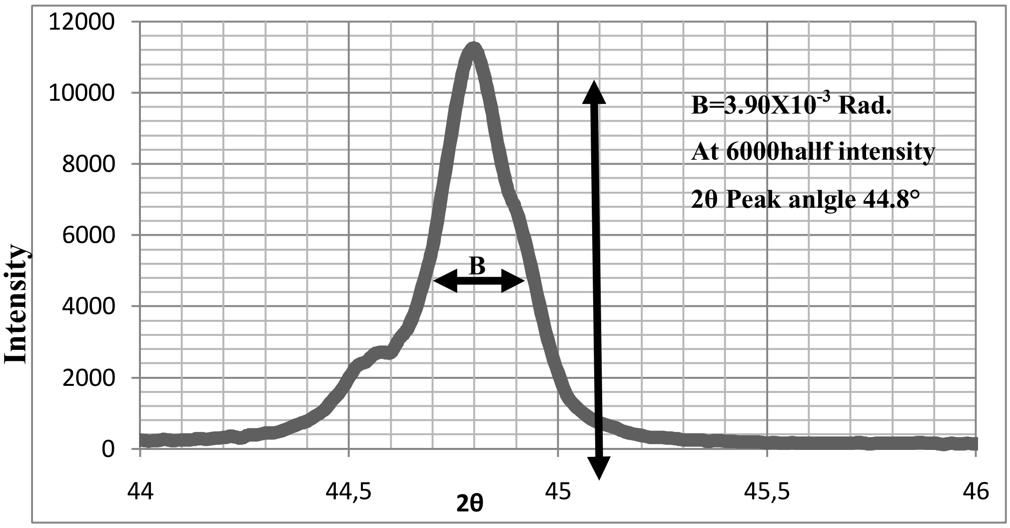

b %5 vol.TiB_2-A356

Figure 4. 30 Diffraction patterns of A356-TiB_2 composite showing (200) peaks broadening because of secondary dendrite arm spacing's

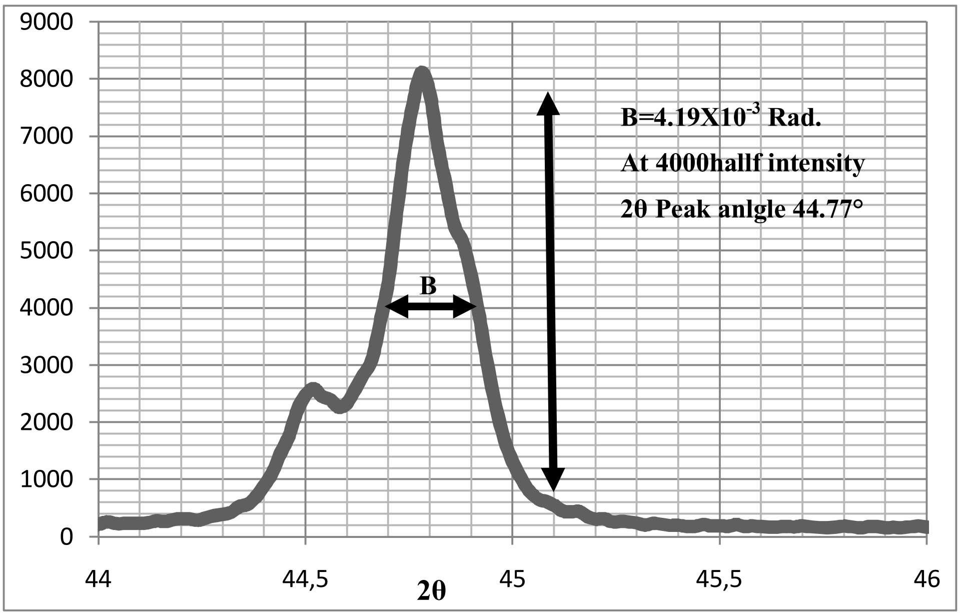

c %7.5 vol.TiB_2-A356

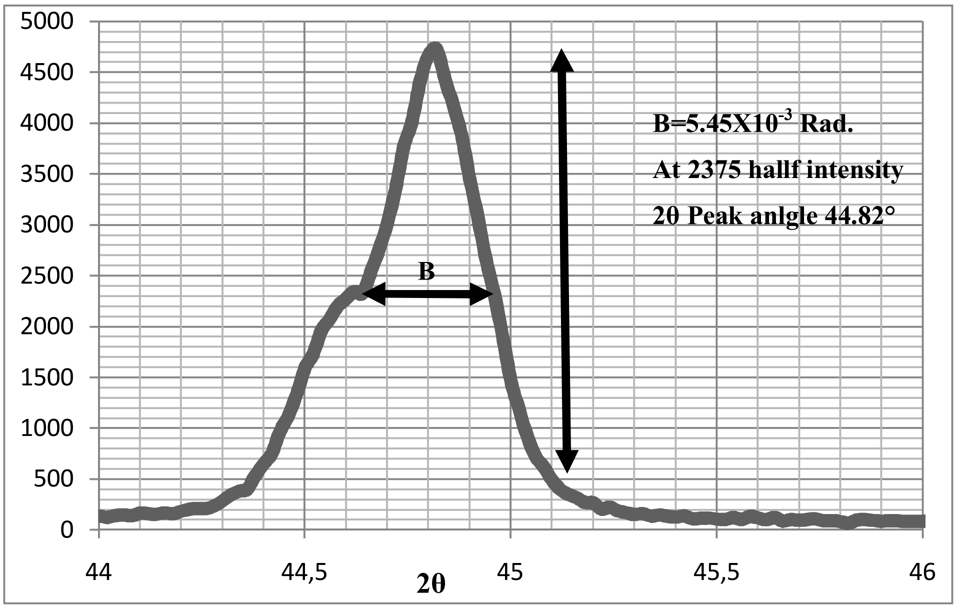

d %10 vol.TiB_2-A356

Figure 4. 30 Diffraction patterns of A356-TiB_2 composite showing (200) peaks broadening because of secondary dendrite arm spacing's **(continued)**

Clearly seen in Figure 4.30, the broadening of the (200) peak increases with the increase of the percentage of reinforcement TiB_2 particles. To determine the grain size of the aluminum alloy matrix for each sample, Equations 3.1 and 3.2 are given in Chapter III were applied. Calculation results showed which are presented in Table 4.7; the increase in the volume percentage of TiB_2 causes a decrease in the grain size.

In addition the broadening calculations, using the special metallographic microscope and suitable software, the secondary dendrite arm spacing measurement was performed and results are shown in Figure 4.31.

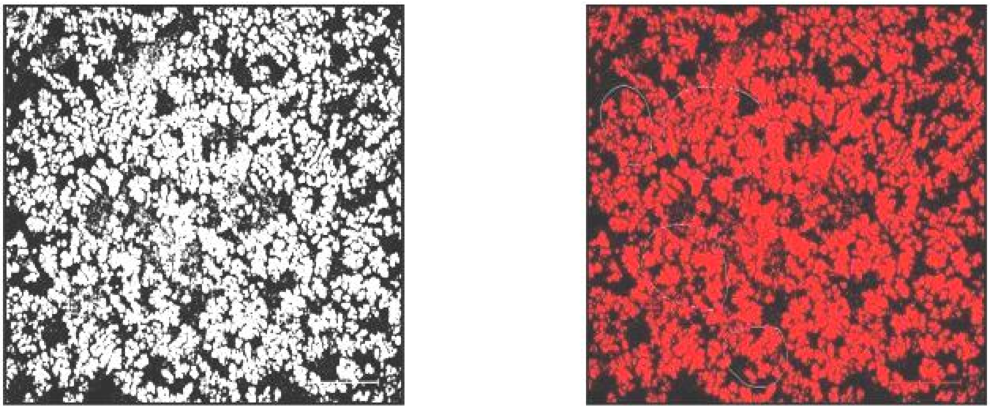

Secondary Dendrite Arm Spacing Measurement

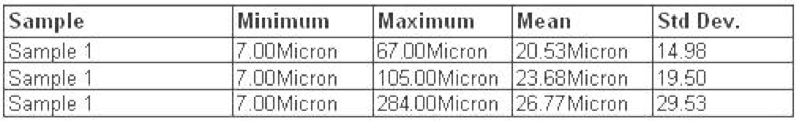

Sample	Minimum	Maximum	Mean	Std Dev.
Sample 1	7.00Micron	67.00Micron	20.53Micron	14.98
Sample 1	7.00Micron	105.00Micron	23.68Micron	19.50
Sample 1	7.00Micron	284.00Micron	26.77Micron	29.53

Figure 4. 31 Secondary Dendrite arm spacing measurement of A356 reference sample via to special metallographic light microscope and software. X200 magnification and etched with Keller' reagent

Secondary dendrite arm spacing results are given in Table 4.7.

Table 4.7 Reinforcement Content and SDAS Size*

Vol. % Reinforcement	**SDAS Size (μm)**
0	23±3
5 [% Increment]	21±2 [-8.6]
7.5 [% Increment]	19±3 [-17.4]
10 [% Increment]	14±2 [-38.6]

*The broadening measurements were correlated to the experimental composite's SDAS size measured by optical microscope. Since the effect of subgrain reflections cannot be distinguished, the SDAS size information deduced from the linear trend line is may not be the actual SDAS size.

4.5 Mechanical Properties of A356 –TiB_2 Composites

The mechanical test results, which were conducted on the composite samples, are summarized in Table 4.8. The values listed in the table indicate the average of 15 values determined for each parameter. The results indicate that the ultimate tensile strength (UTS), yield strength (YS), modulus of elasticity (E, Young's Modulus), flexural strength and microhardness increase with increasing amount of TiB_2 particles in the composite.

Table 4.8 Mechanical Testing Results of A356-TiB_2 Composite

TiB_2 reinforcement vol. %	**0**	**5**	**7.5**	**10**
UTS (MPa) [Increment %]	173	182±3 [+5]	192±2 [+9]	205±4 [+19]

Table 4.8 (cont'd)

YS (MPa) [Increment %]	148±2	159±2 [+7]	169±2 [+14]	174±3 [+18]
E (GPa) [Increment %]	19±2	22±1 [+15.7]	23±2 [+21.1]	25±1 [+31.1]
% Reduction in Area [Increment %]	10.2±2	9.7±2 [-4.9]	8.3±2 [-18.6]	7.5±1 [-26.5]
% Elongation [Increment %]	11.1±1	10.5±1 [-5.4]	9.2±1 [-17.1]	8.6±1 [-22.5]
Hardness (HV 0.2) [Increment %]	101±2	104±3 [+2.9]	111±3 [+9.9]	127±5 [+25.7]
Flexural Strength (MPa) [Increment %]	332±4	358±3 [+7.8]	372±3 [+12.0]	387±5 [+16.6]

The macro and micro hardness results are shown in Table 4.9. Micro-hardness test was applied at X200 magnification. 200 grf test load was applied with common Vickers indenter. Brinell macro-hardness test was applied with 500 kgf test load and 10 mm steel ball indenter.

Table 4. 9 Brinell Macro and Vickers Micro Hardness Numbers of A356-TiB_2 Composite

TiB_2 reinforcement vol. %	HV 0.2 [Increment %]	HBS [Increment %]
0	101±2	88±2
5	104±3 [+2.9]	90±4 [+2.2]
7.5	111±3 [+9.9]	95±3 [+7.9]
10	127±5 [+25.7]	109±4 [+23.86]

Graphical forms of the results are shown in Figure 4.32. These graphs also indicate that the ultimate tensile strength (UTS), yield strength (YS) and hardness (HV0.2) increases with the increasing amount of particles in the composite.

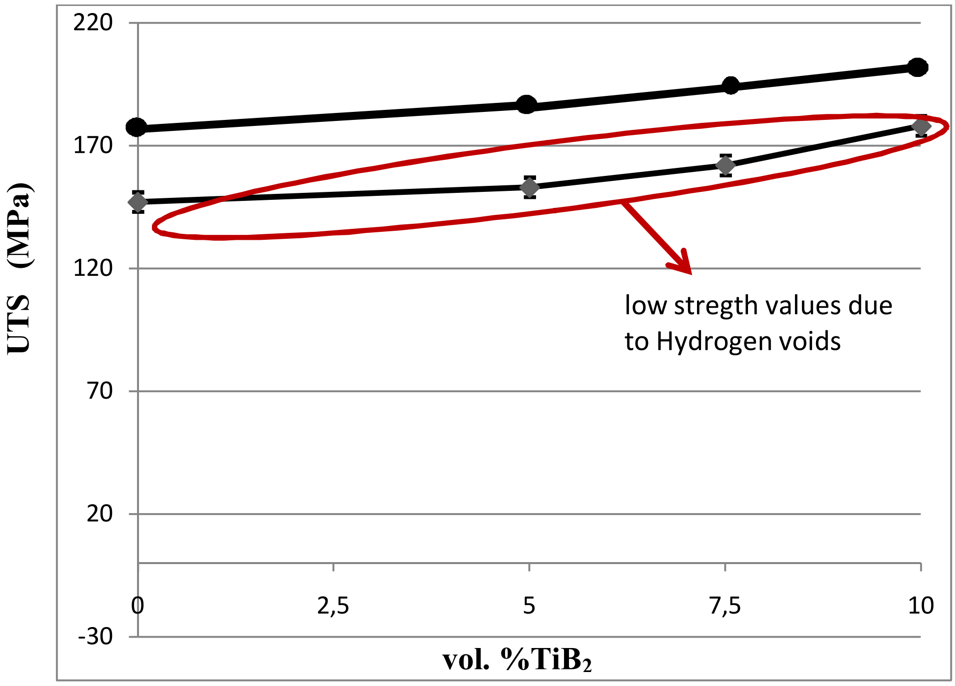

(a)

Figure 4. 32 (a) Variation of ultimate tensile strength (UTS) with volume percent of reinforcements.(b)Variation of yield strength (YS) with volume percent of reinforcements.(c)Variation of flexural strength with volume percent of reinforcements.(d)Variation of hardness (HV0.2) with volume percent of reinforcements. (e) Variation of elastic modulus (E) with volume percent of reinforcements

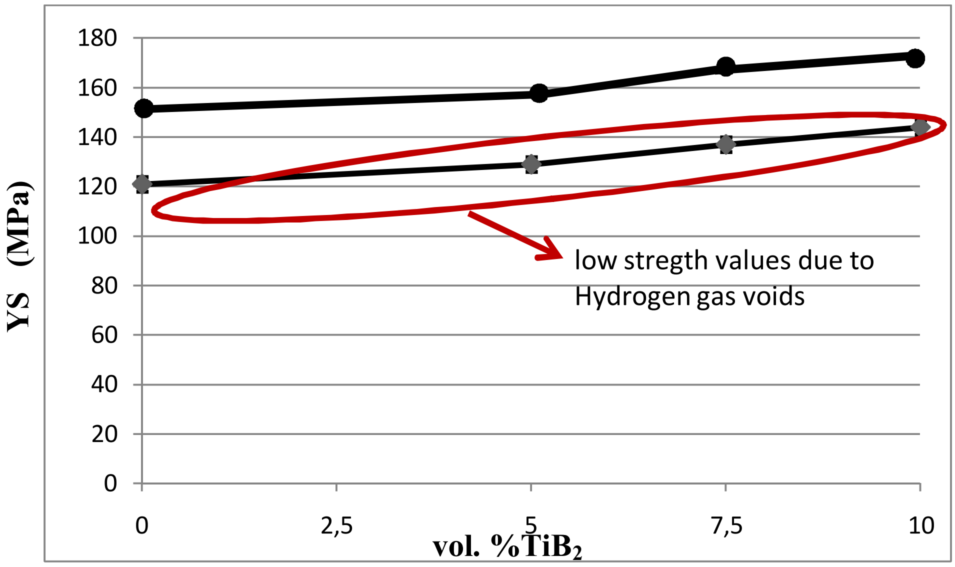

(b)

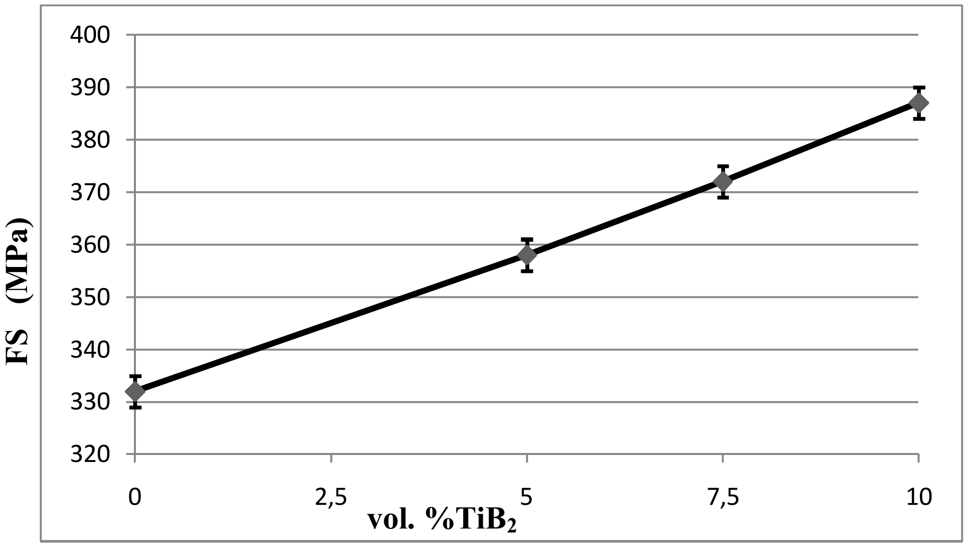

(c)

Figure 4. 32 (a) Variation of ultimate tensile strength (UTS) with volume percent of reinforcements.(b)Variation of yield strength (YS) with volume percent of reinforcements.(c)Variation of flexural strength with volume percent of reinforcements.(d)Variation of hardness (HV0.2) with volume percent of reinforcements. (e) Variation of elastic modulus (E) with volume percent of reinforcements **(continued)**

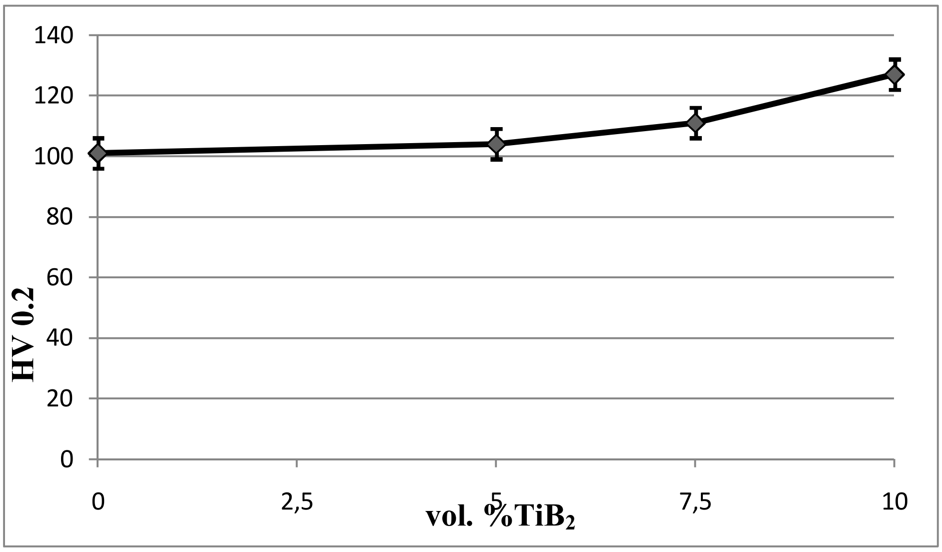

(d) .

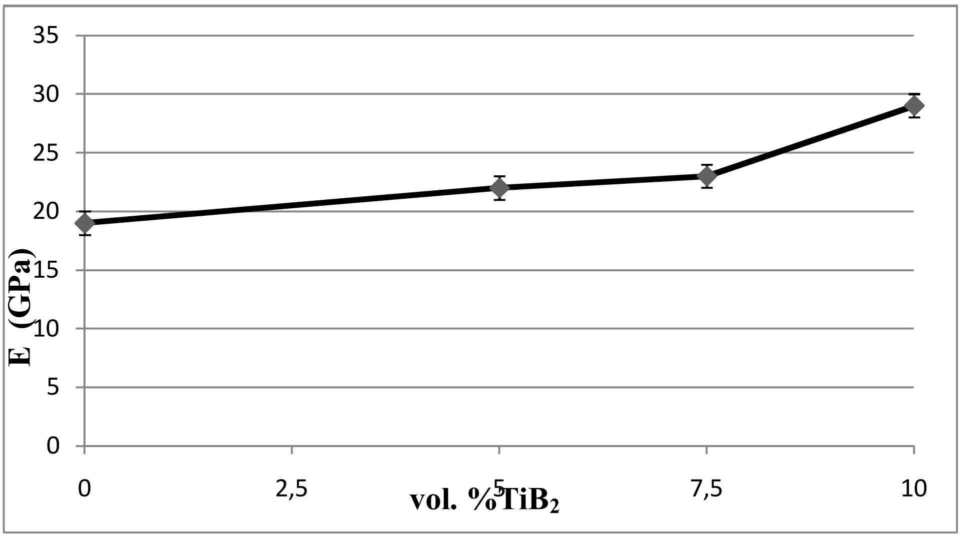

(e)

Figure 4. 32 (a) Variation of ultimate tensile strength (UTS) with volume percent of reinforcements.(b)Variation of yield strength (YS) with volume percent of reinforcements.(c)Variation of flexural strength with volume percent of reinforcements.(d)Variation of hardness (HV0.2) with volume percent of reinforcements. (e) Variation of elastic modulus (E) with volume percent of reinforcements **(continued)**

Some ultimate and yield strength values were abnormally low. These low data were not included in average ultimate tensile and yield strength calculations. Macro examinations were carried out on the fracture surface of these specimens. Some voids were observed which are given below in Figure 4.33.

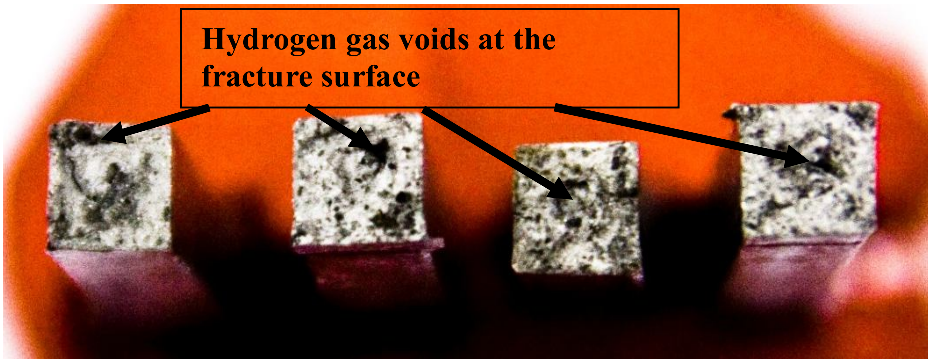

Figure 4. 33 Fracture surfaces of the defected tensile specimens

Most probably, Hydrogen picking of liquid aluminum caused these defects, Because, hydrogen is the only gas which is soluble in liquid aluminum. With increasing temperature hydrogen solubility increases enormously; this is shown below in Figure 4.34.

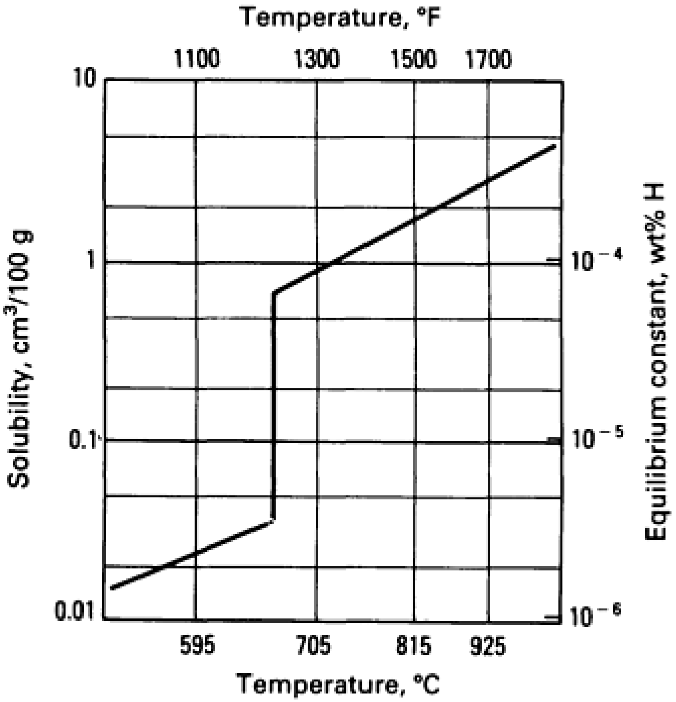

Figure 4. 34 Hydrogen solubility (pH_2=1 atm) with increasing temperature **[57]**

The ductility change is shown in Figure 4.35 in terms of reduction in area % and elongation %, with amount of reinforcement. As it is seen, the ductility decreases with the increase of reinforcement in composite.

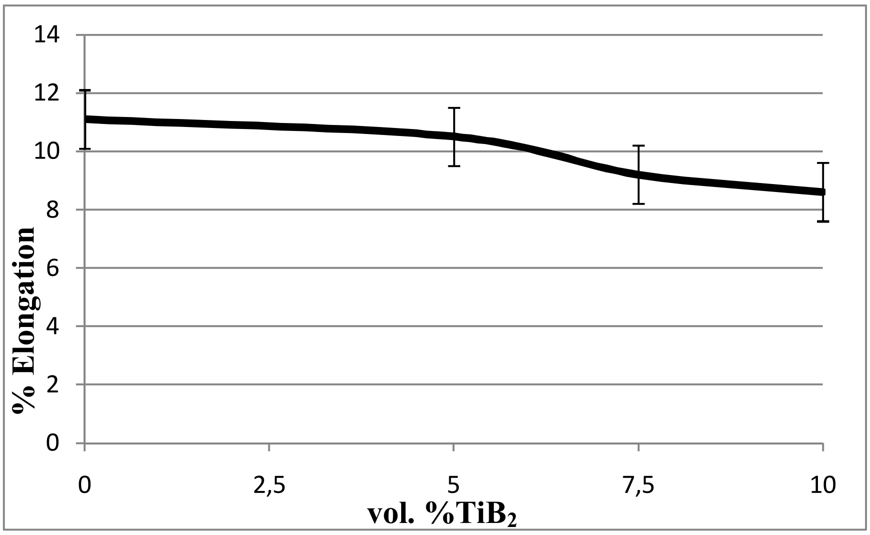

(a)

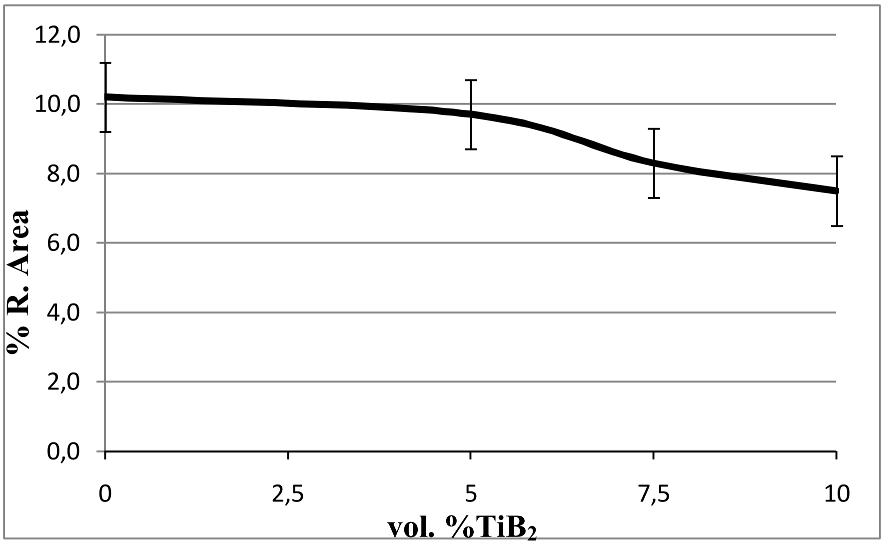

(b)

Figure 4. 35. (a)Variation of elongation with volume percent of reinforcements. (b)Variation of ductility with volume percent of reinforcements

The results shown in Figure 4.32 and 4.35 were consistent with the strengthening mechanisms of discontinuously reinforced metal matrix composites mentioned in section 2.4.2.1 which is explained in detail. Four main aspects, which are directly related with the mechanical properties and discontinuously reinforcing ceramic particles, available for supporting mechanical results of the present study are:

- Thermal expansion coefficients of ceramic TiB_2 particles and A356 metal matrix are 8.28 µm/m°K and 23.5 µm/m°K, respectively. During cooling, metal matrix is more contracted than the discontinuously reinforced TiB_2 particles. As a result of CTE difference, the plastic deformation zones and high dislocation densities are created around the TiB_2 particles. The uniformly distributed TiB_2 particles cause effective strengthening due to the CTE mismatch.
- During solidification, TiB_2 particles generate heterogeneous nucleation sites and produce considerably smaller grain size compared with the unreinforced matrix alloy. The smaller grain size directly increases the strength: this phenomenon is explained by the Hall-Petch formulation which is initially developed for describing the strengthening due to the pinning of the dislocations at the grain boundaries.
- Eutectic silicon morphology is another crucial aspect for the strengthening of Al-Si casting alloys. This is transformation of coarse silicon needles to small fibrous ones. In the present study, TiB_2 particles fulfilled this modification. The difference is clearly seen in SEM micrographs; In Figure 4.22b coarse Si needles were observed on the specimen containing no TiB_2 Modified Si particles were observed on specimen containing TiB_2 as can be seen in Figures 4.23, 4.24, 4.25.
- Load transfer between matrix and the ceramic particles is other crucial mechanism that is responsible for strengthening in the discontinuously reinforced composites. Ductile A356 matrix and hard reinforcement is excellent combination during the service loads.

Lastly, mechanical properties of A356-discontinuosy reinforced TiB$_2$ composites produced in present study were compared with the properties of composites produced by other methods found in literature. Comparisons are summarized in Table 4.10. Processing methods, such as heat treatment and extrusion, were applied to the composites in these methods. As compared with the other methods, the in-situ slag metal reaction method used in the current work supplies a more significant increase in the strength parameters with the incremental increase in the percentage of reinforcements.

Table 4.10 Comparison of Mechanical Properties of Al-TiB$_2$ Metal Matrix Composites

Process	Vol % Reinfor..	%EL	%RA	UTS MPa	YS MPa	Flexural Stress	Hardness HB
In-situ A356 - TiB$_2$ Composite formed by slag-metal reaction (present work)	**0**	**11.1**	**10.2**	**147**	**121**	**332**	**56**
	5	**10.5**	**9.7**	**153**	**129**	**358**	**58**
	7.5	**9.2**	**8.3**	**162**	**137**	**372**	**62**
	10	**8.6**	**7.5**	**178**	**144**	**387**	**71**
Al - 2%Mg - Al$_2$O$_3$ - TiB2 Composite formed by melt string [58]	0	13.4	24.7	150	-	-	39
	3.54	10.3	16.7	164	-	-	53
	5.84	11.6	20.7	154	-	-	44.5
Al - 3%Mg - Al$_2$O$_3$ - TiB$_2$ Composite formed by melt -stirring [22]	0	29.6	22.9	162	80.5	-	52.6
	2.03	28.2	21.9	163	94.5	-	57.7
	3.58	23.5	19.1	169	99.5	-	64.5
	4.42	20	16.7	175	108	-	73.2
In-situ Al-4.5 Cu -TiB$_2$ by in melt reaction [59]	5	1.9	-	358	258	-	83
	7	2.8	-	387	283	-	84
	10	3.3	-	417	317	-	87
AA1100-TiB$_2$ in-situ stir casting [60]	7.3	4.6	-	223	171.3	-	-
Al - 4.5Cu-TiB$_2$ in-situ stir casting [60]	15	2.3	-	333	202.8	-	-
Al- TiB$_2$ Composite by stir casting[61]	5	9.2	-	124	96	-	-
	10	6.3	-	164	128	-	-
	15	5.5	-	153	124	-	-

CHAPTER V

CONCLUSIONS

In the present study, discontinuously TiB_2 reinforced aluminum A356 alloy matrix composites were successfully produced and metallographic and mechanical properties were carefully investigated. Slag/metal reaction method was applied during the in-situ production route. Commercially pure Aluminum, Boric acid (H_3BO_3), Rutile (TiO_2) and Cryolite (Na_3AlF_6) were used as ingredient materials. The amounts of TiB_2 particles in the produced composites were 5%, 7.5%, 10% by volume. The matrix was well known A 356 aluminum casting alloy which has 7 weight % Si and 0.3 weight % Mg. Squeeze casting process was applied and mechanical testing specimens were prepared by use of a special die.

Microstructural studies were performed by both light and scanning electron microscopes. In order to identify the phases present, and the microstructural charteristics, energy dispersive X-ray spectroscopy and X-ray diffraction analysis were conducted.

Tensile tests, three point bending tests and hardness tests were carefully carried out. Furthermore, the effect of reinforcement amount on the mechanical properties was determined.

The main results which were obtained in the present study are shown below:

1. TiB_2 particles were formed in-situ in the aluminum matrix through the reaction of TiO_2 and B_2O_3 in the Na_3AlF_6 based slag by liquid Aluminum.

2. TiB_2 particles formed by slag-metal reaction were found to have formed in roughly spherical shapes having 1-4 μm in size.

3. TiB_2 particles were found no to have penetrated into the first solidified proeutectic α-dendrites. TiB_2 particles were distributed around the proeutectic α-dendrites and a more homogenous distribution compared with other processing techniques such as solid state reactive sintering, was obtained.

4. Grains and dendrite arm spacings were significantly refined with the formation of TiB_2 particles.

5. The eutectic silicon phase was modified and the flake eutectic silicon transformed into a fibrous form between the proeutectic α-Al dendrites.

6. Ultimate tensile strength, yield strength, flexural strength and hardness of the material increased with increasing TiB_2 reinforcement amount in the metallic matrix.

7. Elongation and reduction in area decreased with increasing reinforcement amount in the metallic matrix.

Finally, it can be stated that in-situ technique used in this study can successfully be applied to produce an A356-TiB_2 composite

REFERENCES

[1] T.S. Srivatsan, I.A. Ibrahim, F.A. Mohamed, E.J. Lavernia, Journal of Materials Science, 26 (1991), p. 5965-5978.

[2] C.A. Smith, Discontinuous Reinforcements for Metal-MatrixComposites, in: D.B. Miracle, S.L. Donaldson (Eds.) ASM Metals Handbook, Vol:21, 10th ed., 2001, p. 51-56

[3] H.J. Rack, Processing and Properties of powder metallurgy composite, in: P. Kumar, K. Vedula, A. Ritter (Eds.), The Metallurgical Society, Warrendale, PA, 1988, p. 155.

[4] D.E. Alman, Properties of Metal-Matrix Composites, in: D.B. Miracle, S.L. Donaldson (Eds.) ASM Metals Handbook, Vol:21, 10th ed., 2001, p. 838-842.

[5] Y. Han, X. Liu, X. Bian, Composites Part A: Applied Science and Manufacturing, 33 (2002), p. 439-444.

[6] D.B. Miracle, S.L. Donaldson, Introduction to Composites, in: D.B. Miracle, S.L. Donaldson (Eds.) ASM Metals Handbook, 2001, p. 39-40

[7] K.U. Kainer, Metal Matrix Composites, Custom-made Materials for Automotive and Aerospace Engineering, in: K.U. Kainer (Ed.), Wiley-VCH, 2006, p. 2

[8] K.U. Kainer, Metal Matrix Composites, Custom-made Materials for Automotive and Aerospace Engineering, in: K.U. Kainer (Ed.), Wiley-VCH, 2006, p. 3.

[9] R.W. Hertzberg, Deformation and Fracture Mechanics of Engineering Materials, 3rd ed., John Wiley & Sons, 1989.

[10] C.A. Smith, Discontinuous Reinforcements for Metal-MatrixComposites, in: D.B. Miracle, S.L. Donaldson (Eds.) ASM Metals Handbook, Vol:21, 10th ed., ASM, 2001, p. 51.

[11] I.A. Ibrahim, F.A. Mohamed, E.J. Lavernia, Journal of Materials Science, 26 (1991), p. 1137-1156.

[12] G.S. Murty, M.J. Koczak, W.E. Frazier, Scripta Metallurgica, 21 (1987), p. 141-146.

[13] E.L. Rooy, Introduction to Aluminum and Aluminum Alloys, in: ASM Metals Handbook, ASM, 2001, p. 22-23.

[14] A. Kearney, E.L. Rooy, Aluminum Foundry Products, in: T. Lyman (Ed.) ASM Metals Handbook, Vol:2, 9th ed., ASM 1979, p. 140.

[15] D.A. Granger, Solidification of Eutectic Alloys: Aluminum-Silicon Alloys, in: R. Elliott (Ed.), ASM Metals Handbook, Vol:15, 1988, p. 160-168.

[16] J. Ejiofor, R. Reddy, JOM Journal of the Minerals, Metals and Materials Society, 49 (1997), p. 31-37.

[17] A. Kearney, E.L. Rooy, Aluminum Foundry Products, in: T. Lyman (Ed.) ASM Metals Handbook, Vol:2, 9th ed., ASM, 1979, p. 164-165.

[18] B.K. Hwu, S.J. Lin, M.T. Jahn, Materials Science and Engineering A, 207 (1996), p. 135-141.

[19] Y. Cui, L. Ceng, C. Yao, X. Li, in Proceedings of ICCM-11, III (1997), p. 215-220.

[20] A. Changizi, Productıon and Properties of In-Sıtu Aluminum Titanum Diboride Composites Formed by Slag-Metal Reactıon Method, MSc thesis, METU. , February 2005. p. 9.

[21] D.M. Stefanescu, Trans Tech Publications Inc., Vol: 79-80, (1993), p. 75-90.

[22] M. Elmadagli, A Study on the Production of Al-TiB2 Particulate Reinforcement Al Composite, MSc thesis, METU, July 2000. p. 5.

[23] Y. Liu, S. Yin, Z. Guo, L. Hoyi, Journal of Materials Research, 13 (1998), p. 1749-1752.

[24] M.A. Meyers, E.A. Olevsky, J. Ma, M. Jamet, Materials Science and Engineering A, 311 (2001), p. 83-99.

[25] K.U. Kainer, Metal Matrix Composites, Custom-made Materials for Automotive and Aerospace Engineering, in: K.U. Kainer (Ed.), Wiley-VCH, 2006, p. 24

[26] A. Changizi, Productıon and Properties of In-Sıtu Aluminum Titanum Diboride Composites Formed by Slag-Metal Reactıon Method, MSc thesis METU, February 2005. p. 17.

[27] A. Changizi, Productıon and Properties of In-Sıtu Aluminum Titanum Diboride Composites Formed by Slag-Metal Reactıon Method, MSc thesis, METU, February 2005. p. 18.

[28] K.U. Kainer, Metal Matrix Composites, Custom-made Materials for Automotive and Aerospace Engineering, in: K.U. Kainer (Ed.), Wiley-VCH, 2006, p. 20-25.

[29] F.J. Humphreys, Deformation and annealing mechanisms in discontinuously reinforced metal-matrix composites, Proc. 9th Risø Int. Symp ed., On Mechanical and Physical Behavior of Metallic and Ceramic Composites, Risø National Laboratory, Roskilde 1988. p. 51-74.

[30] F.J. Humphreys, A. Basu, M.R. Djazeb, The microstructure and strength of particulate metal-matrix composites, Proc. 12th Risø Int. Symp ed., on Materials Science, Metal-Matrix Composites -Processing, Microstructure and Properties, Risø National Laboratory, Roskilde, 1991. p. 51-66.

[31] A. Hollemann, E. Wiberg, Lehrbuch der anorganischen Chemie, de Gruyter, (1985), p.

[32] Company prospectus Nicalon Fiber, Nippon Carbon Co., Ltd., Tokyo, Japan, (1989), p.

[33] N.L. Yue, L. Lu, M.O. Lai, Composite Structures, 47 (1999), p. 691-694.

[34] I. Maxwell, A. Hellawell, Metallurgical and Materials Transactions B, 3 (1972), p. 1487-1493.

[35] A. Abdel-Hamid, F. Durand, Z. Metallkd. , 76 (1985), p. 744.

[36] J. Murray, P. Liao, K. Spear, Journal of Phase Equilibria, 7 (1986), p. 550-555.

[37] J. Marcantonio, L. Mondolfo, Metallurgical and Materials Transactions B, 2 (1971), p. 465-471.

[38] F. Zupanic, S. Spaic, A. Krizman, Materials Science and Technology, 14 (1998), p. 1203-1212.

[39] J. Moriceau, Revue De L'Aluminium, (1972), p. 977.

[40] H.-G. Lee, Chemical Thermodynamics for Metals and Materials, Imperial College Press, 1999. p. 283-295.

[41] H. Zhu, H. Wang, L. Ge, W. Xu, Y. Yuan, Materials Science and Engineering: A, 478 (2008), p. 87-92.

[42] Y. Zhang, X. Wu, R. Rapp, Metallurgical and Materials Transactions B, 34 (2003), p. 235-242.

[43] L. Murray, in: H. Baker (Ed.) ASM Metals Handbook, Vol:3, ASM. , 2001, p. 51.

[44] S.V. Devyatkin, G. Kaptay, Journal of Solid State Chemistry, 154 (2000), p. 107-109.

[45] Handbook of Ternary Alloy Phase Diagram, ASTM, 1995.

[46] M.M. Schwartz, Processing,Fabrication, and Applications, in: D.B. Miracle, S.L. Donaldson (Eds.) ASM Metals Handbook, Vol:21, 10th ed., ASM, 2001, p. 579-584.

[47] J.R.R.M. Aikin, J. Metals, 8 (1997), p. 35.

[48] V. Shtessel, S. Sampath, M. Koczak, In-Situ Composites /Science and Technology, TMS, Pennsylvania, 1994. p. 37.

[49] A.K. Kuruvilla, K.S. Prasad, V.V. Bhanuprasad, Y.R. Mahajan, Scripta Metall. Mater, 32 (1995), p. 873-877.

[50] K.U. Kainer, Metal Matrix Composites, Custom-made Materials for Automotive and Aerospace Engineering, in: K.U. Kainer (Ed.), Wiley-VCH, 2006, p. 28.

[51] Russell, S.Y. Oh, A. Figueredo, MRS Bull., 16 (1991), p. 46-52.

[52] M.J. Koczak, Fundamentals of Metal Matrix Composites, Butterworth-Hemmann, New York, 1993.

[53] A. Mortensen, I. Jin, International Materials Reviews, 37 (1992), p. 101-128.

[54] A. Kurtoglu, Aluminum Oxide and Titanium Diboride Reinforced Metal Matrix Composite and Its Mechanical Properties, MSc thesis, METU August 2004. p. 58.

[55] A. Kurtoglu, Aluminum Oxide and Titanium Diboride Reinforced Metal Matrix Composite and Its Mechanical Properties, MSc thesis, METU August 2004. p. 59-60.

[56] A. Kurtoglu, Aluminum Oxide and Titanium Diboride Reinforced Metal Matrix Composite and Its Mechanical Properties, MSc thesis, METU, August 2004 p. 53.

[57] A. Kearney, E.L. Rooy, Aluminum Foundry Products, Metals Handbook, ASM, 2001. p. 510.

[58] Kuroglu. A, Aluminum oxide titanium diboride reinforced metal matrix composite and its mechanical properties, MSc thesis, METU, July 2004. p. 86

[59] Z. Chen, Y. Chen, G. An, Q. Shu, D. Li, Y. Liu, Metallurgical and Materials Transactions A, 31 (2000), p. 1959-1964.

[60] K.L. Tee, L. Lu, M.O. Lai, Composite Structures, 47 (1999), p. 589-593.

[61] K.L. Tee, L. Lu, M.O. Lai, Journal of Materials Processing Technology, 89-90 (1999), p. 513-519.